PHOTOCONDUCTIVITY IN A MAGNETIC FIELD AND SOME RELATED EFFECTS IN SEMI-INSULATED GALLIUM ARSENIDE

by

H. A. MILNER-BROWN

Submitted in partial fulfillment
of the requirements for the degree of
Master of Science

Department of Physics,
Faculty of Pure and Applied Science,
The University of Ottawa,
Ottawa, Canada.

1969

ABSTRACT

It has been observed in semi-insulating GaAs at both $90^{o}K$ and $300^{o}K$, that the photocurrent (I_p) could be decreased (I_p^-) or increased (I_p^+) depending upon whether the photoexcited carriers are deflected towards or away from the surface of photoexcitation. These effects are attributed to differences in surface and volume lifetimes of the photoexcited carriers.

Results obtained varied with surface treatment, temperature and wavelength of excitation as well as with the magnitudes of the applied electric (E) and magnetic fields (B) and are quantitatively expressed in terms of the ratios $A = I_p^+/I_p$ and $R = I_p^+/I_p^-$. A sample which had undergone abrasive surface treatment gave $R = 40$, $A = 4.5$ at $90^{o}K$ and $R = 10$, $A = 4.5$ at $300^{o}K$ for $B = 2.2\ Wb/m^2$, $E = 6 \times 10^4$ volt m^{-1} and $\lambda = 7500\ \mathring{A}$: a chemically polished sample under the same conditions gave $R = 3.5$, $A = 1.5$ at $300^{o}K$. The maximum ratios obtained were $A = 23$, $R = 54$ at $90^{o}K$ for $B = 2.2 Wb/m^2$, $E = 6 \times 10^4$ volt m^{-1} and $\lambda = 4500\ \mathring{A}$.

A simple phenomenological theory of this effect has been formulated based on a previously developed model and independent Photo-Hall, Photoconductivity and Photo-electromagnetic (PEM) measurements gave the magnitudes of the principal phenomenological parameters involved. The parameters are a mean harmonic of mobilities $\mu \simeq 6 \times 10^{-2}$ metre volt^{-1} sec^{-1}, a mean volume lifetime $\tau_2 \simeq 6 \times 10^{-7}$ sec., a mean surface

lifetime $\tau_2 \simeq 1.3 \times 10^{-7}$ sec all at $300^{o}K$, and it was then possible to compare experimental data with calculated values using the Simple model and a satisfactory agreement was obtained.

ACKNOWLEDGEMENTS

The author wishes to thank Dr. E. Fortin for suggesting the problem and for his supervision throughout the course of the research, and to Dr. E. van Tongerloo for the GaAs crystals. Thanks are also due to Mr. R. Senechal and Mr. G. Dionne for helpful discussions and to Mr. C. N. Goodchild and the Technicians for construction of the cryostat. Finally, the author is grateful to the Canadian International Development Agency for their financial support during the period of this research.

LIST OF ILLUSTRATIONS

LIST OF TABLES

TABLE OF CONTENTS.

CHAPTER I

INTRODUCTION

This chapter summarizes the various effects to be discussed in this thesis; these are the Photoconductivity process, the PEM effect, the Photo-Hall effect and photoconductivity in a magnetic field. There is also a review of the literature as far as the effect of a magnetic field on the photoconductivity is concerned and a description of the project.

1-1 Photoconductivity Process

The principal purpose of this section is to introduce the characteristic parameters necessary for a simple description of photoconductivity.

The conductivity of an insulator or a semiconductor is expressed as $\sigma = e(n\mu_n + p\mu_p)$ (1-1)

Where n and p are the densities of free electrons and holes, respectively, and μ_n and μ_p are the electron and hole mobilities.

When an insulator or a semiconductor is illuminated with light of wavelengths lying in the fundamental absorption region, the absorption of light quanta produces electron transitions from the valence band to the conduction band and consequently generates non-equilibrium electrons and holes. The photoconductivity resulting is

then given by

$$\Delta\sigma = e(\Delta n\mu_n + \Delta p\mu_p) \tag{1-2}$$

where Δn and Δp are the excess electron and hole densities respectively. In insulators the values of Δn and Δp may be much larger than the corresponding free-carrier densities in the dark, n_o and p_o. In semiconductors, the reverse is often true, and the effect of radiation can be considered as a small perturbation on a large dark carrier density. The semi-insulating GaAs under consideration in this work belongs to the former group.

Now if the light falling on the photoconductor creates G electron-hole pairs per second per unit volume of the photoconductor, then

$$G\tau_n = \Delta n \tag{1-3}$$

and

$$G\tau_p = \Delta p$$

where τ_n is the free lifetime of an electron, τ_p is the free lifetime of a hole, and Δn and Δp are respectively the additional steady state free electron and hole densities present due to the light absorption. The photoconductivity equation (1-2) can then be rewritten as

$$\Delta\sigma = Ge(\mu_n\tau_n + \mu_p\tau_p) \tag{1-4}$$

This relation shows that the lifetime is the dominant parameter in photoconductivity. By definition the free lifetime is the time that the charge carrier is free to contribute to the conductivity. It is the time that an excited hole spends in the valence band. The free lifetime of a charge carrier can be terminated by recombination or inter-

rupted if the carrier is trapped, to be resumed when the carrier is freed from the trap.

All through the analysis however, we shall be concerned with the pair lifetime, which is the free lifetime of an electron-hole pair. If either electron or hole is captured, the pair lifetime is terminated.

Now the change in conductivity resulting from excitation is normally terminated by the recombination of the photoexcited electrons and holes. This recombination can occur either by direct recombination of free electrons and holes without one of the carriers being first captured at an imperfection or by the recombination of a free carrier of one type with a bound carrier of the opposite type, previously captured at an imperfection in the crystal. In most cases, recombination through an imperfection dominates for low-carrier densities, and direct recombination becomes important only for high-carrier densities.

Whenever recombination between photoexcited electrons and holes occurs, some means must be provided for the dissipation of the excess energy of the excited carriers. There are three basic ways in which this energy dissipation can occur: (1) by the emission of photons, the energy of each photon being equal to the energy difference between the two carriers before recombination.

(2) by the emission of a number of phonons with total energy equal to the excess energy to be dissipated.

(3) by a three-body collision, the excess energy being given up to a third carrier in what is called an Auger or impact recombination.

The Auger recombination process might make use of an exciton (bound electron-hole system), one member of the exciton carrying off the excess energy to be dissipated in the capture of the other member. It is therefore the recombination process which determines the lifetime of the free carriers, and hence the sensitivity of the photoconductor.

The effect of a magnetic field on the photocurrent has been explained in terms of a surface lifetime, which is the lifetime of the carriers in the surface region and a volume lifetime, the carrier lifetime in the bulk of the sample. A brief discussion of these lifetimes will be given in the next section.

1-2 Surface and Volume Lifetimes

The surface of a crystal is a macroscopic deviation from the periodic nature of the structure and therefore trapping and recombination processes at the surface of a semiconductor are substantially different from those in the volume of the same material.

Differences between surface and volume recombination can be examined in terms of differences in steady-state photoconductivity excited by surface-absorbed (exciting photon energy greater than band gap) or volume-absorbed (exciting photon energy smaller than band gap) radiation. One of the most commonly observed results of such differences is the maximum near the absorption edge in the photoconductivity response measured as a function of exciting wavelength.

The variation of photoconductivity decay time with exciting wavelength for a typical sensitive crystal as shown in (1) indicates

that the decay time for surface excitation is much smaller than the decay time for volume excitation. Thus for a photosensitive material, the volume lifetime of photocarriers is usually larger than the surface lifetime, and a maximum in the spectral response occurs when a change is made from surface excitation to volume excitation with increasing wavelength. One possible reason for the lifetime differences is that strongly absorbed excitation creates a high density of photocarriers in a small volume near the surface, resulting in a predominance of bimolecular recombination and hence a decreased lifetime for the free carriers. A second possible reason is that either there is a greater density of recombination centers near the surface than in the volume or that their capture cross-section is larger. Lifetime measurements which will be reported on in Chapter IV clearly indicate that the volume lifetime is greater than the surface lifetime.

1-3 Photoconductivity in a Magnetic Field

When a semiconductor is illuminated with light of energy $h\nu$ greater than the forbidden gap, electron-hole pairs are created, and thus, photoconductivity should result under an applied electric field. However, in the region of very high absorption where the absorption constant (α) is about 10^6 m^{-1}, the radiation can only penetrate a

thin surface film of thickness $1/\alpha$, and thus can only produce photoconductivity in this film . Firstly, surface imperfections will tend to obstruct the flow of this photocurrent more than photocurrents through the bulk of the material. Secondly, the fact that the incident radiation is absorbed in a thin surface film means that the density of photoelectrons produced will be high, and therefore the recombination probability of electrons and holes will be high. For these reasons, the specific sensitivity of many photoconductors drops appreciably on the short wavelength side of the spectrum. Now if a magnetic field is applied in a direction such that before recombination the photocarriers are dragged down by the Lorentz force into the bulk of the sample where a longer lifetime prevails, the photocurrent could be enhanced. Conversely, if the direction of the magnetic (or electric) field is reversed, carriers created in the bulk will be pushed towards the surface causing a decrease in photocurrent. In the I-V characteristics at constant magnetic field one would therefore expect to observe something reminiscent of a diode rectifier characteristics.

From a phenomenological viewpoint, the above effect is not unlike the photoelectromagnetic (PEM) effect. In the latter, electron-hole pairs are produced at the illuminated surface, set up a concentration gradient, and diffuse naturally into the bulk. Under the influence of a magnetic field the electrons and holes separate and there is a net charge transport along the sample,

creating the PEM current. In the former, the magnetic field forces electron-hole pairs into the bulk of the sample, and the electric field creates the current. Thus the same factors controlling the PEM current will have an influence on the magnitude of the photo-current in a magnetic field, as will be shown by the identical behaviour of both effects with the same parameters. This will be considered in Chapter IV.

1-4 Terminology

In our analysis we shall assume a simple model in which a rectangular photoconducting slab is in the Voigt geometry with a mean carrier lifetime τ_1 from the illuminated surface ($Z = 0$) to a depth Z_1 (region no. 1) and mean volume lifetime τ_2 for $Z > Z_1$ (region no. 2). In actual fact, however, the carrier lifetime is probably a continuous function of Z, increasing smoothly towards the interior of the sample. Now the experimental results will be expressed quantitatively in terms of Rectification (R) and Amplification (A) ratios; the former term originates from the shape of the I - V characteristics. R and A are defined as follows: If I_p^- , I_p^+ are the photocurrents when the magnetic field deflects the photoexcited carriers towards and away from the illuminated surface respectively and I_p the photocurrent in the absence of a magnetic field, then Rectification ratio $R = I_p^+/I_p^-$ and Amplification ratio $A = I_p^+/I_p$. It should be clarified here that owing to diffusion effects and the fact that in region no. 1 the lifetime increases smoothly from $Z = 0$ to $Z = Z_1$, $I_p^- \neq I_p$ because while I_p^- is a measure of only the equilibrium number of photocarriers concentrated at the very top of the surface region where τ_1 is very small, I_p on the other hand includes even the photocarriers which actually diffuse into the volume. Thus, I_p is always greater than I_p^- and therefore the rectification ratio R is always greater than the amplification ratio A. This fact will be very evident when results are presented in Chapter IV.

1-5 Photo-Hall Effect

One of the best and most widely used methods of determining the mobilities of charge carriers in solids is the Hall effect: when the crystal is illuminated, it is referred to as the Photo-Hall effect: the conductivity $\sigma = ne\mu$, where n is the density of free carriers and μ their mobility; the Hall constant $R = K/ne$, where K is a constant between 1 and 2 depending on the scattering mechanism and the band structure, and the Hall Mobility $\mu_H = \sigma R = K\mu$. The variation of Hall mobility with photoexcitation intensity L can be expressed:

$$d\mu_H/dL = \mu \quad dK/dL + K\, d\mu/dL$$

The term involving the variation of K with L can be neglected for present purposes; not only is the variation less than a factor of 2, for a complete change over for impurity-dominated to phonon-dominated scattering (32), but K decreases with L under these conditions. The variation of μ with L can be illustrated by the simple case where photoexcitation raises the fermi-level to fill positively charged centers and hence greatly reduces their scattering.

When both carriers are making an appreciable contribution to the conductivity, the measured Hall Constant R is given by

$$R = p\mu_p^2 - n\mu_n^2/e(p\mu_p + n\mu_n)^2$$

if we assume K is unity.

Since for two-carrier conductivity $\sigma = pe\mu_p \quad ne\mu_n$, the Hall mobility $\mu_H = \sigma R$ is given by

$$\mu_H = p\mu_p^2 - n\mu_n^2/p\mu_p + n\mu_n$$

Thus μ_H goes to zero when $p\mu_p^2 = n\mu_n^2$, with R changing sign as this point is reversed.

1-6 Literature Review

Changes of photocurrent in the presence of a magnetic field have been previously reported in CdS single crystals at 300°K by Shōji Tanaka and co-workers (2) using wavelengths 436 mμ and 548mμ. From their observations they gave a probable expression $(I_p^+ - I_p)/I_p = CEB$, where I_p is the photocurrent in the absence of a magnetic field, I_p^+ the photocurrent when the magnetic field (B) is applied and C an unspecified constant. The fractional change in photocurrent was about 0.1 for E = 10^4 volt/cm and B = 1 Wb/m^2.

Frankevitch and Balabanov (3) (4) observed a change in the photoconductivity of organic semiconductors in a magnetic field. According to their theory, the rate of formation of free carriers is governed by the total concentration of transport excitons which are formed after the absorption of light. The magnetic field can alter the concentration of transport excitons if the steady-state concentrations of the para- and ortho-excitons with m = o are not equal.

The fractional change in photocurrent observed in both anthracene and naphthalene was however less than 20% at V = 600 volts and B = 2 Wb/m^2.

Zielinger, Zouachi, Fortin and Weichman (5) reported a Photomagneto-rectification effect in Cu_2O at 77^oK in which a rectification ratio R = 10 was obtained for B = 1.9 Wb/m^2, V = 300 volts and λ = 4700 $\mathring{A}$. They attributed the effect to differences in the surface and volume lifetimes of the photocarriers, however, the photocurrents were small $\sim 10^{-12}$ Amps.

A simple model of the above effect has been developed by Fortin (6) which has a form similar to the equation given in (2). However, the previously unspecified constant C was identified as equal to $\frac{\mu^2(\tau_2 - \tau_1)}{Z_1}$, where μ is the mean harmonic of the electron and hole mobilities, τ_2 and τ_1, the mean volume and surface lifetimes respectively, and Z_1 the depth of the surface region. This linear relation is however only true at low electric and magnetic fields, but offers a means of measuring lifetimes which will be considered later in Chapter IV.

Using the same basic model another equation has been derived by the author which satisfies the behaviour at higher fields and reduces to (6) at low fields (ie: valid at all fields). This will be given in Chapter II.

1-7 Summary of Project

Detailed study of the photoconductivity in a magnetic field of semi-insulating GaAs were pursued partly because the increase in photocurrent was much larger than previously reported (40 times larger than that reported in (2) under the same conditions and up to 250 times larger at $90^{o}K$) and also indicated a potential for being practically applicable.

Studies were made on the behaviour of the effect with respect to surface treatment, temperature, wavelength and intensity of excitation as well as to applied electric and magnetic fields.

The principal phenomenological parameters of the simple model are a mean harmonic of mobilities and a mean surface and volume lifetimes. In order to test the validity of the model an effort was made to measure these parameters. Using Photo-Hall and PEM effect measurements, these parameters were evaluated with reasonable accuracy. In addition, the behaviour of the PEM effect with certain parameters (magnetic field, intensity of excitation) were studied in comparison with the above effect in order to substantiate the initial hypothesis that the PEM effect and the Photocurrent amplification effect were from a phenomenological viewpoint similar. A satisfactory agreement was obtained of the experimental data with the theoretical predictions. No combined detailed experimental and theoretical analysis of this effect has previously been made.

CHAPTER II

THEORY

The following topics will be discussed in this chapter:

1. A theoretical treatment of photoconductivity with special emphasis on surface effects.
2. A simple model explaining the effect of a magnetic field on the magnitude of the photocurrent.
3. The principles involved in the PEM measurements which were used in evaluating the carrier mobilities and lifetimes.

1. Photoconductivity

A simple theoretical treatment of photoconductivity will now be given (7) for completeness to enable us to explain quantitatively the spectral distribution of photoconductivity.

A photoconductor is illuminated on one surface by monochromatic radiation of frequency ν.

The symbols used throughout are:

ω = width of sample (m)

d = thickness of sample (m)

$b = \mu_n/\mu_p$ - Mobility ratio

L = Ambipolar diffusion length (m)

S = Surface recombination velocity

($m\ sec^{-1}$)

α = Absorption coefficient

(m^{-1})

Q = Intensity of radiation

(quanta m^{-2} sec)

D = Ambipolar diffusion constant

($m^2\ sec^{-1}$)

τ = Carrier lifetimes in volume

= τ_2 in the previous sections

q = Quantum efficiency

The rate of creation of electron-hole pairs is given by

$$R = \frac{q\ \alpha Q}{h\nu} \tag{1-1}$$

Neglecting trapping effects, the equation of continuity satisfied by the excess carrier density Δn is:

$$D \frac{d^2\ \Delta n}{dz^2} - \frac{\Delta n}{\tau} = - Re^{-\alpha z} \tag{1-2}$$

where

$D \frac{d^2 \Delta n}{dz^2}$ is the rate of change of the number of excess carriers crossing unit area in the z-direction per unit time, due to diffusion;

$\frac{\Delta n}{\tau}$ is the recombination rate and $Re^{-\alpha z}$ is the rate of change of the electron-hole pairs created along the z-axis.

If d >>L, the appropriate solution of equation (1-2) is:

$$\Delta n = Ae^{-z/L} - \frac{\tau R e^{-z}}{(L^2\alpha^2 - 1)} \tag{1-3}$$

where A is a constant to be determined by the boundary condition at Z = 0.

$$D \frac{\partial \Delta n}{\partial z} = S\Delta n \tag{1-4}$$

where

$D \frac{\partial \Delta n}{\partial z}$ is the number of excess carriers crossing unit area in the z-direction per unit time, due to diffusion, and $S\Delta n$ is the net rate at which excess carriers are absorbed by the surface per unit area.

This conditions then gives:

$$\frac{DA}{L} - \frac{\alpha L^2 R}{(\alpha^2 L^2 - 1)} = - SA + \frac{S\tau R}{(\alpha^2 L^2 - 1)} \tag{1-5}$$

Hence, from equation (1-3)

$$\Delta n = \frac{R\tau}{(\alpha^2 L^2 - 1)} \cdot \frac{\alpha^2 L^2 + S\tau}{L + S\tau} \cdot (e^{-z/L} - e^{-\alpha z}) \tag{1-6}$$

The photocurrent is given by:

$$I_p = eE\,(1 + b)\,\mu_n\,\omega \int_0^{\infty} \Delta n\,dz \qquad (1\text{-}7)$$

$$= \frac{eq\,\omega LQ\,\mu_n\,\tau\,(1 + b)\,E}{h\nu\,(L + S\tau)} \cdot (1 + \frac{S\tau}{L}) \cdot \frac{1}{1 + \alpha L} \qquad (1\text{-}8)$$

When α is very large, the penetration depth is of the order of L and and the photocurrent $I_p = I_p(\infty)$ say, where

$$I_p(\infty) = \frac{eq\,LQ\,\mu_n\,\tau\,(1 + b)E}{h\nu\,(L + S\tau)} \qquad (1\text{-}9)$$

and hence,

$$(I_p/I_p(\infty)) = 1\quad \frac{S\tau}{L}\quad \frac{1}{(1 + \alpha L)} \qquad (1\text{-}10)$$

If $S\tau >> L$, a large increase in I_p will take place as α decreases sufficiently to make $\alpha \sim L^{-1}$, equation (1-10) becomes

$$I_p/I_p(\infty) = 1 + S\tau/L \qquad (1\text{-}11)$$

When $S\tau >> L$ the photocarriers will recombine mainly at the surface if they are formed at a distance less than L from the surface, while if they are formed mainly at a distance greater than L, bulk recombination will predominate with correspondingly longer lifetimes. When α becomes small enough at longer wavelengths, to enable an appreciable amount of radiation to pass through the sample, I_p begins to fall again as shown in Fig. 1.

Now in equation (1-11), $1 + S\tau/L = F$, the Surface factor which

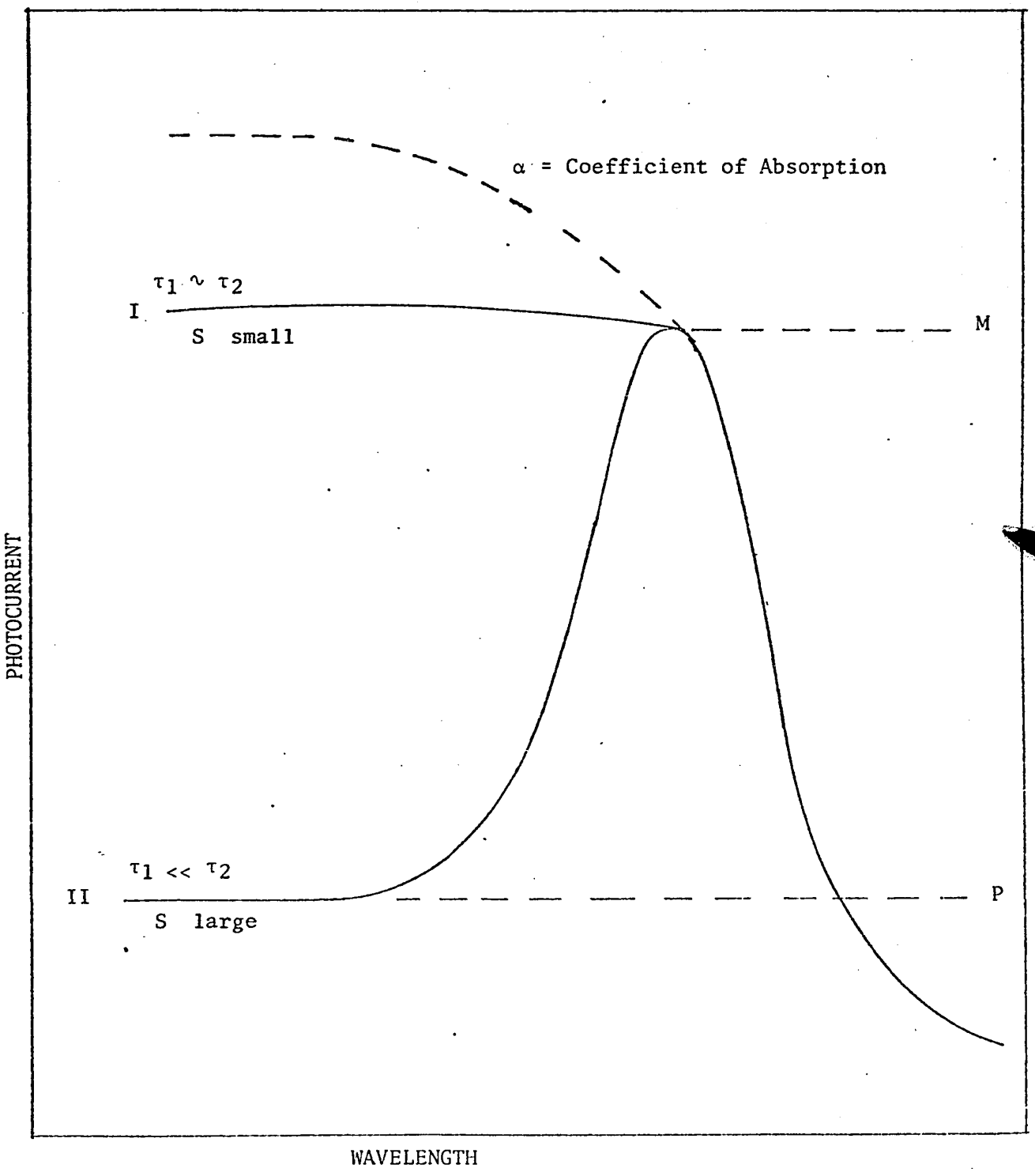

Figure 1: Variation of Photocurrent with Wavelength
(I) $\tau_1 \sim \tau_2$ (II) $\tau_1 << \tau_2$

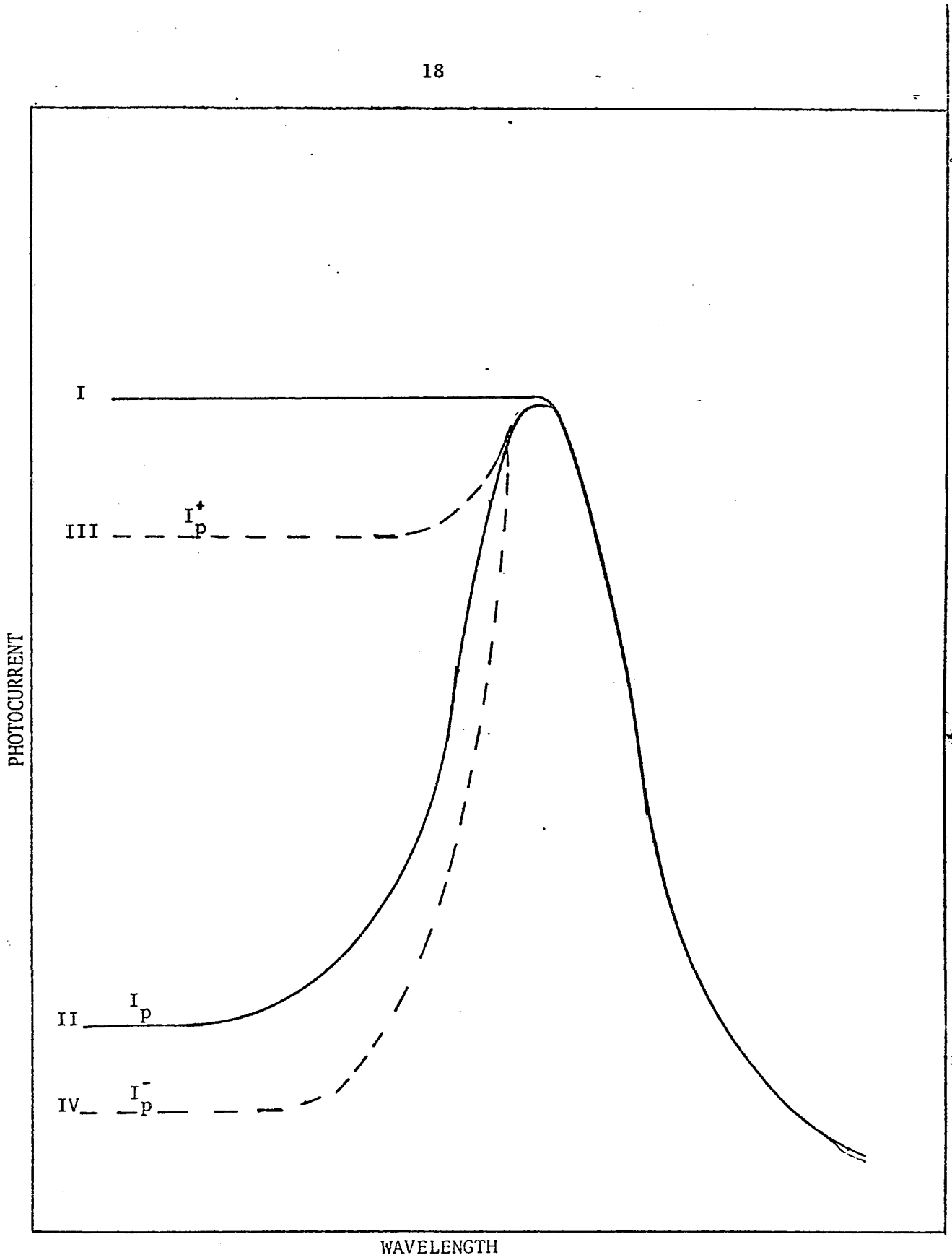

Figure 2 EFFECT OF A MAGNETIC FIELD ON THE SPECTRAL RESPONSE CURVE
Curve II (B=0) Curve III (B^+) Curve IV (B^-)

is defined as the ratio of the maximum photocurrent to the photocurrent at the "plateau". i.e. $F = M/p$ (see Fig. 1). $L \sim 10^{-5}$m, $\tau \sim 10^{-6}$ sec. Thus, when $S << 10$ m sec^{-1}, $F \sim 1$, the surface lifetime $\tau_1 \sim$ the volume lifetime τ_2 and therefore $I_p \sim I_p(\infty)$. Hence the photocurrent stays almost constant even at short wavelengths. However when S is larger than 30 m sec^{-1}, $\tau_1 << \tau_2$, F is large and the photocurrents at short wavelengths drops by a factor F, since $I_p/I_p(\infty) = F$. (Fig. 2 Curve II).

The magnetic field in deflecting the carriers into the volume, should raise Curve II to Curve III, and as a result reduce the effective surface factor as shown in Fig. 2. Theoretically, Curve II could be raised as far up as Curve I. Conversely, when the carriers are drawn more towards the illuminated surface, Curve II should be lowered to the level of Curve IV, increasing the effective surface factor. In general, at the short wavelength end of the spectral response curve, the Rectification ratio $R = \frac{I_p^+ \text{ (Curve III)}}{I_p^- \text{ (Curve IV)}}$

and the Amplification ratio $A = \frac{I_p^+ \text{ (Curve III)}}{I_p \text{ (Curve II)}}$

these predictions will be illustrated in Chapter IV. A simple model which explains the essential features of, and the parameters involved in this effect will be given in the next section.

$$\text{AMPLIFICATION RATIO} \quad A = \frac{I_p^+}{I_p} = \frac{1 + \dfrac{\mu^2 EB\tau_2}{Z_1}}{1 + \dfrac{\mu^2 EB\tau_1}{Z_1}} .$$

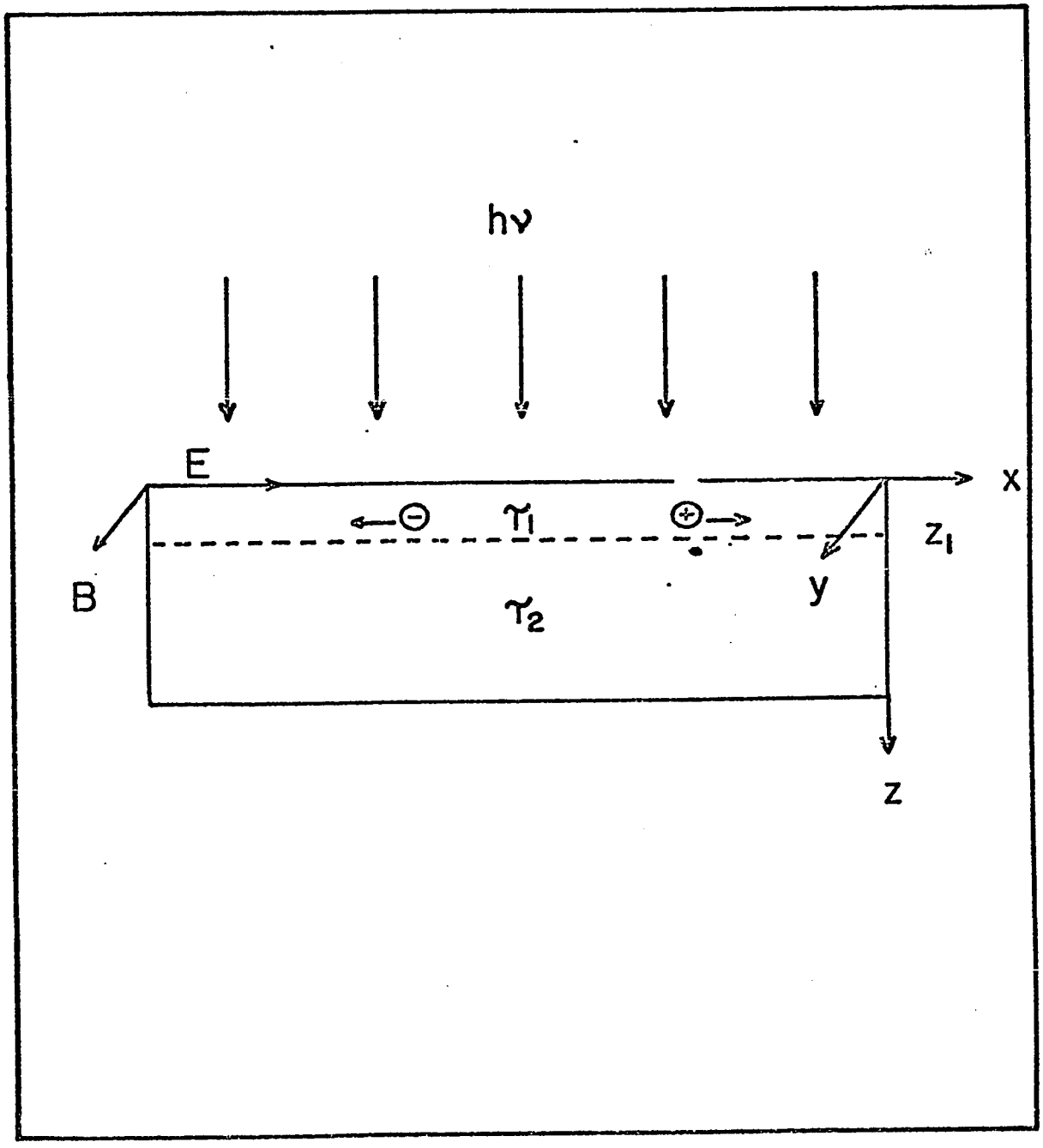

Figure 3 PHOTOCONDUCTING SLAB IN THE VOIGT GEOMETRY

2 Phenomenological Theory

2.1

A simple model of the above phenomenon has been developed by Fortin (6) from the arrangement illustrated in Fig 3 in which a rectangular photoconducting slab is in the Voigt geometry. The assumptions are:

a) A mean carrier lifetime τ_1 exists from the illuminated surface to a depth Z_1 (region no. 1) and τ_2 for $Z > Z_1$ (region no. 2)

b) Photoexcitation rate per unit volume is also a step function of Z, i.e. a Constant G up to $Z = Z_1$ and zero elsewhere, and also the dark current is zero.

c) The existence of surface states and thus of a space charge layer at the free surface of the semiconductor is neglected.

Under illumination, an electric field E, will yield a photocurrent

$$I_p = G\tau_1 \, e \, Z_1 \, (\mu_n + \mu_p)E \qquad (2\text{-}1)$$

where

μ_n, μ_p are the electron and hole mobilities.

If a magnetic field B is applied, the carriers are dragged into the bulk of the sample at a constant "drift" velocity $V_z = \mu^2 E_x B_y$ under equilibrium conditions, were $\mu = \frac{2\mu_n \mu_p}{\mu_n + \mu_p}$ is the mean harmonic of mobilities (11).

μ represents the effective mobility of an electron-hole pair, when 'pair' motion is considered,; it is derived from the relation

$$\frac{\frac{1}{\mu} = \frac{1}{\mu_n} + \frac{1}{\mu_p}}{2}$$

i.e. the average of the harmonic of electron and hole mobilities.

Since the electron mobility is larger than the hole mobility, the electrons will be deflected further into the volume of the sample when a magnetic field is applied. This could set up a concentration gradient resulting in a photovoltage which will tend to slow down the electrons and accelerate the holes. For this reason, it is to a first approximation reasonable to use the mean harmonic of mobilities μ, rather than μ_n and μ_p explicitly (10).

The number n_2 of photocarriers entering region no. 2 per second (also the number leaving region no. 1 per second) is given by:

$$n_2 = G\tau_1 V_Z \tag{2-2}$$

The steady state numbers of carriers in the respective regions are then:

$$\begin{aligned} N_2 &= n_2\tau_2 = G\tau_1 V_Z \tau_2 \\ N_1 &= G\tau_1 Z_1 - G\tau_1{}^2 V_Z \end{aligned} \tag{2-3}$$

The total photocurrent I_p in the presence of the magnetic field comes to:

$$\begin{aligned} I_p^+ &= (N_1 + N_2) e V_x \omega (\mu_n + \mu_n) E_x \\ I_p^+ &= I_p \left(1 + \frac{\mu^2}{Z_1} (\tau_2 - \tau_1) E_x B_y\right) \end{aligned} \tag{2-4}$$

According to this analysis, maximum Amplification ratio occurs when $\mu^2 EB\tau_1 = Z_1$, i.e.: when all the carriers generated in region no. 1 are dragged into region no. 2 before recombination, and is equal to τ_2/τ_1.

This linear amplification relation holds only at low fields, but has some practical applications which will be utilized in Chapter IV.

2-2

Since equation (2-4) predicts a linear amplification and does not account for the saturation effects which occur at high fields, an attempt has been made in evaluating the carrier densities at steady state using a different approach. The assumptions (a) and (c) of section (2-1) will also be made in this derivation; the dark current is also assumed to be zero.

The symbols used throughout are:

Q = illumination in quanta m^{-2} sec^{-1} absorbed on xy face

μ_n, μ_p = Electron and hole mobilities ($m^2 volt^{-1}$ sec^{-1})

μ = harmonic mean of mobilities defined by $\mu = \dfrac{2\mu_n \mu_p}{\mu_n + \mu_p}$

E = Electric field ($V\ m^{-1}$)

B = Magnetic Induction ($Wb\ m^{-2}$)

We consider photoconducting slab in the Voigt geometry in Fig. 3. Under constant source of illumination, if the quantum efficiency is unity, then the electron-hole pairs created up to a depth Z_1 per second equals $\int_0^{Z_1} Q\alpha e^{-\alpha Z}\, dZ$

$$= Q(1 - e^{-\alpha Z_1}) \qquad (2\text{-}5)$$

The carriers created at depths greater than $Z_1 = \int_{Z_1}^{\infty} Q\alpha e^{-\alpha Z}\, dZ$ is comparatively very small for α large and can be neglected.

If we consider a unit area of illuminated surface, then the rate of creation of electron-hole pairs per unit volume equals

$$\frac{Q}{Z_1}\,(1 - e^{-\alpha Z_1})$$

Hence, at steady-state the total number of carriers in region no. 1

$$= Q(1 - e^{-\alpha Z_1})\tau_1$$

giving rise to a photocurrent

$$I_p = Q(\mu_n + \mu_p)e\omega(1 - e^{-\alpha Z_1})\tau_1 E \qquad (2\text{-}6)$$

Now, when a magnetic field is applied along the y-axis electron-hole pairs moving along the x-axis with a velocity μE are deflected through a hall angle $\tan \theta = \mu B$. In a time τ_1, before recombination, the deflection of the pair along the z-axis into the volume is given by $\mu E\tau_1 \tan \theta = \mu^2 EB\tau_1$. This means that carriers at $Z = Z_1$ will be deflected a maximum distance of $\mu^2 EB\tau_1$ inside region no. 2 and the general distribution of carriers will be from $Z = o$ to $Z = \mu^2 EB\tau_1 + Z_1$

Owing to the random motion of the carriers, the displacements will not be equal and hence the distribution of carriers in the whole region will by no means be simple. However, any attempt to introduce a complex distribution function will result in complicated expressions difficult to interpret. A reasonable approximation to reality is to assume a uniform carrier distribution in both regions. The carrier pairs

created per unit volume is then equal to:

$$\frac{Q(1 - e^{-\alpha Z_1})}{\mu^2 EB\tau_1 + Z_1}$$

Thus the steady-state total number of carriers in the respective regions are

$$\frac{Z_1}{\mu^2 EB\tau_1 + Z_1} \cdot Q(1 - e^{-\alpha Z_1})\tau_1$$

$$\frac{\mu^2 EB\tau_1}{\mu^2 EB\tau_1 + Z_1} \quad Q(1 - e^{-\alpha Z_1})\tau_2 \qquad (2\text{-}7)$$

and the resultant photocurrent comes to

$$I_p = Q(\mu_n + \mu_p)\omega e\tau_1(1 - e^{-\alpha Z_1}) \quad \frac{Z_1}{\mu^2 EB\tau_1 + Z_1} \quad \frac{\mu^2 EB\tau_1}{\mu^2 EB\tau_1 + Z_1} \cdot \frac{\tau_2}{\tau_1} \quad E$$

(2-8)

$$I_p = I_p \quad \frac{Z_1 + \mu^2 EB\tau_2}{Z_1 + \mu^2 EB\tau_1}$$

$$I_p = I_p \quad \frac{1 + \mu^2 EB\tau_2/Z_1}{1 + \mu^2 EB\tau_1/Z_1}$$

Amplification ratio

$$A = \frac{I_p}{I_p} = \frac{(1 + \mu^2 EB\tau_2/Z_1)}{(1 + \mu^2 EB\tau_1/Z_1)} \qquad (2\text{-}9)$$

Eq. (2-9) indicates that when EB is very large such that $\frac{\mu^2 EB\tau_1}{Z_1} >> 1$, $A = \tau_2/\tau_1$ which is the theoretical maximum amplification ratio.

It will be interesting to know that Eq. (2-8) approximates to Eq. (2-4) at low fields, i.e.: when $\frac{\mu^2 EB\tau_1}{Z_1} << 1$. Now applying the binomial theorem to Eq. (2-8), we have

$$I_p^+ = I_p (1 + \mu^2 EB\tau_2/Z_1)(1 + \mu^2 EB\tau_1/Z_1)^{-1}$$

$$= I_p \left(1 + \frac{\mu^2 EB\tau_2}{Z_1} - \frac{\mu^2 EB\tau_1}{Z_1} - \frac{\mu^2 E^2 B^2 \tau_1\tau_2}{Z_1^2}\right)$$

Neglecting the last term gives

$$I_p^+ = I_p \left(1 + \frac{\mu^2 EB}{Z_1} (\tau_2 - \tau_1)\right)$$

which is the same as Eq. (2-4)

The principal parameters μ, τ_2 and τ_1 were measured using PEM effect methods. The principles involved in these methods will be outlined in the next section.

3. Principles of PEM Effect Measurements

One PEM method was used in the mobility measurements (in addition to the Photo-Hall measurements) whilst two independent methods were employed in the carrer life-time measurements. The principles

involved in all three methods will be given in this section.

(1) The mobility was deduced from the relation (8)

$$V_{PEM} = C \cdot B/1 + (\mu B)^2 \qquad (2\text{-}10)$$

where V_{PEM} is the PEM voltage, B is the magnetic field and C a constant of proportionality.

From the initial hypothesis of phenomenological similarity between PEM effect and Photocurrent Amplification effect, the value of μ expected from Eq. (2-10) was the mean harmonic of mobilities $\mu = 2\mu_n\mu_n/\mu_n + \mu_p$. The value actually obtained was the electron mobility.

From their theoretical postulate, Aigrain and Bulliard (9) (10) expected to measure $\mu = 2\mu_n\mu_p/\mu_n + \mu_p$ in germanium, but ended up measuring the electron mobility. This discrepancy is due to the basic assumptions made in all the derivations of the PEM effect. In his derivation of the PEM effect Bulliard (11) predicted a mean harmonic of mobilities μ, but then he assumes in his derivation that $\mu_n \sim \mu_p$. However, if μ_n is very different from μ_p the theory fails.
Kurnick and Zitter (8) obtained from the relation

$$I_{PEM} \propto \frac{\mu B}{(1 + \mu^2 B^2)^{1/2}}$$

the electron mobility in p-type InSb.

Thus the PEM effect derivations made so far give the minority carrier mobility and not the mean harmonic of mobilities.

From Eq. (2-10)

$$\frac{B}{V_{PEM}} = \frac{\mu^2 B^2}{C} + \frac{1}{C} \qquad (2\text{-}11)$$

and therefore a plot of B/V_{PEM} as a function of B^2 gives μ_n. We then assume a mobility ratio $\mu_n/\mu_p = 10$ to obtain μ_p, and hence μ.

(2) In the first method of lifetime measurements, use is made of the relation between the PEM voltage and Intensity of Excitation given by (12)

$$V_{PEM} = AI_o/C + I_o \qquad (2\text{-}12)$$

where A and C are constants as far as the Intensity I_o is concerned. A is obtained from the intercept of the graph of V_{PEM}^{-1} versus I_o^{-1}. Alternatively $A = V_{PEM}$ at high Intensities when $I_o >> C$.

Now A follows the relation (12)

$$A = BD\beta h \frac{\alpha}{\alpha + \beta + \frac{S}{D}} \qquad (2\text{-}13)$$

where

B = magnetic field

D = Constant of Diffusion related to the mobility by the Einstein relation $D = \mu KT/e$

In the nearly intrinsic specimen $D = 2D_nD_p/D_n + D_p$

$$= \frac{2\mu_n\mu_p}{D_n + D_p} \frac{KT}{e}$$

or $D = \mu KT/e$

h = length of sample

β = coefficient of recombination defined by $D\beta^2 = \frac{1}{\tau}$

where τ is the carrier lifetime.

α = Absorption constant

S = Surface recombination velocity.

When the absorption constant is high, Eq. (2-13) approximates to $A = BD\beta h$ (2-14)

Substituting the value of A from Eq. (2-12) into (2-14) gives β. Finally τ is calculated from

$$\tau = \frac{1}{D\beta^2} \qquad (2\text{-}15)$$

Now A was measured for different wavelengths, i.e., different depths of excitation. Thus, the final τ's calculated for different wavelengths give the lifetimes at different depths in the sample. The same method has been used by Zielinger (13) to obtain a profile of lifetimes across depth in Cu_2O.

(3) The second method used for lifetime measurements involved the relative magnitudes of the PEM and PC currents. This method has been shown to give misleading results when carrier trapping is present (14). Results, however, obtained using the simple analysis agreed very well with those obtained by the previous method. The fact that negligible optical quenching was detected when the sample was simultaneously illuminated by a monochromatic source of wavelength $\lambda = 7000\text{Å}$ and an infrared source, indicated a low trap density (15).

Optical quenching occurs when light raises electrons from the valence band to the sensitizing centers, thus freeing holes which subsequently are captured at sites where recombination with free electrons is probable. There is thus sufficient evidence to indicate that high resistivity GaAs is nearly trap free as pointed out earlier by Hilsum and Holeman (14).

The expression used in evaluating the lifetimes in this method will now be outlined (16)

If we include the effect for both electrons and holes we may express the short-circuit PEM current as

$$I_{PEM} = \frac{qQeB}{l} (D\tau)^{1/2} (\mu_n + \mu_p) \qquad (2\text{-}16)$$

where

q = Quantum efficiency

Q = incident radiation in quanta/unit time/unit area

D = ambipolar diffusion constant

$$= \frac{2D_n D_p}{D_n + D_p} = \frac{2\mu_n \mu_p}{\mu_n + \mu_p} \frac{KT}{e} = \mu \frac{KT}{e}$$

Eq. (2-16) satisfies the condition that the PEM effect vanishes when one of the carrier mobilities is effectively zero.

The corresponding photocurrent is given by

$$I_{pc} = \frac{qQe}{l} (\mu_n + \mu_p) E\tau \qquad (2\text{-}17)$$

where E is the applied electric field.

Combining (2-16) and (2-17) we obtain

$$\tau = (B/E)^2 \; D \; (I_{pc}/I_{PEM})^2 \qquad (2\text{-}18)$$

Results of carrier mobilities and lifetime measurements using the equations outlined in this section will be given in Chapter IV.

CHAPTER III

EQUIPMENT AND EXPERIMENTAL TECHNIQUE

This chapter describes

1. The general apparatus used in the photoconductivity and PEM measurements.
2. Sample preparation
3. Experimental procedure
4. Photo-Hall apparatus

1. General Apparatus

The OPTICAL CRYOSTAT was made of stainless steel and brass, with the lower portion surrounded by a detachable copper radiation shield. At liquid nitrogen temperature, the vacuum obtained was better than 10^{-6} mm of Hg. Fig. 5 shows a simple sketch of the cryostat. Samples were mounted on a BeO plate fixed on the copper tail of the optical cryostat thus achieving high electrical insulation and good thermal contact. Excitation by monochromatic radiation was obtained from a Bausch and Lomb High Intensity grating monochromator, and copper constantan thermocouple in contact with BeO plate was used in the temperature measurements.

The voltage applied to the crystal came from a stabilized D.C. Power Supply, and the current...etc. through the crystal were read on a Keithley Model 602 Solid State Electrometer whose input resistance was

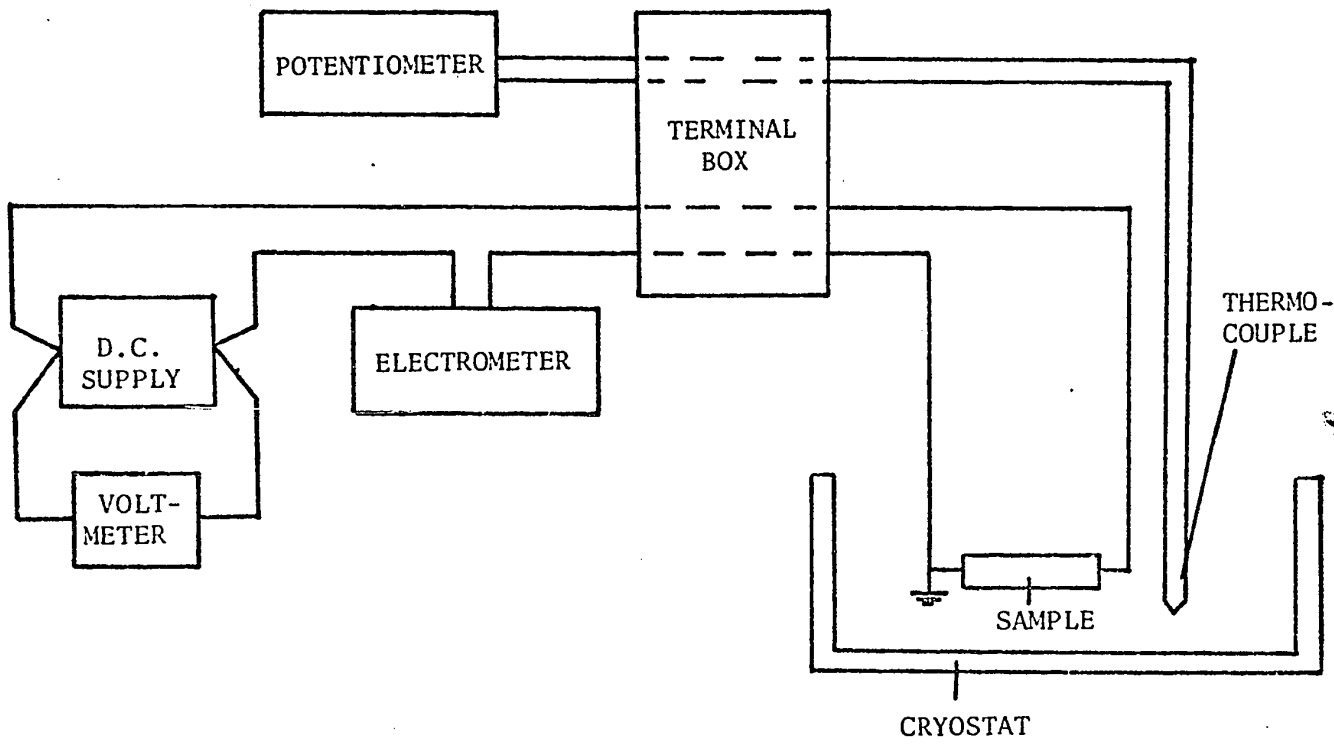

Figure 6 SCHEMATIC BLOCK DIAGRAM OF APPARATUS

greater than 10^{14} ohms. The voltage applied to the crystal was read on a Selectest Model "Super 50" volt-meter. Fig. 6 gives a schematic block diagram of apparatus.

The grating monochromator was calibrated using an Eppley vacuum-type thermopile, with CaF_2 windows and the case connected from the binding posts to the terminals of a KIPP and ZONEN high sensitivity "Microva" Multirange Microammeter. In the lower infra-red spectral range Kodak No. 29 filter was placed in the holder provided at the entrance of the slit end of the monochromator to eliminate unwanted orders of spectra. The widths of the Entrance and Exit slits were always kept at 5.36 mm and 3.00 mm respectively, and the Spectral range of operation was between 0.4μ to 1.1μ.

A black opaque tube was connected directly from the exit slit to fit the quartz window rim of the cryostat. This ensured complete exclusion of background radiation. Uniform magnetic fields were provided by a Magnion-Harvey-Wells 15" electromagnet model L-158 along with the HS-10200 Power Supply and EFC-4 field regulator. With a gap of 1 1/4" and a maximum current of 205 A, a maximum field of 3.2 Wb/m^2 is obtained. The desired field is simply dialed on the 5 decade switches and the power supply automatically drives up to that field. The general arrangement is shown in Fig. 4.

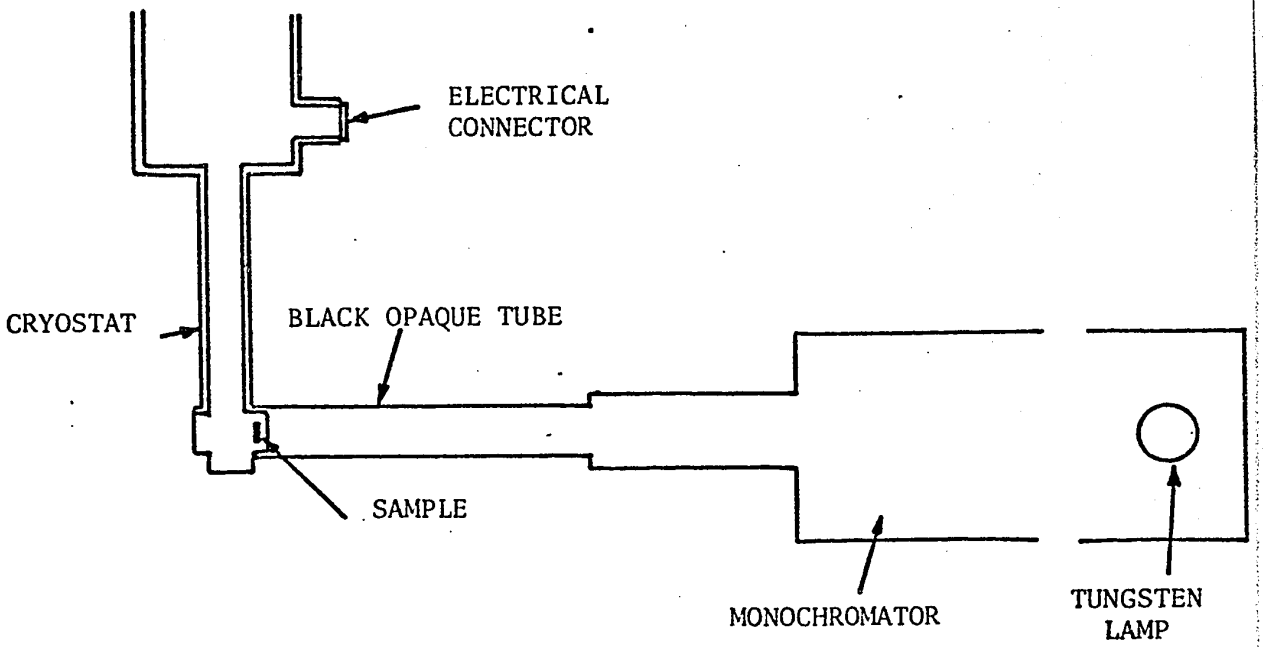

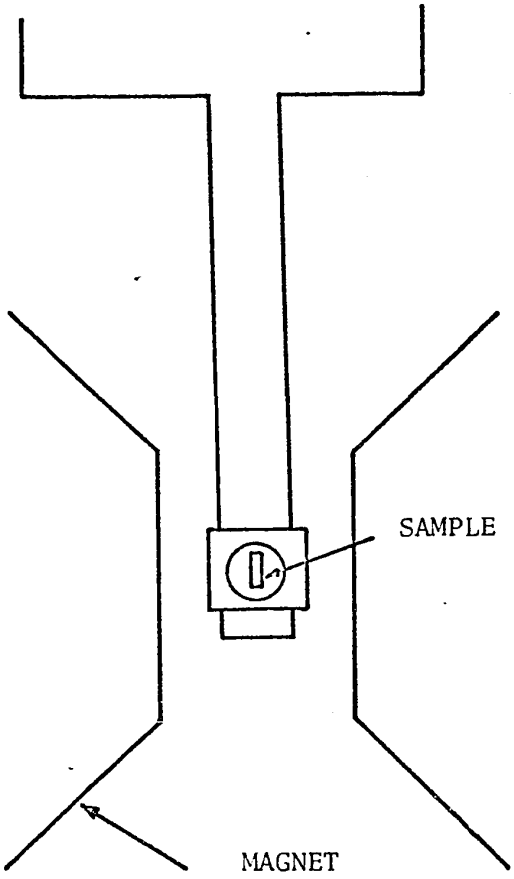

Figure 4 EXPERIMENTAL ARRANGEMENT

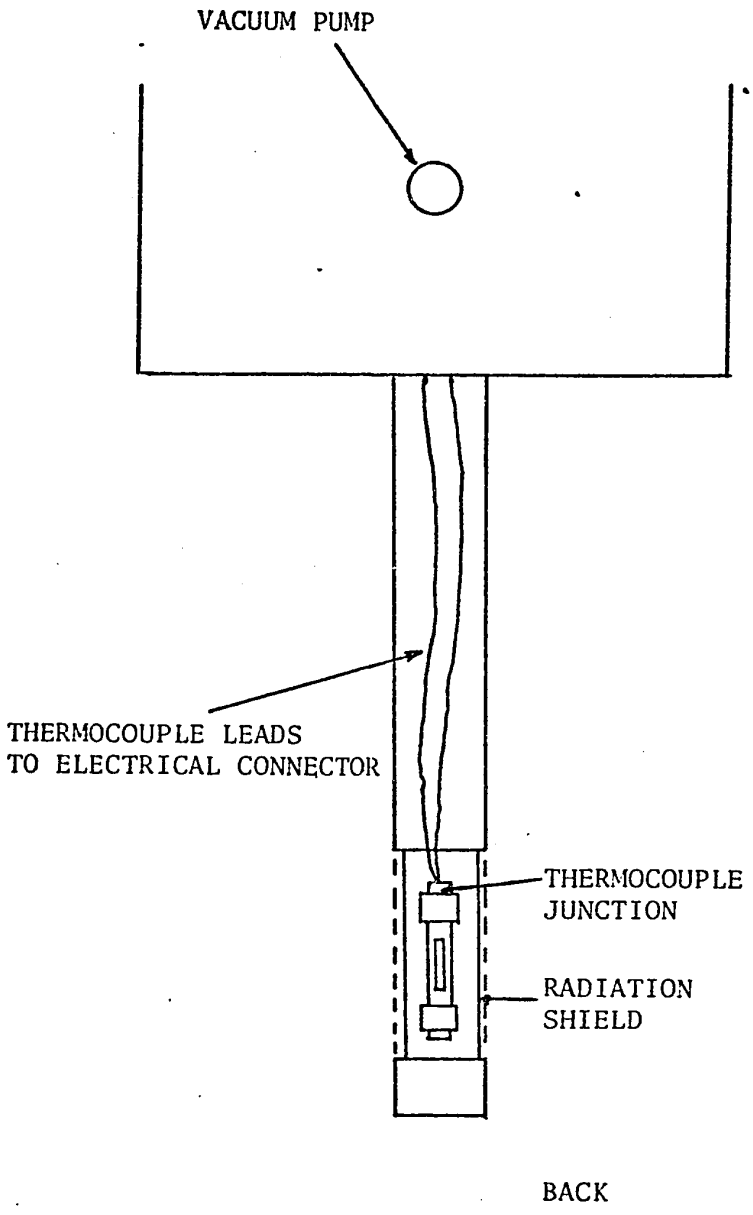

Figure 5 OPTICAL CRYOSTAT

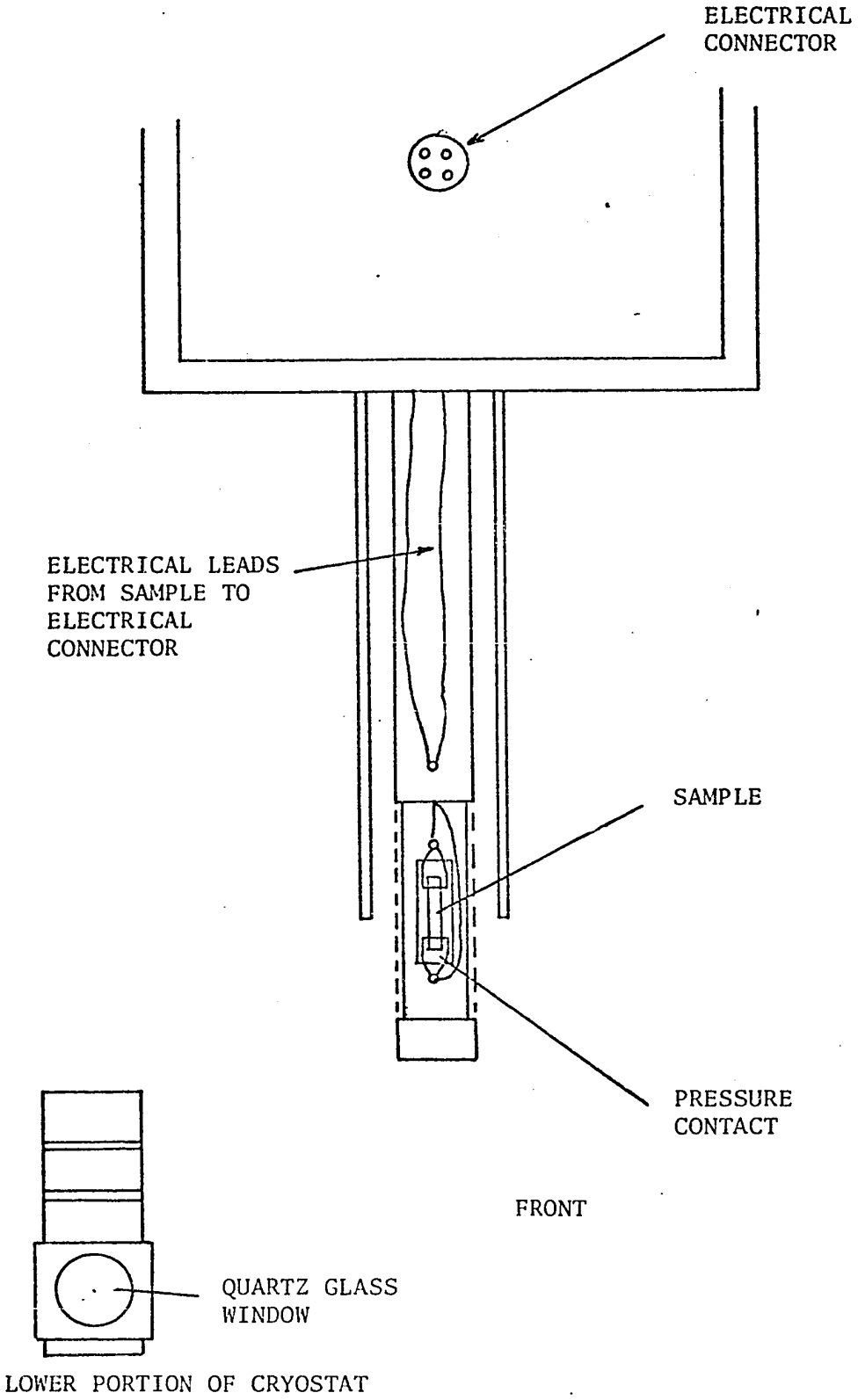

Figure 5 OPTICAL CRYOSTAT

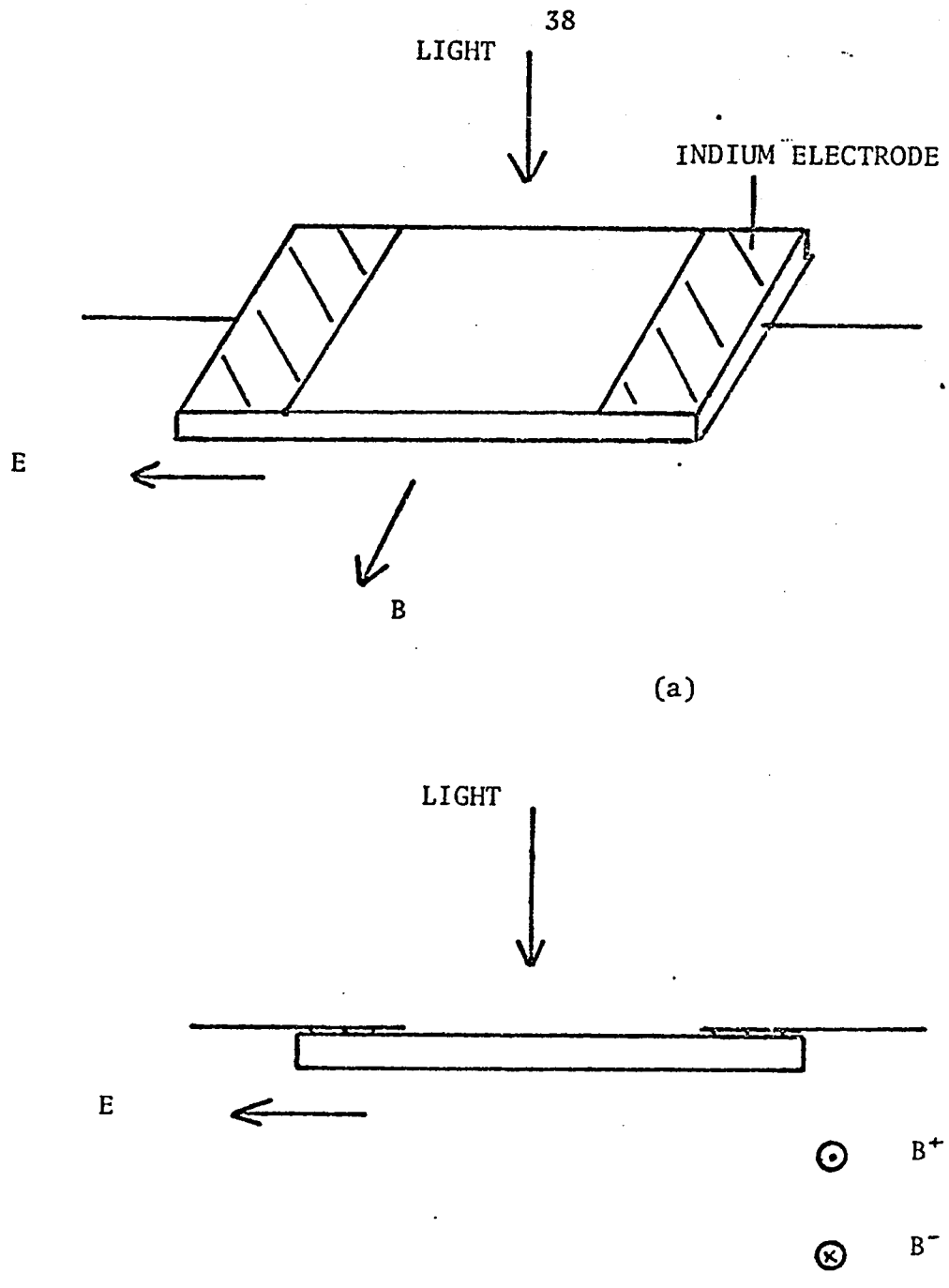

Figure 7 GaAs SAMPLE WITH INDIUM CONTACTS

2. Sample Preparation

The Cr compensated high-resistivity GaAs slab ($\rho \sim 10^7$ ohm cm) obtained from Monsanto (St.Louis) was cut into rectangular parallelepipeds of dimensions (9 x 1.8 x 0.9 mm^3).

Indium wire of 99.999% purity was evaporated onto the ends of the sample (after the surface treatment) under vacuum of 10^{-6} mm Hg in a Veeco-400 Evaporator. Samples were then placed in a helium atmosphere and the contacts alloyed at 500^oC for 5 minutes; the end contacts resulting were ohmic up to V = 400 volts.

Specimen dimensions were measured by means of a Vernier microscope, the scale of which could read to an accuracy of 2×10^{-2} mm. Fig. 7 shows a typical sample with In contacts in the Voigt geometry.

Sample 7

The surface of the original slab viewed under a microscope indicated it had undergone abrasive surface treatment and so ohmic contacts were applied to cut sample without further surface treatment. This is sample 7.

Sample 9A

Original sample was mechanically polished using a 1μ alumina polishing powder. Sample was first glued to an adjustable lapping holder, by means of glyptol thinned with acetone, and then lapped on

a glass plate using the 1μ alumina powder moistened with distilled water. Sample was then chemically polished in an etchant of H_2SO_4:H_2O_2: H_2O in a 2:1:2 ratio for 10 minutes at 70°C.

Sample 30

Sample was lapped using a 5μ alumina polish fluid rinsed. in distilled water and alloyed Indium contacts put on.

Sample 11

Original Sample which already had alloyed Indium contacts was lapped with a 5μ alumina polish just to remove the contacts. Sample was then rinsed in distilled water and new Indium end contacts alloyed on.

Sample 33

Sample was placed in an etchant of $AgNo_3$ + $K_2Cr_2O_7$ at 70°C for 5 minutes. This surface treatment could result in an increase in the capture cross-section of the surface recombination centers.

3. Experimental Procedure

In all the samples investigated the experimental procedure followed a similar pattern. Initial measurements of photocurrents in a magnetic field were made at both 300°K and 90°K, but this practice

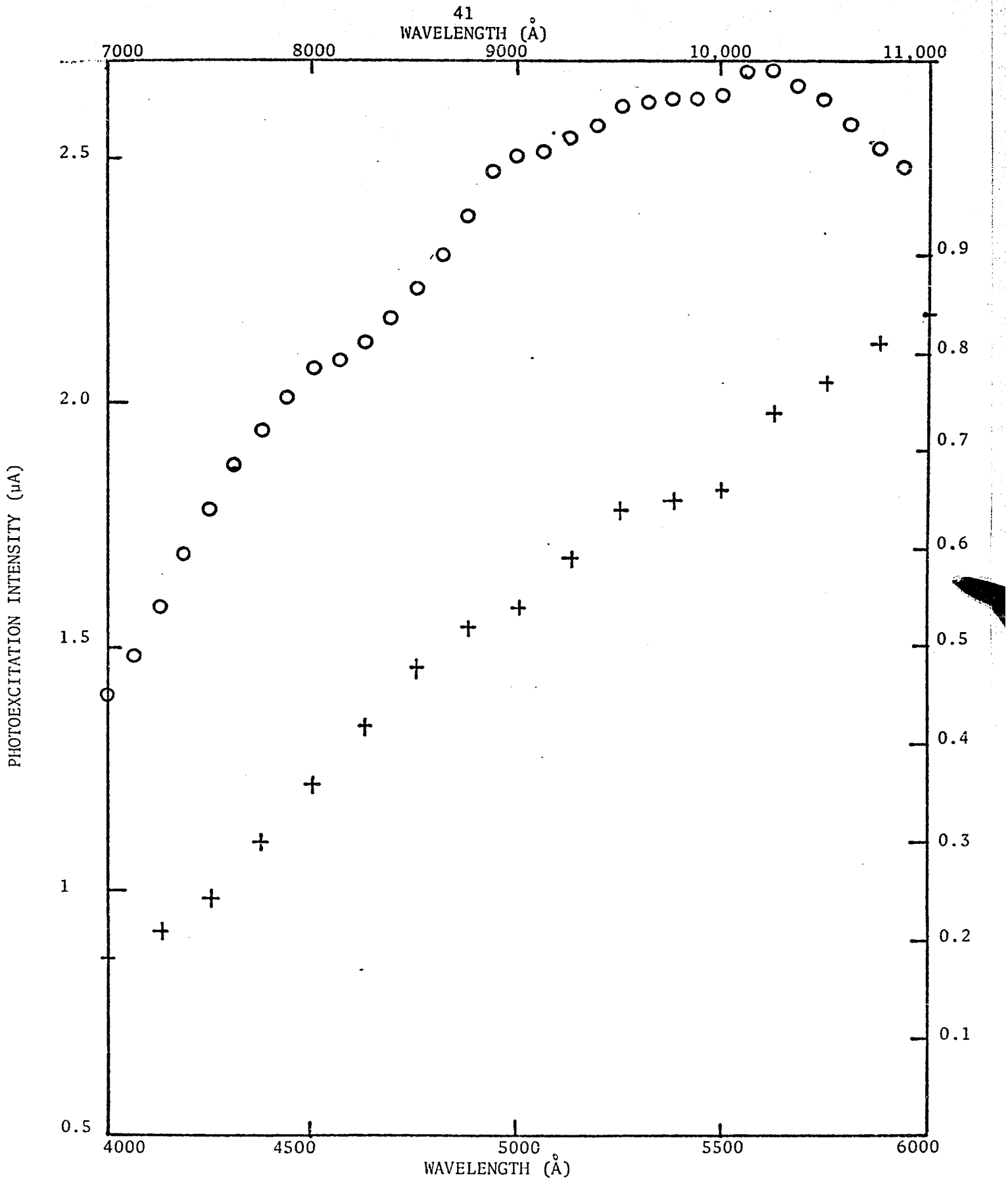

Figure 8 CALIBRATION CURVE OF MONOCHROMATOR INTENSITY

continued only when significant results were obtained at both temperatures.

At 300°K the dark current was always subtracted from the measured current to get the actual photocurrent; the dark currents at 90°K however, were negligible. For example in Sample 7 for V = 400 Volts, at 300°K, the dark current is 0.2 μA and the current when the wavelength = 7500Å is 2.2μA, while at 90°K the corresponding currents are 8×10^{-10} Amp. and 3×10^{-7} Amp. respectively.

Spectral Response Curve

400 volts was applied across sample and the photocurrent read for wavelengths 4000Å - 8000Å using the visible grating, and 7000Å - 11,000Å using the low infra-red grating. The monochromator had been previously calibrated (see Fig. 8) within this spectral region, and so a normalized spectral distribution of photoconductivity was plotted.

Wavelength Dependence

With the applied voltage V = 400 Volts, photocurrents I_p^+, I_p^- were recorded with the applied magnetic field at $B^+ = 2.2$ Wb/m^2 and $B^- = 2.2$ Wb/m^2 respectively.

Amplification ratios $A = I_p^+/I_p$ and Rectification ratio: $R = I_p^+/I_p^-$ were calculated and plotted against different wavelengths. This gave the wavelengths for which the effect was a maximum--usually the maximum was spread over a certain range of wavelengths ($\sim$ 500Å).

Magnetic Field Dependence

The monochromator grating was set at one of the wavelengths which gave maximum effect in the previous run, and applied voltage at 400 V. Photocurrents I_p^+, I_p^- were recorded for magnetic field B^+, B^- respectively, within the range of 0.11 - 3.0 Wb/m^2. Using I_p values from the spectral response curve, A and R were plotted as a function of the magnetic field.

Dependence On Photoexcitation Intensity

The monochromator was connected to a variac, and the different intensities obtained by varying the variac were calibrated using the Eppley vacuum-type thermopile. The wavelength, applied voltage and magnetic field were kept constant. I_p^+, I_p^-, I_p were recorded at different Intensities, A and R calculated and their dependence on Photoexcitation Intensity plotted.

I - V Characteristic

For a fixed wavelength, the photocurrent is plotted as a function of applied voltage (both positive and negative directions) with B = 0, B^+ and B^- respectively.

4. Photo-Hall Measurements

The Standard Hall equipment in the semiconductor Laboratory could not be used since it was designed for low resistivity samples

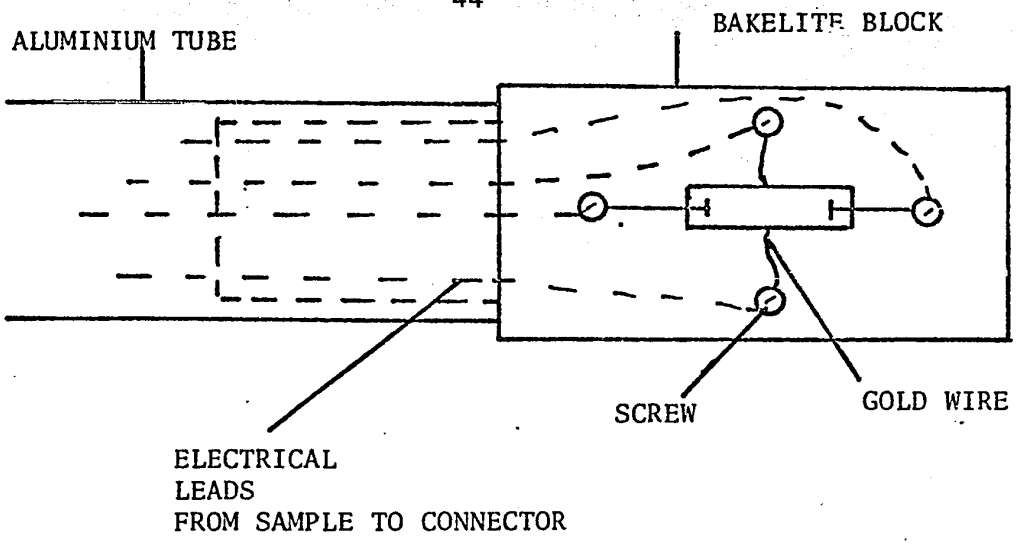

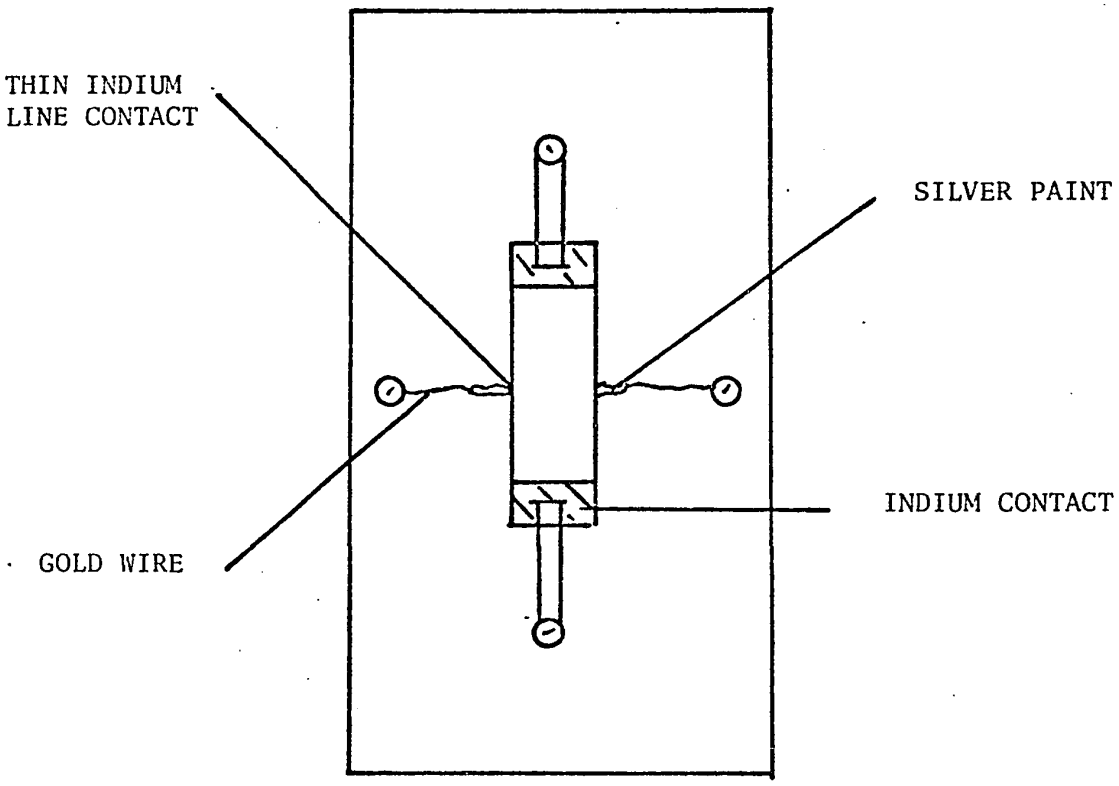

Figure 9 PHOTO-HALL PROBE

($\rho \sim 1\Omega$ cm).

A simple Hall Probe was made which allowed for four contacts to the sample, two at the ends and two at the sides. Indium wire of 99.999% purity was evaporated onto the ends of one of the faces of the sample, as well as on opposite edges along the length of sample in the form of very thin lines 0.2 mm thickness. The two Indium lines were almost exactly aligned (the evaporation was done several times until it was perfect) in order to reduce the misalignment voltage to a minimum. All the contacts were alloyed at 500^{o}C for 5 minutes in a helium medium --they were all ohmic.

Electrical contacts were made at the sides of the sample by means of thin gold wires and silver paint as indicated in Fig. 9 of the Hall Probe.

The resistivity of the sample was determined by measurement of the current through the sample using contacts 1 and 2, and the Hall Potential was measured between contacts 3 and 4. The voltage applied to the crystal came from a stabilized D.C. Supply and both the current through the crystal and the Hall Voltage were read on a Keithley Model 602 Solid State Electrometer. Fig. 10 gives a schematic block diagram of the Hall Apparatus. Monochromatic radiation was obtained from a Bausch and Lomb High Intensity grating monochromator, with the wavelength fixed at 9000$\mathring{A}$. Both the radiation and the applied magnetic field were perpendicular to the face of the sample. The misalignment voltage was small, however, its effect was nullified by applying the magnetic field in both directions

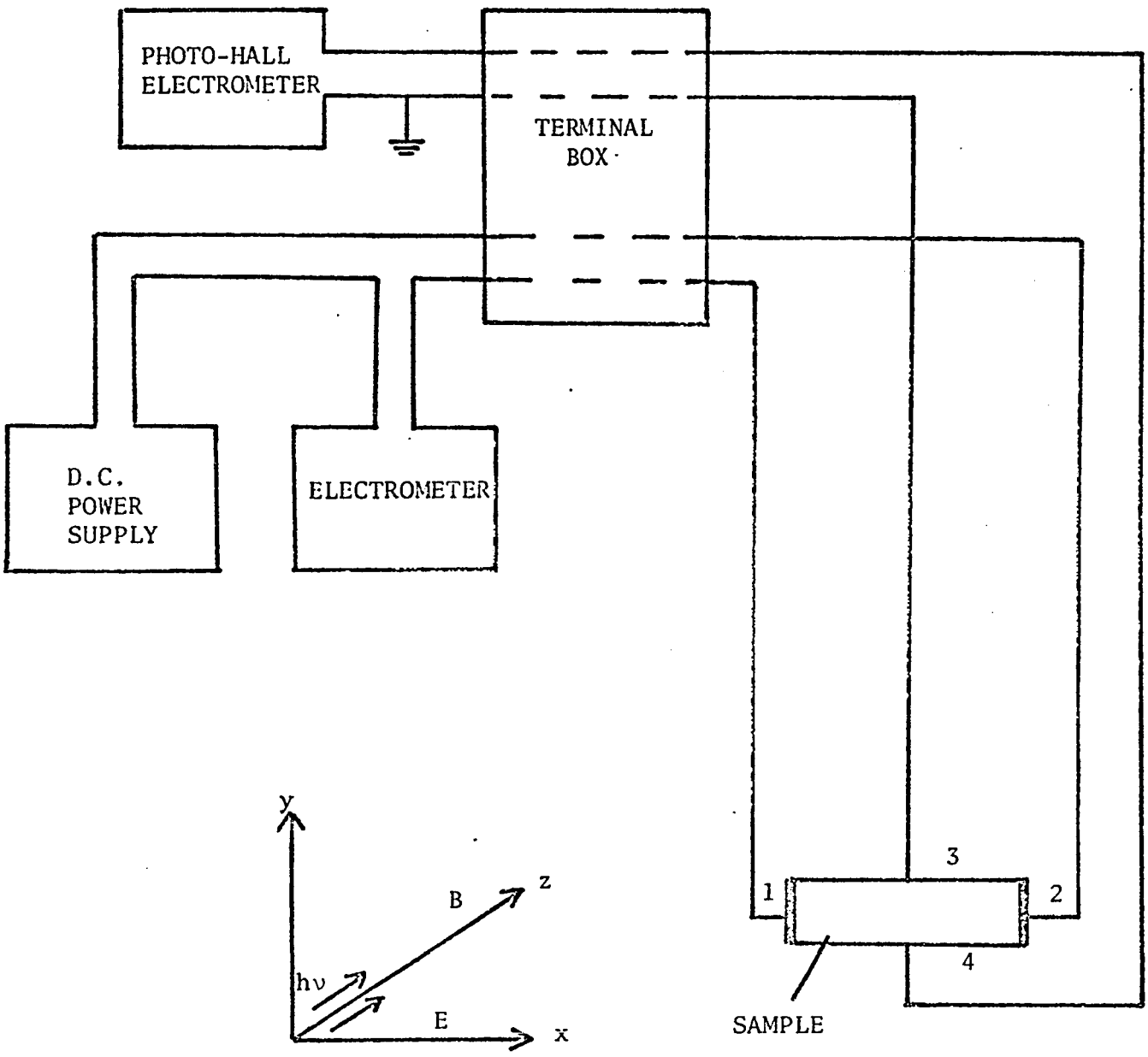

Figure 10 SCHEMATIC BLOCK DIAGRAM OF PHOTO-HALL APPARATUS

for a particular direction of the electric field. i.e., if V_H is the actual Hall Voltage and V_m the misalignment voltage, then for one direction of the magnetic field we read across contacts 3 and 4 the voltage $V_m + V_H$. When the magnetic field is reversed, we read $V_m - V_H$, and the difference is $2 V_H$. Thus, the misalignment voltage does not affect the results.

The Hall constant R, the resistivity ρ, and hence the mobility were calculated for different intensities of radiation.

The Hall constant was calculated from the relation

$$R_H = \frac{V_H t}{IB}$$

where V_H is the Hall Voltage, t is the thickness of the sample and B is the magnetic field. The resistivity was evaluated using the relation

$$\rho = \frac{AV}{Il}$$

where V is the applied voltage, A the cross-sectional area, and l the length of specimen.

The Hall Mobility is given by

$$\mu_H = \frac{R}{\rho}$$

The results of the Photo-Hall measurements will be given in Cahpter IV.

CHAPTER IV

RESULTS AND DISCUSSION

This chapter is divided into two main parts. Part I deals with photoconductivity measurements in a magnetic field while Part II gives results of carrier mobility and lifetime measurements.

A comparison of some experimental data with calculated values using the Simple model will also be considered.

PART I

In this section, five samples with different surface treatments will be considered. However, since the general behaviour of the Amplification and Rectification ratios with respect to wavelength of excitation, electric and magnetic fields are the same in all the samples, detailed results will be given for only the original sample (sample 7). Results for the other samples will be restricted to particular aspects of the effect which were affected by the surface treatments, as far as the magnitudes of the Amplification and Rectification ratios are concerned.

To make direct comparison easier, the spectral response curve and the variation of the Amplification and Rectification ratios with wavelength given by Samples 7 and 9A will be jointly discussed.

PEM measurements will be introduced when convenient either as a means of comparison or as supporting evidence to justify certain

conclusions.

A. SAMPLE 7

1. Wavelength Dependence

The normalized spectral response curves of Samples 7 and 9A are shown in Fig 11. The surface factor F of Sample 7 which had undergone abrasive surface treatment is 5, and that of the chemically polished samples 9A is 2. Thus, from our previous considerations we expect sizeable Amplification and Rectification ratios in Sample 7 but a smaller effect in Sample 9A.

Fig 12 shows a plot of A and R vs wavelength at $300^{o}K$ for both samples. Sample 7 gave a maximum A and R of 4.3 and 10.5, while the corresponding ratios for Sample 9A were only 1.5 and 3.5 respectively as expected from the surface factors. All the curves, however, behave in the same way, increasing to a maximum at wavelength = 8250Å and falling rapidly to $\sim$ 1 when wavelength is greater than or equal to 9000Å.

These results can be explained on the basis of the Simple model as follows:

The photogeneration of carriers occurs in a layer of thickness (t) $\sim 1/\alpha$ (α = absorption coefficient) in the neighbourhood of the surface. To obtain any photocurrent amplification, the transit time of the carriers deflected across this photoexcited layer must therefore be of the order of the carrier lifetime ($\sim 10^{-7}$sec). In the wavelength range, wavelength = 7000 - 8,300Å, α is larger than $10^{6}m^{-1}$, the excitation layer

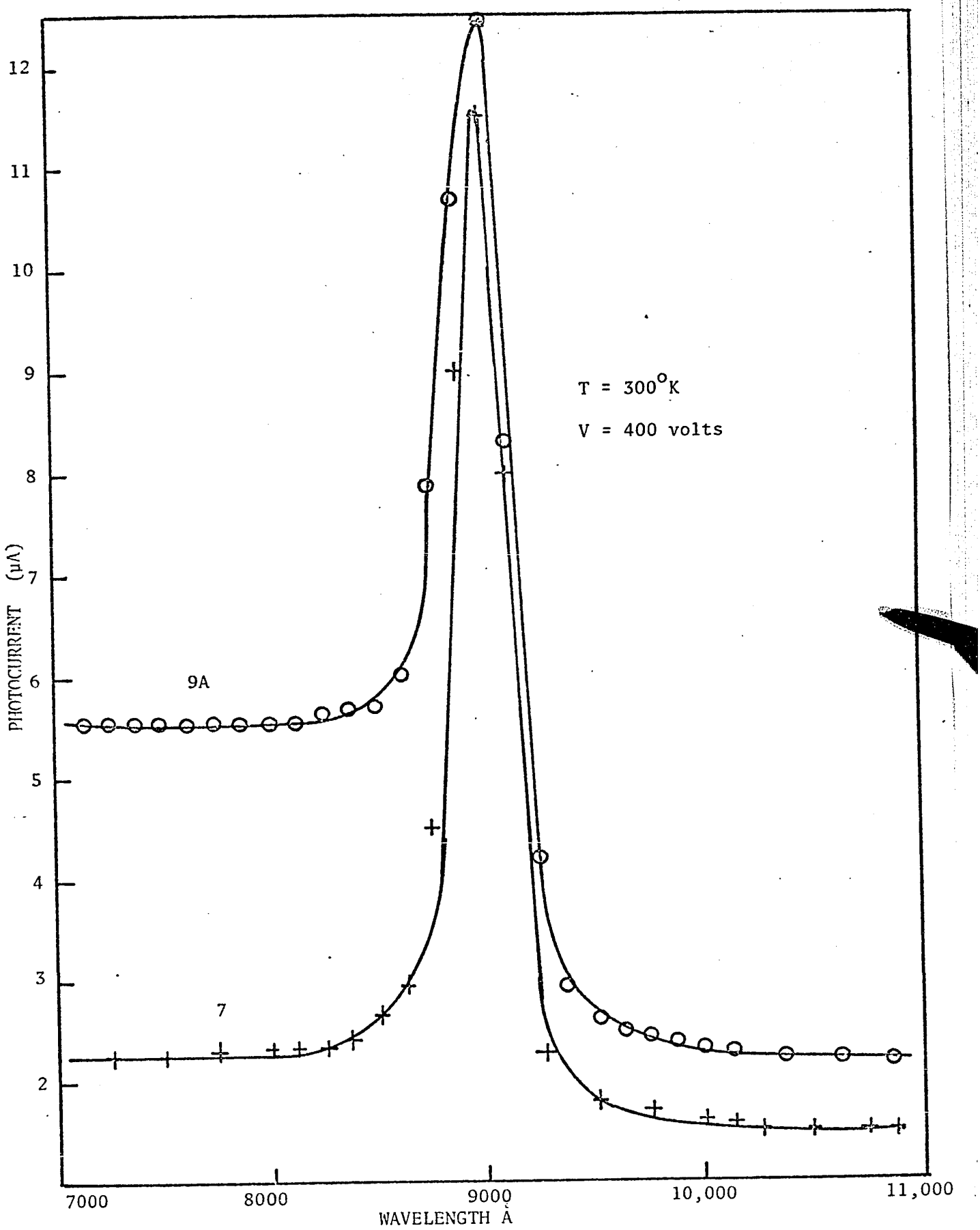

Figure 11 COMPARISON OF SPECTRAL RESPONSE CURVES OF SAMPLES 7 and 9A

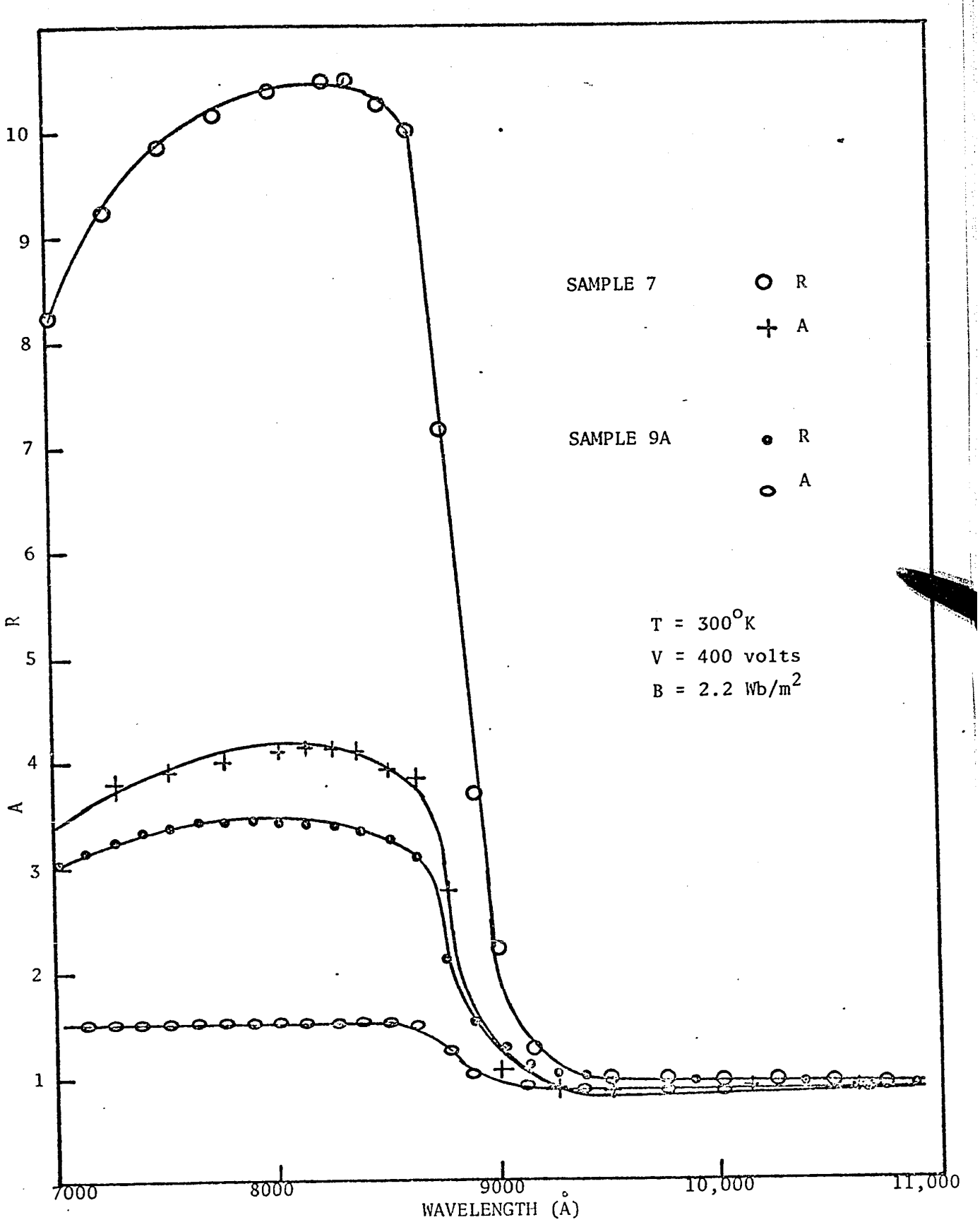

Figure 12 R AND A VERSUS WAVELENGTH

is thin and, hence, within region no. 1 where a mean surface lifetime τ_1, exists. When the magnetic field (B^+) is applied the carriers are deflected into the volume (region no. 2) where a longer lifetime τ_2 prevails resulting in an Amplification of the photocurrent. At λ = 9000Å, $\alpha \sim 10^5 m^{-1}$ and $t \sim 10^{-5} m$. Since the effect disappears at this point, it indicates that $Z_1 \sim 10^{-5} m$. Thus, at longer wavelengths when α is less than $10^5 m^{-1}$, t is greater than Z_1. i.e: there is already volume excitation.

Fig 13 illustrates the effect of the magnetic field (B^+) on the spectral response curve. The curve is "raised" at the shorter wavelength end, resulting in an effectively reduced surface factor (as predicted in Chapter II) and a better detection characteristics at shorter wavelength.

In the field of device applications this effect could provide photocurrent control and flatten the spectral sensitivity curves of detectors.

Experiments at 90°K were confined within the wavelength range, wavelength = 4000 - 8000Å using the visible-low Infra-red Grating: the effect is small at larger wavelengths as the absorption edge is now at 8400Å.

Fig 14 shows results obtained at 300°K and 90°K in the wavelength range 4000 - 8000Å.

The amplification ratio at 300°K is very small (less than 2) at very short wavelengths (4000Å - 5000Å), increasing to ∿3 at wavelength = 7250Å (Curve I). The corresponding results at 90°K show an

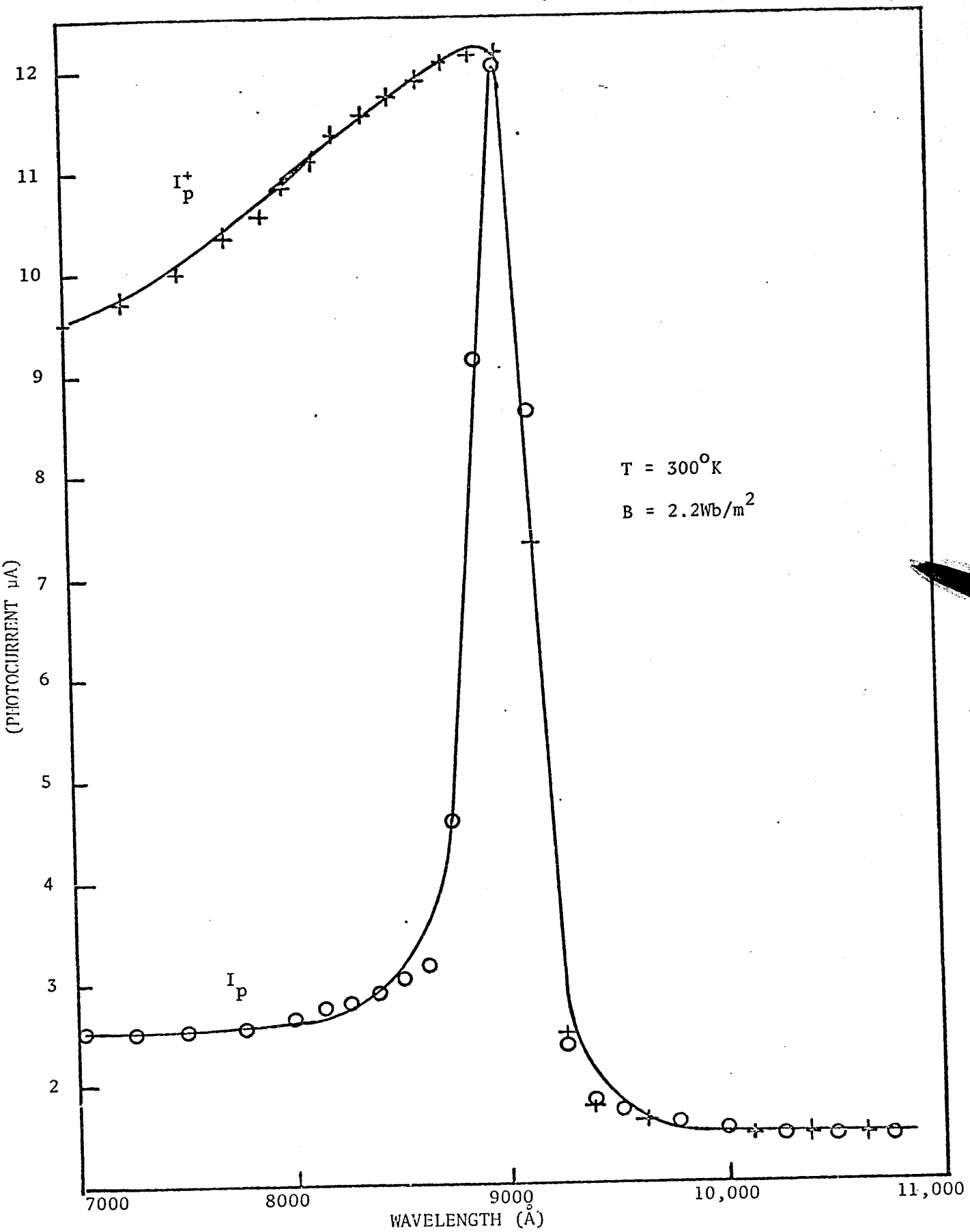

Figure 13 EFFECT OF A MAGNETIC FIELD ON THE SPECTRAL RESPONSE CURVE

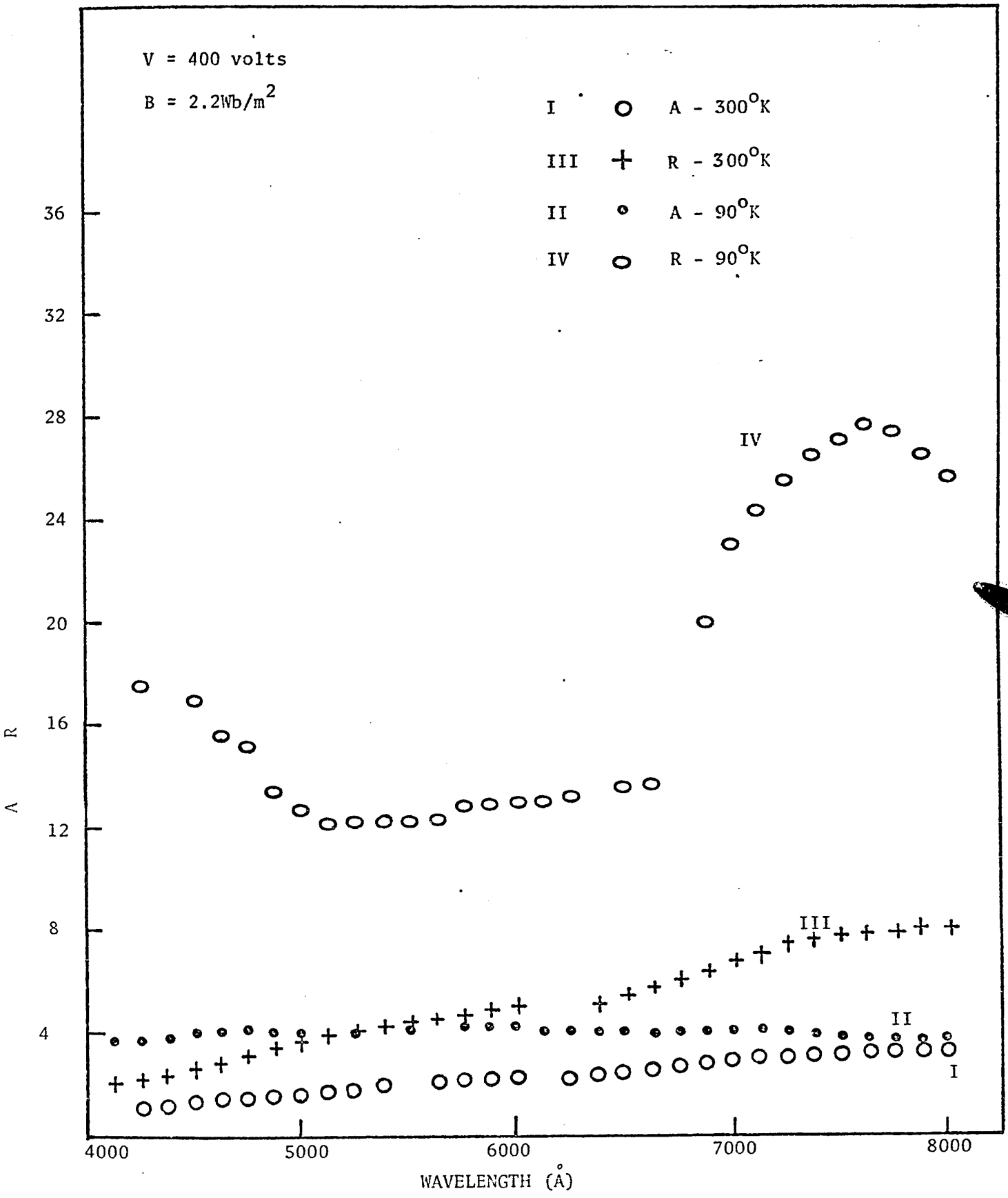

Figure 14 A and R VERSUS WAVELENGTH

almost constant amplification ratio of 4 throughout the wavelength range (Curve II). At 300°K the Rectification ratio (R) shows a gradual increase from R = 2 at 4000Å, to 8 at 8000Å (Curve III). This is consistent with the results obtained using the Infra-red Grating (see Fig 12).

The R versus λ plot at 90°K (Curve IV) has a rather peculiar shape. R = 22 at 4000Å, dropping to an almost constant value of ∿12 between 5125Å and 6250Å, increasing to a maximum of 28 at wavelength = 7625Å, and then a slight decrease to 25.5 at wavelength = 8000Å. This behaviour is not exactly clear, however, the general increase in R at 90°K indicates that the low temperature has a greater effect on the lifetime at the very top of the illuminated surface than on any other parameter. This accounts for the much reduced values of I_p^- as evident by comparing I_p, I_p^+, and I_p^- at 300°K and 90°K respectively. For an excitation wavelength = 7000Å and B = ±2.2 Wb/m^2

$$I_p\ (300^\circ K)/I_p\ (90^\circ K) = 8$$

$$I_p^+\ (300^\circ K)/I_p^+\ (90^\circ K) = 6$$

$$I_p^-\ (300^\circ K)/I_p^-\ (90^\circ K) = 19$$

Thus, the relatively big drop in I_p^- by a factor of 19 at 90°K, accounts for the large increase in R = (I_p^+/I_p^-)

2. Magnetic Field Dependence

Fig 15 shows the effect of increasing magnetic field (B) on R and A at 300°K.

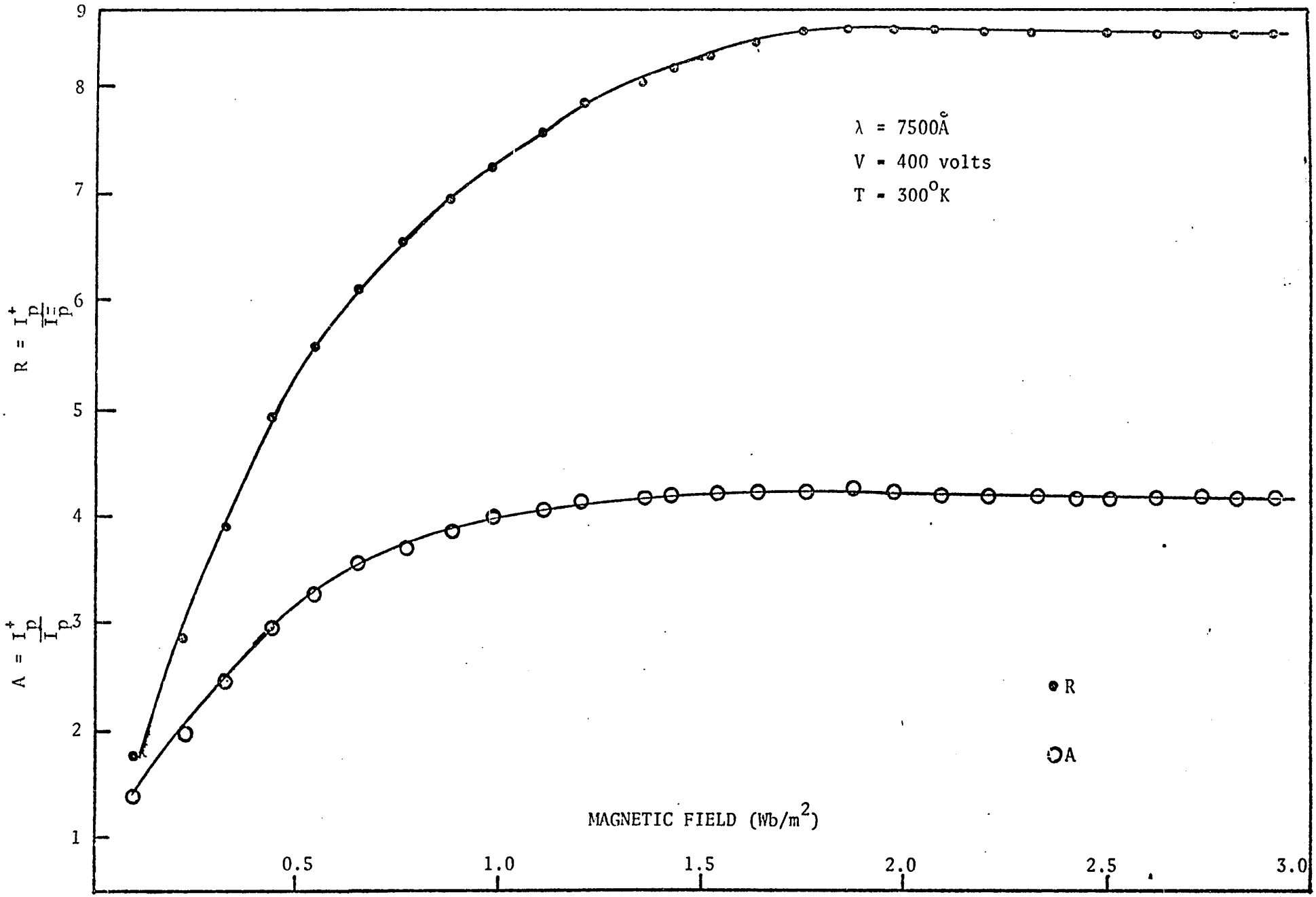

Figure 15 MAGNETIC FIELD DEPENDENCE OF RECTIFICATION AND AMPLIFICATION RATIOS

There is a linear increase at low fields (B less than 0.5 Wb/m^2), saturating at fields B > 1.0 Wb/m^2. This behaviour can be explained quantitatively by studying the variation of I_p^+ and I_p^- with B shown in Fig 16. I_p^- shows a gradual decrease from 1.8 μA at $B^- = 0.11$ Wb/m^2 to 1.2 μA at $B^- = 1.1$ Wb/m^2, a decrease of about 30%, but a further decrease of only 8% from $B^- = 1.1$ Wb/m^2 to 2 Wb/m^2, and finally attaining a constant minimum value for B^- greater than 2.4 Wb/m^2. The explanation is that as B^- increases the photocarriers are pushed further into regions of decreasing lifetimes in the neighbourhood of the surface, I_p^- decreasing slowly until at $B^- = 2.4$ Wb/m^2, the majority of the deflected photocarriers actually reach the very top of the illuminated surface where the lifetime is at a minimum; thus, a further increase in B^- does not affect I_p^-.

Conversely, as B^+ increases, more carriers reach region no. 2 (where a longer lifetime prevails) before recombination, and I_p^+ attains saturation which corresponds to the situation in which all photocarriers generated in region no. 1 are deflected into region no. 2 before recombination. This explains the behaviour of $R = I_p^+/I_p^-$ and $A = I_p^+/I_p$ with B, shown in Fig 15.

Quantitatively, in terms of the Simple model in which

$$A = \frac{\dfrac{(1 + \mu^2 EB\tau_2)}{(Z_1)}}{\dfrac{(1 + \mu^2 EB\tau_1)}{(Z_1)}}$$, saturation occurs when $\frac{\mu^2}{Z_1} EB\tau_2$

and $\frac{\mu^2}{Z_1} EB\tau_1 >> 1$ and A has a maximum value of τ_2/τ_1

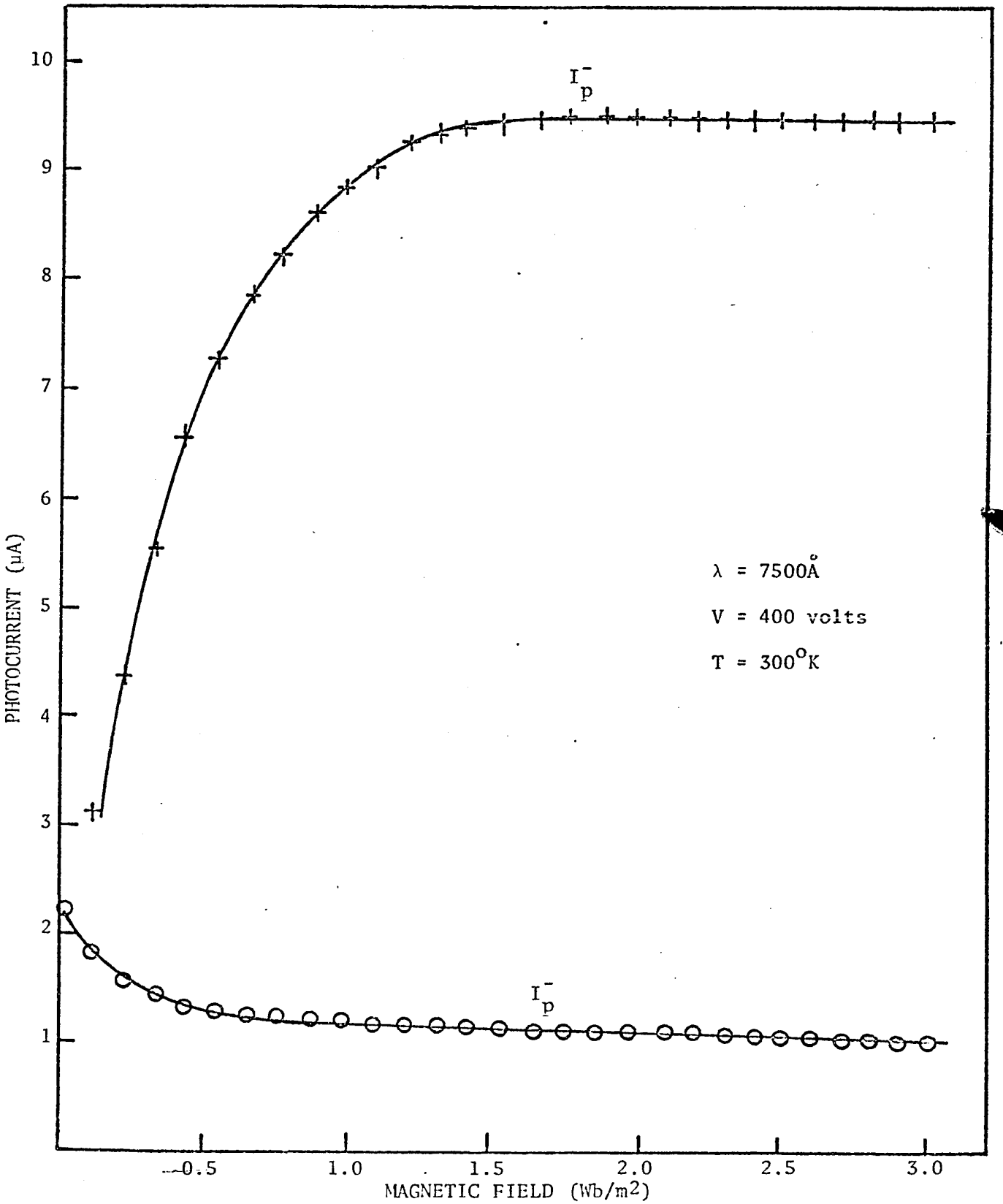

Figure 16 VARIATION OF SURFACE PHOTOCURRENT (I_p^-) AND VOLUME PHOTOCURRENT (I_p^+) WITH MAGNETIC FIELD

In Fig 15, A (maximum) = 4.3 and from lifetime measurements to be discussed later in this chapter, $\tau_1 = 1.3 \times 10^{-7}$, $\tau_2 = 6 \times 10^{-7}$ sec. i.e., $\tau_2/\tau_1 = 4.6$, which agrees reasonably with the experimental value of A (maximum).

The behaviour at 90°K is similar to that at 300°K as illustrated in Fig 17. The remarkable rise of R with increasing B could be attributed to the effect of the low temperature on the lifetime at the very top of the illuminated surface as stated before. A possible explanation for this is as follows: the carrier lifetime of either an electron or hole (assuming $\tau_p = \tau_n$) is given by (17)

$$\tau = \frac{1}{N_r V S}$$

where N_r is the number of recombination centers, S the capture cross-section and V, the thermal velocity. Now $N_r \propto \exp(-\Delta E/KT)$, $\Delta E = |E_f - E_r|$ where E_f is the Fermi level and E_r the level of the recombination states. It is possible that the low temperature has a greater effect on ΔE at the surface, and hence on N_r, which causes a big drop in τ in the surface region.

Comparing magnitudes of I_p, I_p^+, and I_p^- at 300°K and 90°K respectively give for V = 400v, wavelength = 7500Å, B = ±2 Wb/m^2 the following ratios

$$\frac{I_p\ (300^\circ K)}{I_p\ (90^\circ K)} = 16$$

$$\frac{I_p^+\ (300^\circ K)}{I_p^+\ (90^\circ K)} = 20$$

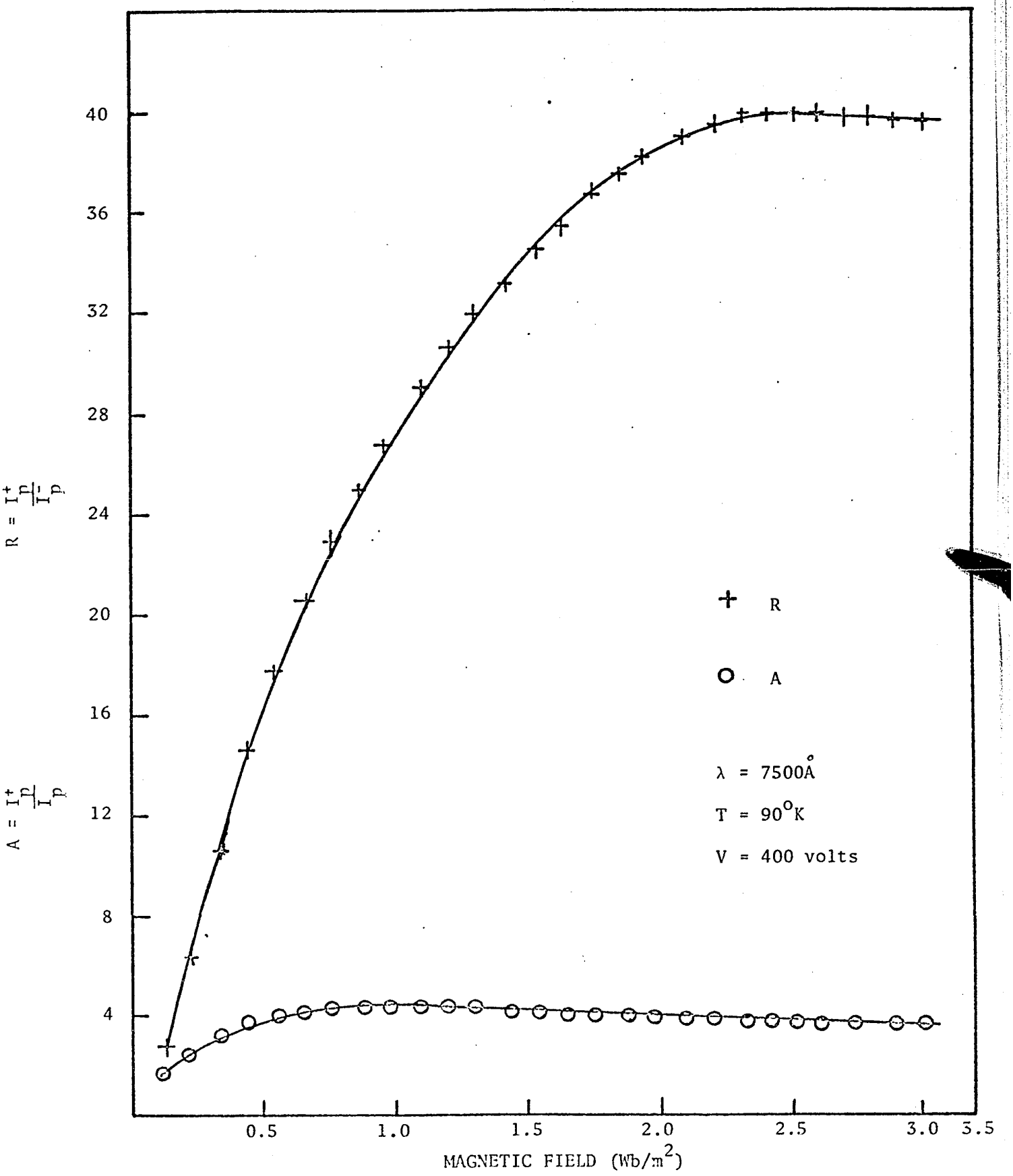

Figure 17 R and A VERSUS B

$$\frac{I_p^-\ (300^oK)}{I_p^-\ (90^oK)} = 100$$

Thus, the big drop in I_p^- is consistent with the large increase of R to almost 40.

3. Magnetic Field Dependence of the PEM Effect

It will be appropriate at this stage to consider an example of the phenomenological similarity between the photocurrent-amplification phenomenon and the PEM effect by comparing their dependence on magnetic field.

Fig (18) shows the dependence of the short-circuit PEM current (I_{PEM}) on magnetic field (B) at 300^oK. The shape of this curve is similar to the I_p^+ versus B plot in Fig 16.

Kurnick and Zitter (8) have shown that the PEM current can be expressed, for a sample with width and length large compared to the diffusion length, as:

$$I_{PEM} = \frac{e\ L\ \mu\ B\ (D\tau)^{1/2}}{(1 + \mu^2B^2)^{1/2}} \cdot \frac{1}{1\ \ \frac{\tau S}{(D\tau)^{1/2}}\ (1 + \mu^2B^2)^{1/2}} \qquad (4\text{-}1)$$

If $\tau S/(D\tau)^{1/2} >> 1$ i.e., high surface recombination

$$I_{PEM} = \frac{e\ L\ \mu\ B\ D}{(1 + \mu^2B^2)S}$$

or simply

$$I_{PEM} \sim \frac{\mu B}{(1 + \mu^2B^2)} \qquad (4\text{-}2)$$

If $\tau S/(D\tau)^{1/2} << 1$. i.e., low surface recombination

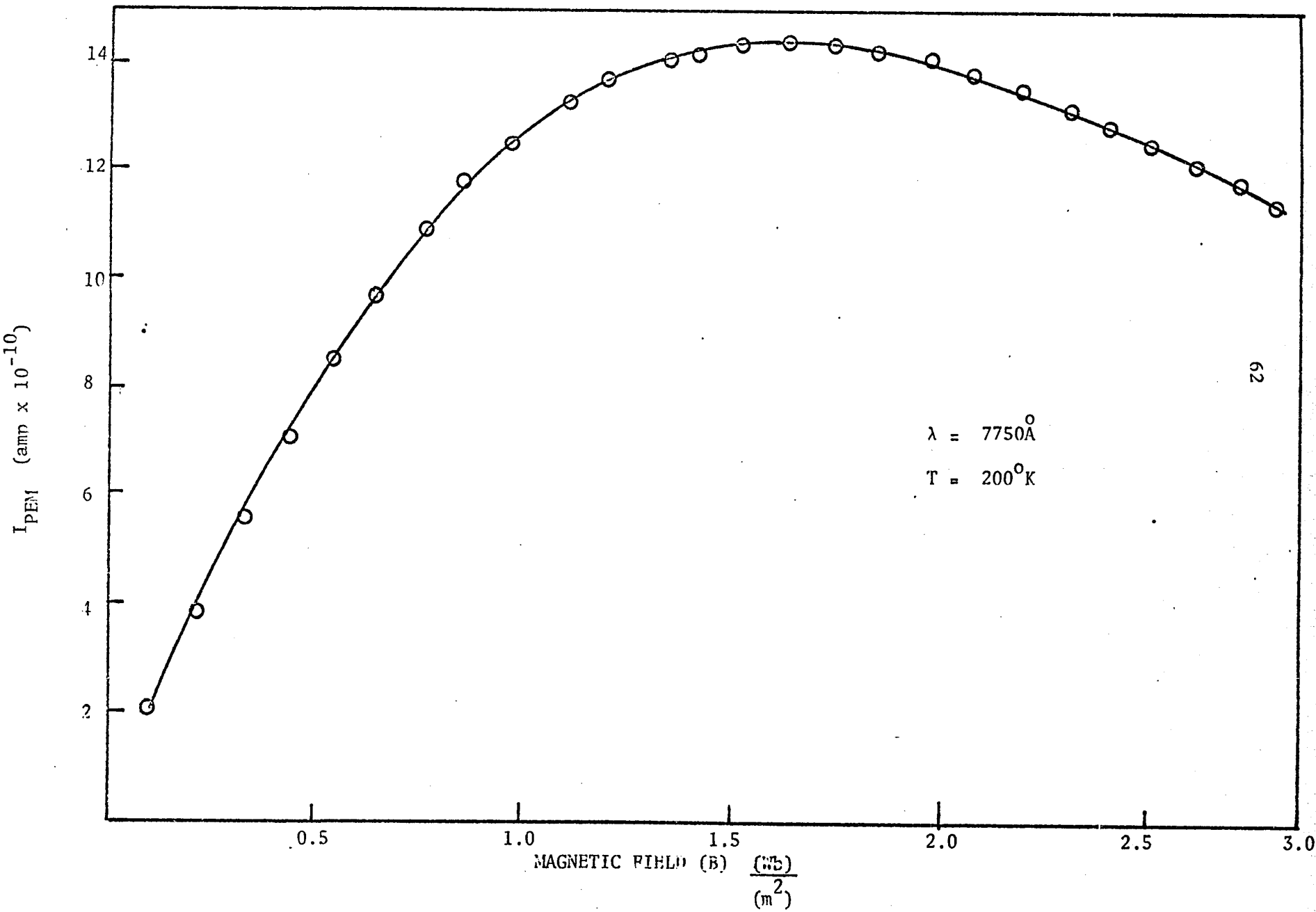

Figure 18 MAGNETIC FIELD DEPENDENCE OF THE PEM SHORT-CIRCUIT CURRENT (Ipem)

$$I_{PEM} = \frac{e\ L\ \mu\ B\ (D\tau)^{1/2}}{(1 + \mu^2 B^2)^{1/2}}$$

i.e.,

$$I_{PEM} \sim \frac{\mu B}{(1 + \mu^2 B^2)^{1/2}} \qquad (4\text{-}3)$$

For high surface recombination, Eq (4-2) shows that I_{PEM} measured as a function of B passes through a maximum, whereas for low surface recombination Eq (4-3) shows that I_{PEM} approaches saturation with increasing B.

In Fig (18), the I_{PEM} versus B surve for Sample 7 passes through a maximum satisfying the relation for high surface recombination (eq 4-2). This is consistent with the relatively large surface factor of the spectral response curve of Sample 7 (Fig 11).

Fig (19) indicates the I_{PEM} versus B plot for Sample 7 at $90^{o}K$: the shape of the curve is similar to that obtained for a mechanically polished InSb sample at $77^{o}K$ in (8). Thus, in general surface properties deduced from PEM effect studies are in qualitative agreement with those obtained from the Photocurrent Amplification effect.

4. Surface Recombination Velocity (S)

a. The PEM effect has been used in the evaluation of surface recombination velocity from the relation (18)

$$\frac{V_{PEM}^{(MAX)}}{\iota} = BS$$

where $V_{PEM}^{(MAX)}$ is the maximum PEM voltage in the V_{PEM} versus B curve,

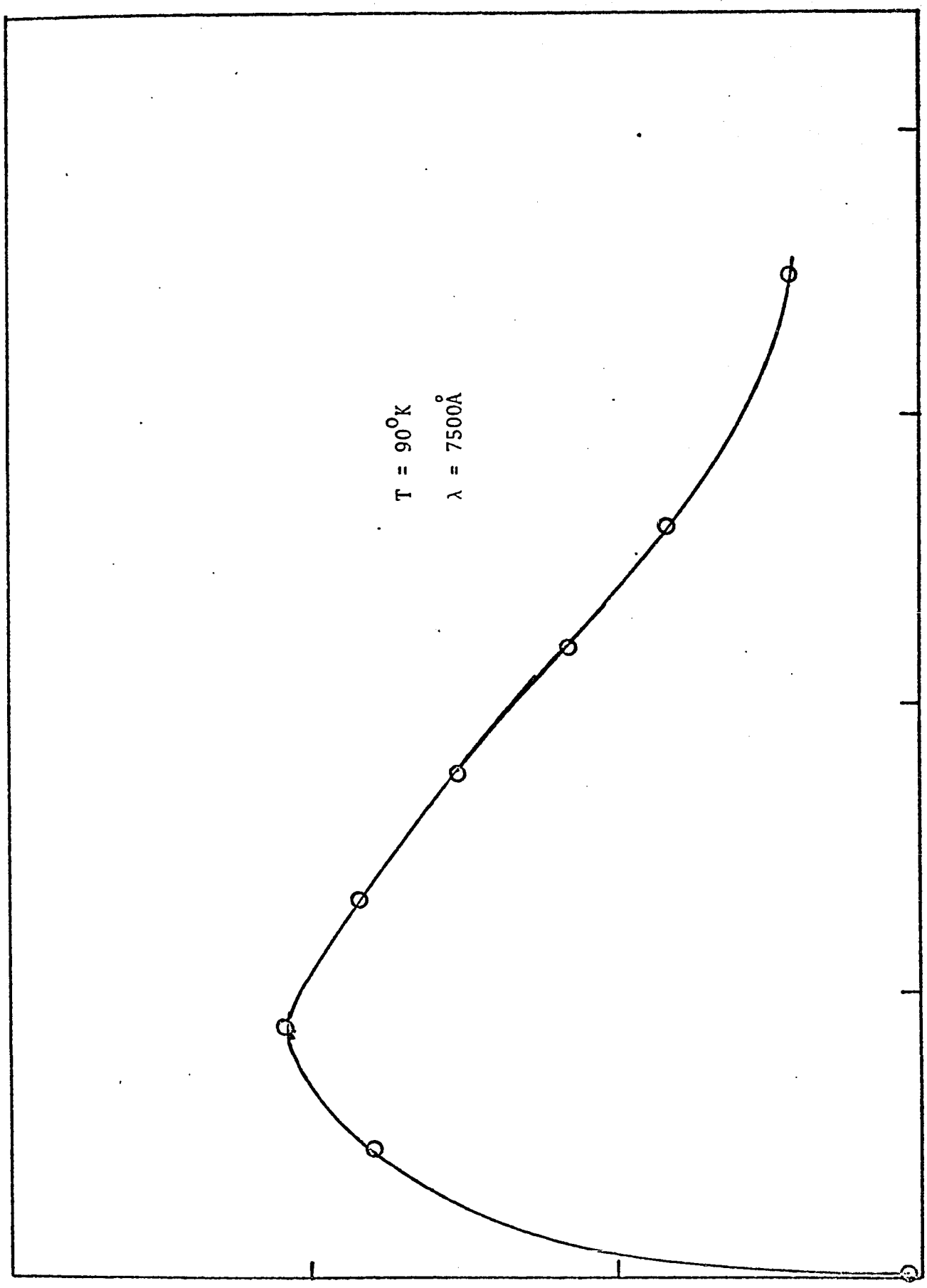

Figure 19 MAGNETIC FIELD DEPENDENCE OF THE PEM SHORT-CIRCUIT CURRENT

B is the corresponding magnetic field and ι the distance between the electrodes. From the graph of V_{PEM} versus B shown in Fig (20), $V_{PEM}^{(MAX)}$ = 0.63 v at B = 1.9 Wb/m^2 and $\iota = 6.6 \times 10^{-3}$m.

Substituting these values into the equation above gives

$\underline{S = 50 \text{ m sec}^{-1}}$

b. Now from the previous theory in Chapter II

$1 + \frac{S\tau}{L}$ = Surface factor $\doteqdot$ Maximum Amplification ratio (4.3)

From lifetime measurements to be considered in Chapter IV

$\tau = 6 \times 10^{-7}$ sec and L $\sim 10^{-5}$m

Thus if $1 + \frac{S\tau}{L} = 4.3$

$\underline{S = 55 \text{ m sec}^{-1}}$

This is in fair agreement with the PEM effect result.

Of course, the latter method is tedious, since it involves two other parameters (τ, L); however, it offers a means of checking the magnitudes of surface recombination velocities calculated from the PEM effect.

So far no surface recombination velocity measurements has been made in s.i. GaAs (to the author's knowledge), but for a ground InSb surface Kurnick and Zitter (8) have found S = 100 m sec^{-1} using the PEM effect while Davis (19) found values as low as 2 m sec^{-1} depending upon the surface treatment. Moss, Pincherle and Woodward(18) obtained S = 33 m sec^{-1} for a ground germanium surface. Thus the values of 55 m sec^{-1} and 50 m sec^{-1} found in this GaAs sample by the two methods seem reasonable.

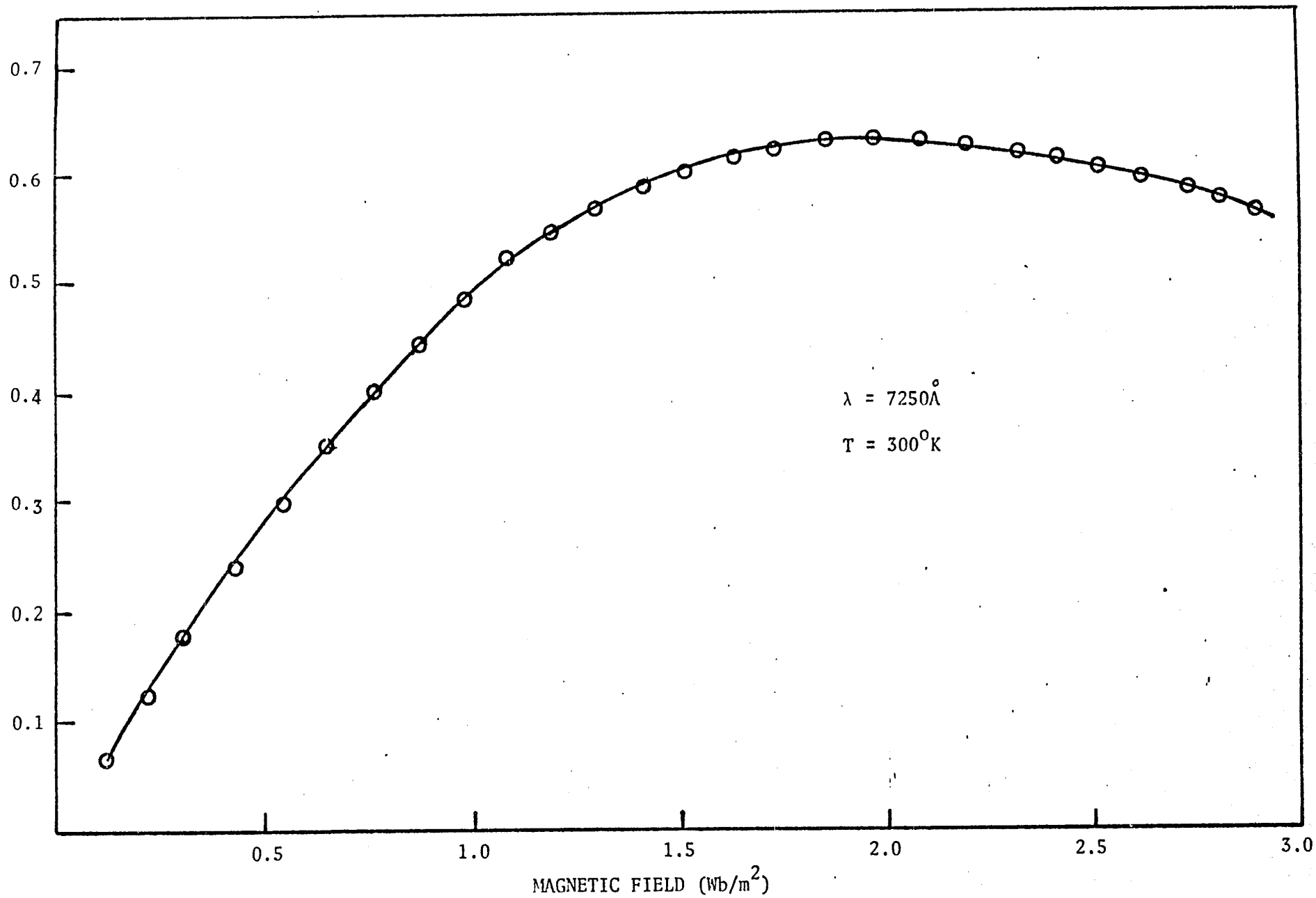

Figure 20 VARIATION OF PEM VOLTAGE WITH MAGNETIC FIELD

5. I - V Characteristics

In Fig (21) is shown the I-V characteristics of Sample 7 at $300^{o}K$ which has a shape somewhat reminiscent of a Diode Rectifier characteristics.

For no magnetic field (B = 0), the I-V curve obeys Ohm's law satisfactorily (Curve II). When both the applied electric and magnetic fields are positive or negative and the carriers are deflected towards the illuminated surface, the resultant photocurrent I_p^- turns towards saturation as the voltage is increased.

When the applied electric and magnetic fields are of opposite sign, and the carriers are drawn into the interior of the sample, the photocurrent I_p^+ varies almost linearly with voltage, with a slope greater than that in the absence of a magnetic field. The I-V characteristics at $90^{o}K$ is shown in Fig (22). The general behaviour of the carriers is the same as in Fig (21), however I_p^+ has a steeper slope than at $300^{o}K$.

This fact and also the very low values of I_p^- are consistent with the high rectification ratios observed at $90^{o}K$ in Fig (17).

6. Dependence on Photoexcitation Intensity

In Fig (23) is shown the effect of increasing photoexcitation intensity on the Amplification and Rectification ratios.

Both A and R increase from low intensities, saturating at high intensities: this probably indicates a lifetime dependence on intensity. Saturation occurs because at higher intensities the extra carriers created recombine before being deflected into the volume.

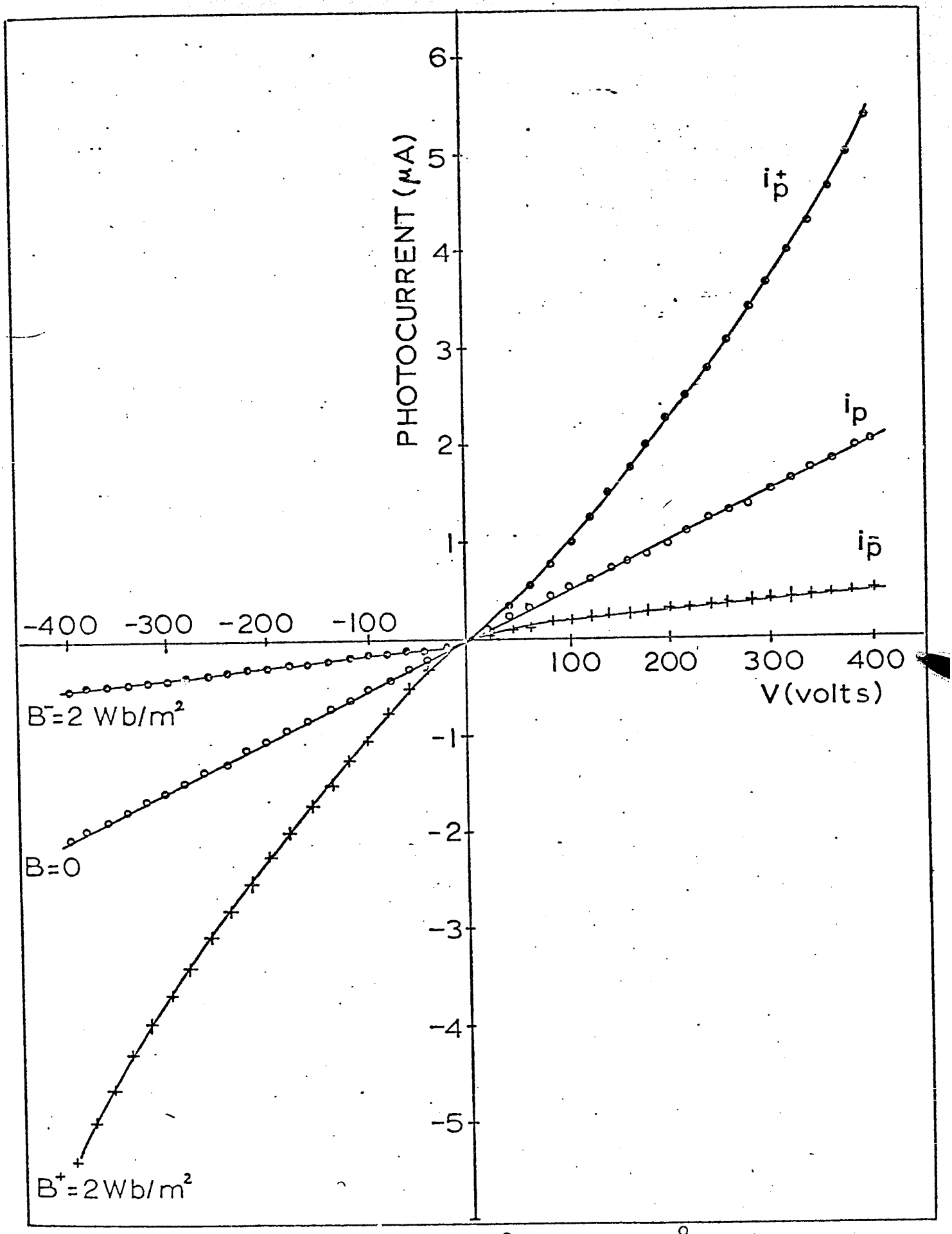

Fig. 21. I-V characteristics at 300°K, λ = 7250 Å

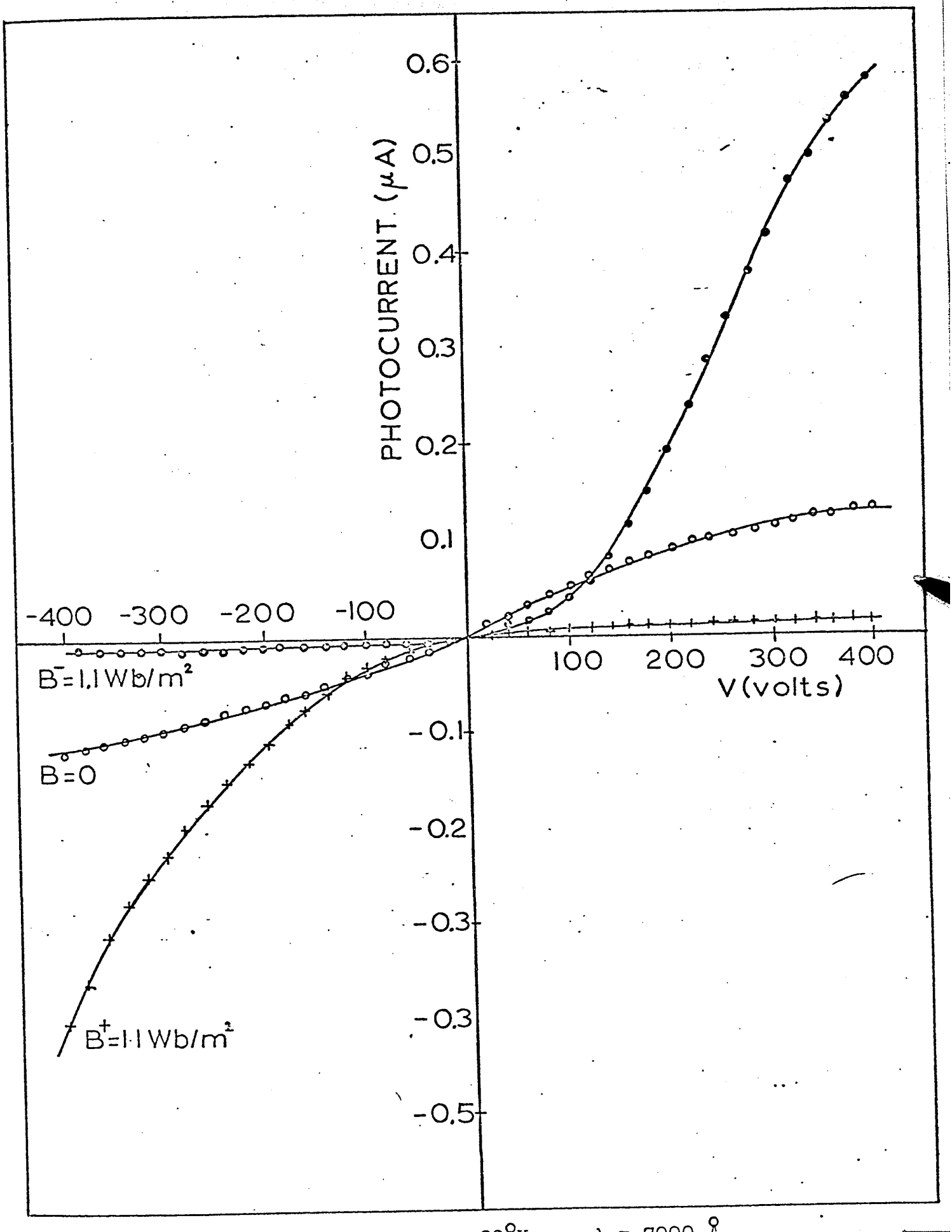
PHOTOCURRENT (μA)
0.6
0.5
0.4
0.3
0.2
0.1
-0.1
-0.2
-0.3
-0.3
-0.5
-400 -300 -200 -100
100 200 300 400
V(volts)
B⁻=1.1 Wb/m²
B=0
B⁺=1.1 Wb/m²

Figure 23: VARIATION OF A AND R WITH PHOTOEXCITATION INTENSITY

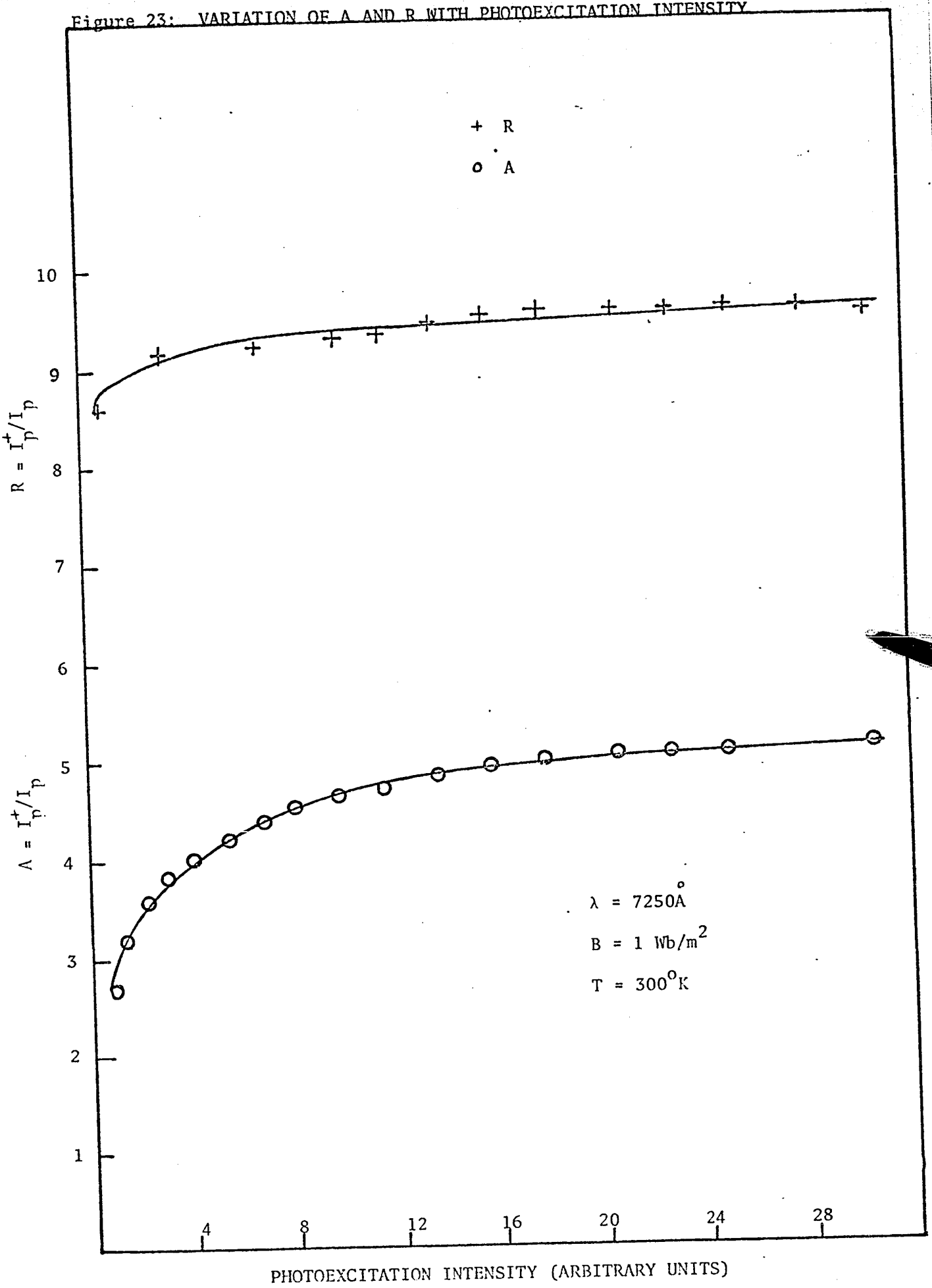

The PEM effect shows a similar behaviour with photoexcitation Intensity as illustrated in Fig (24).

This is another example in which the two effects behave in a similar way with the same parameter.

B. SAMPLE 30

This sample was polished with 5 μ alumina polish. The surface recombination velocity was less than that of Sample 7, but greater than that of the chemically polished Sample 9A, as will be seen from the results below.

The spectral distribution of photosensitivity curve of Sample 30 shown in Fig (25) gives a surface factor F = 2.6. This is less than the surface factor of Sample 7 spectral response curve (F = 5), but greater than that of Sample 9A (F = 2). The maximum Rectification amd Amplification ratios were 4.9 and 2.3 respectively. (Fig 26). The ratios lie between those of Sample 7 (R = 10.5, A = 4.3) and Sample 9A (R = 3.5, A = 1.5) values. The results are therefore consistent.

Further evidence in support of the low surface recombination of Sample 30 is obtained from the I_{PEM} vs B plot in Fig (27) in which I_{PEM} approaches saturation with increasing magnetic fields in accordance with equation (4-2) for low surface recombination. Once again results obtained from both the Photocurrent Amplification and PEM effects on the nature of the photoconductive properties of a surface are consistent.

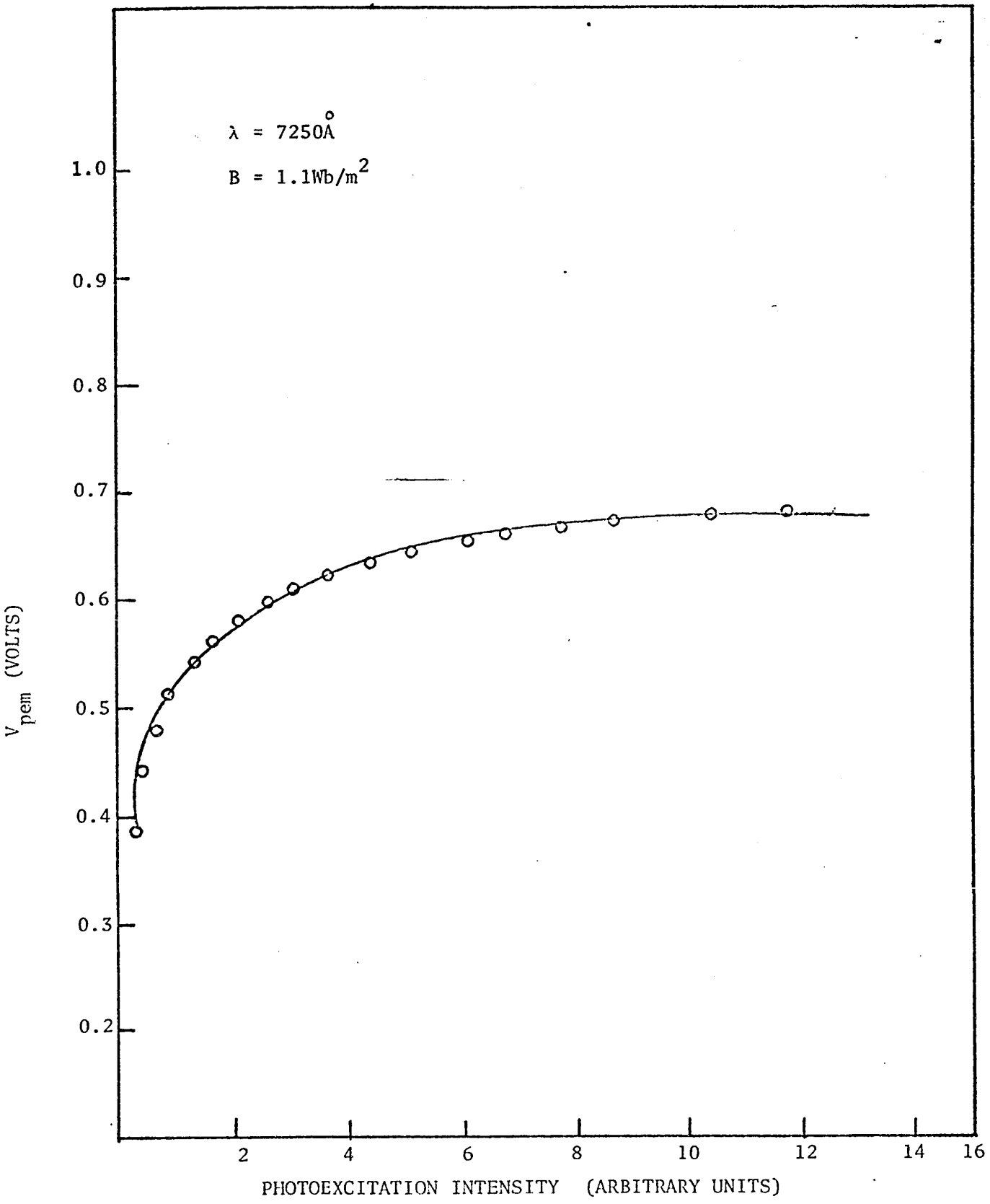

Figure 24 V_{pem} VERSUS PHOTOEXCITATION INTENSITY

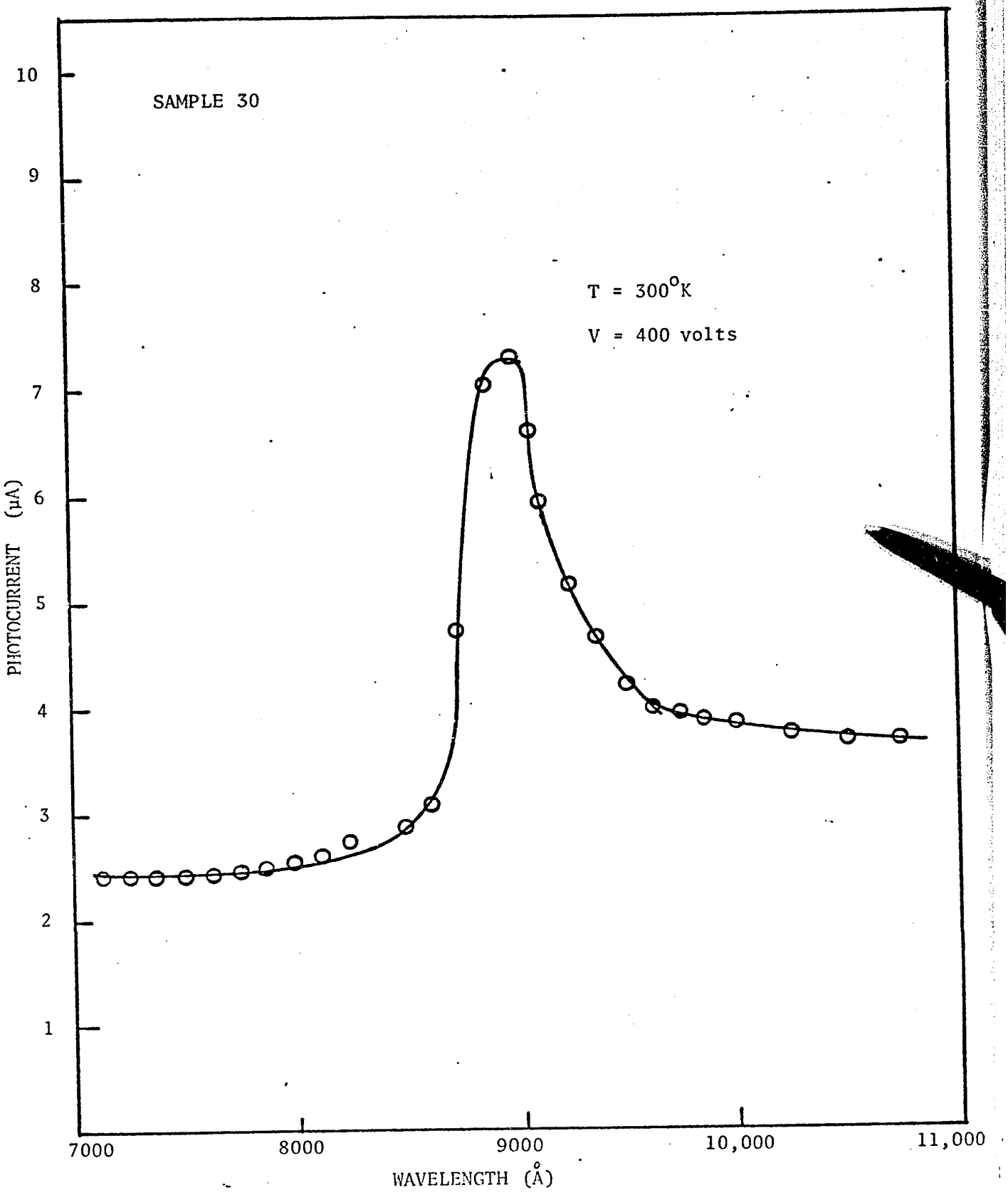

FIGURE 25 NORMALIZED SPECTRAL DISTRIBUTION OF PHOTOCONDUCTIVITY OF SAMPLE 30

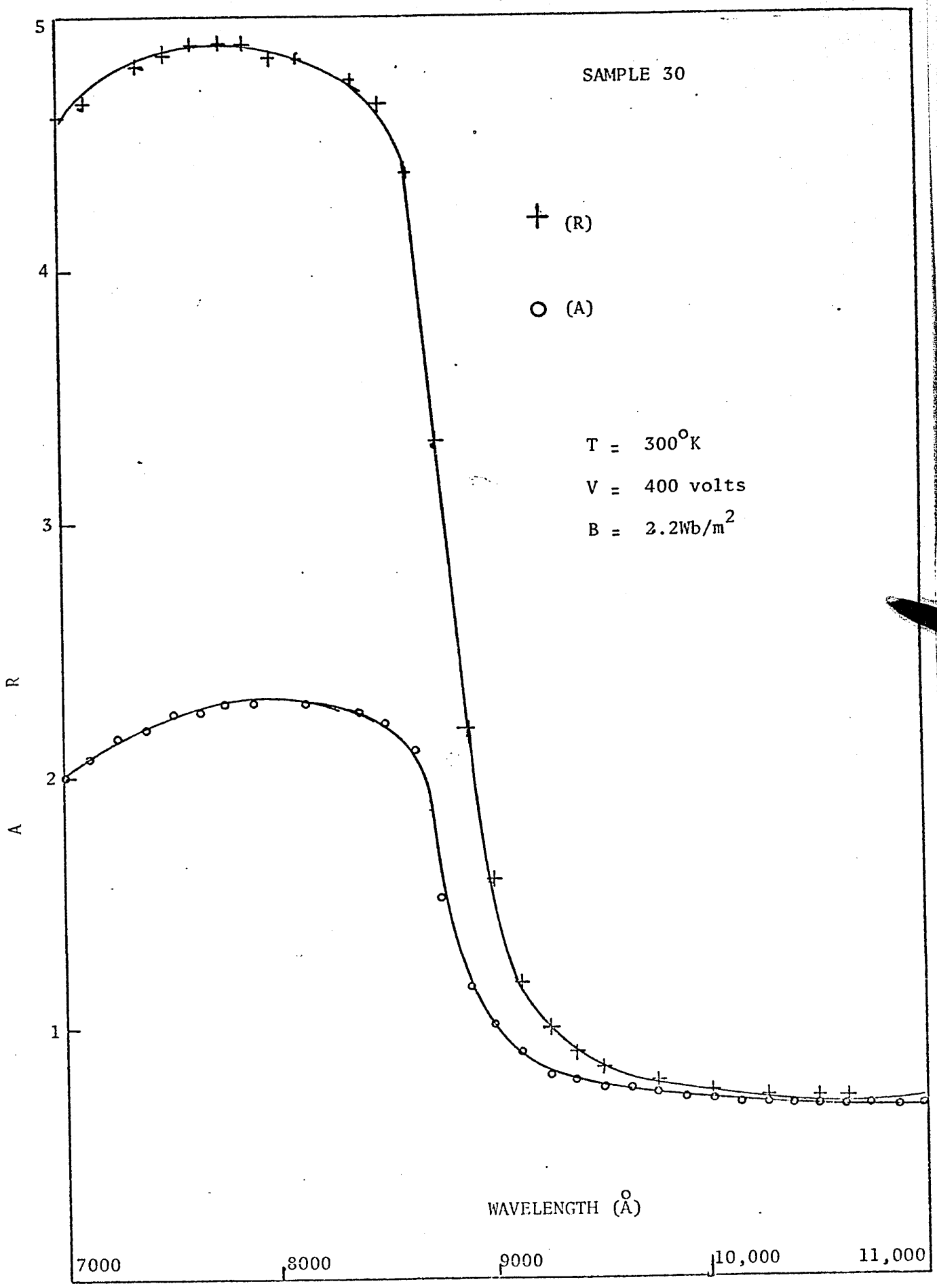

Figure 26 A and R VERSUS WAVELENGTH

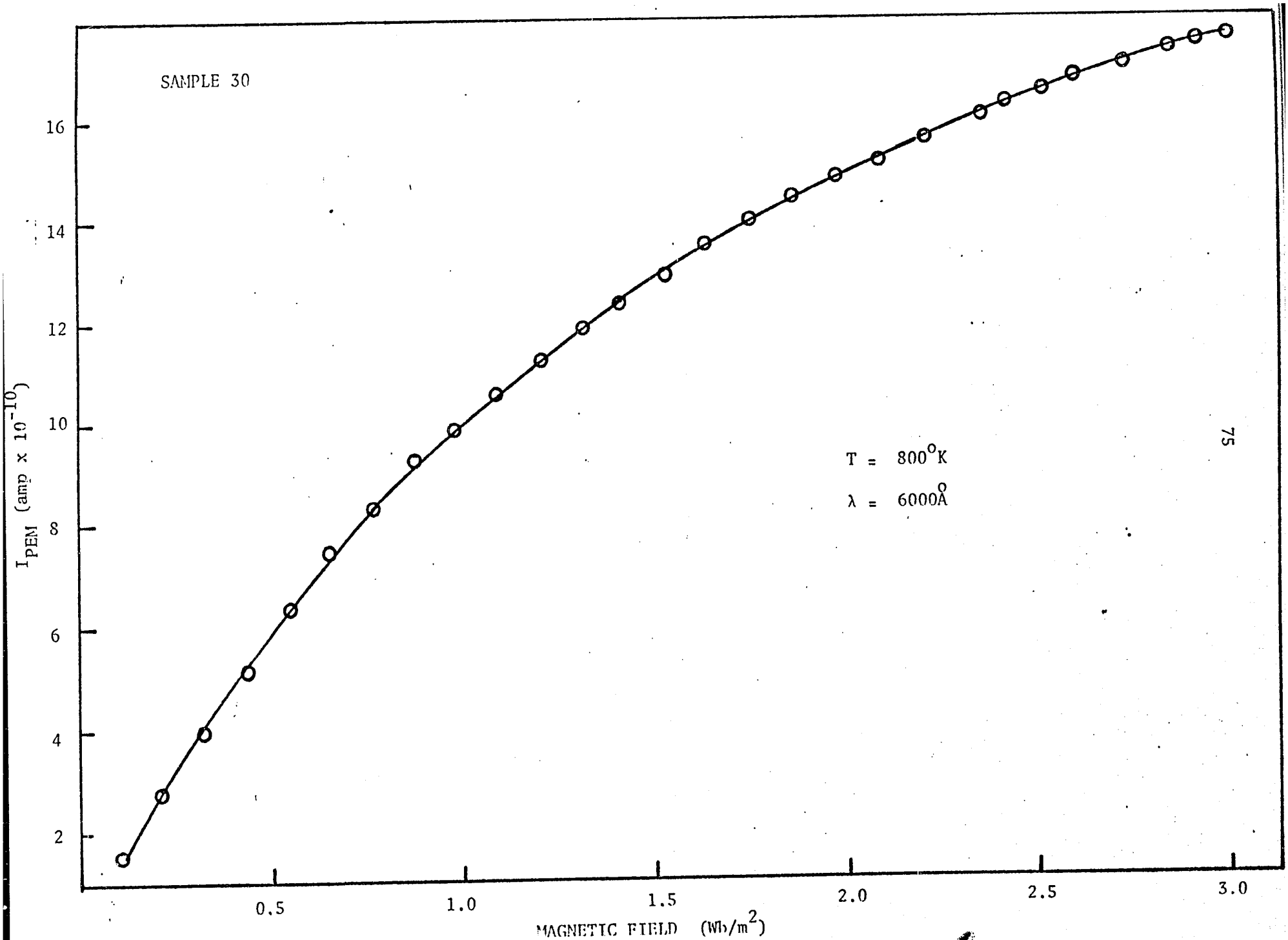

Figure 27 VARIATION OF PEM CURRENT WITH MAGNETIC FIELD

C. SAMPLE 33

Sample 33 was etched in a $AgNo_3$ + $K_2Cr_2O_7$ etchant. The above surface treatment resulted in a slight increase ($\sim$20%) of the Rectification ratio as shown in Fig (28). This is probably due to an increase in the capture cross-section of the recombination centers at the very top of the surface region (20) which lowered the I_p^- values.

D. SAMPLE 11

Original sample with Indium contacts was lapped very briefly and slowly with 5 μ alumina powder just to remove the contacts. Results obtained indicate that probably some of the Indium could have diffused into the surface region. What actually happened is not immediately obvious to the author.

The graph of Rectification and Amplification ratios as a function of wavelength at 90°K given in Fig (29) indicates increased effects at very short wavelengths (wavelength = 4000Å - 5000Å); Maximum R is 54 at 4500Å while maximum A is 23 at 4000Å. The above results could be explained by postulating three distinct regions of different lifetimes across the sample thickness. In Fig (30), region no. 1 represents a very thin film of extremely short lifetime τ_1', while lifetimes τ_1 and τ_2 in regions no. 2 and no. 3 are about the same as in the original sample.

When the sample was illuminated with monochromatic radiation of very short wavelengths (wavelengths < 5000Å), the excited layer was very thin, confined mainly to region no. 1 and part of region no. 2.

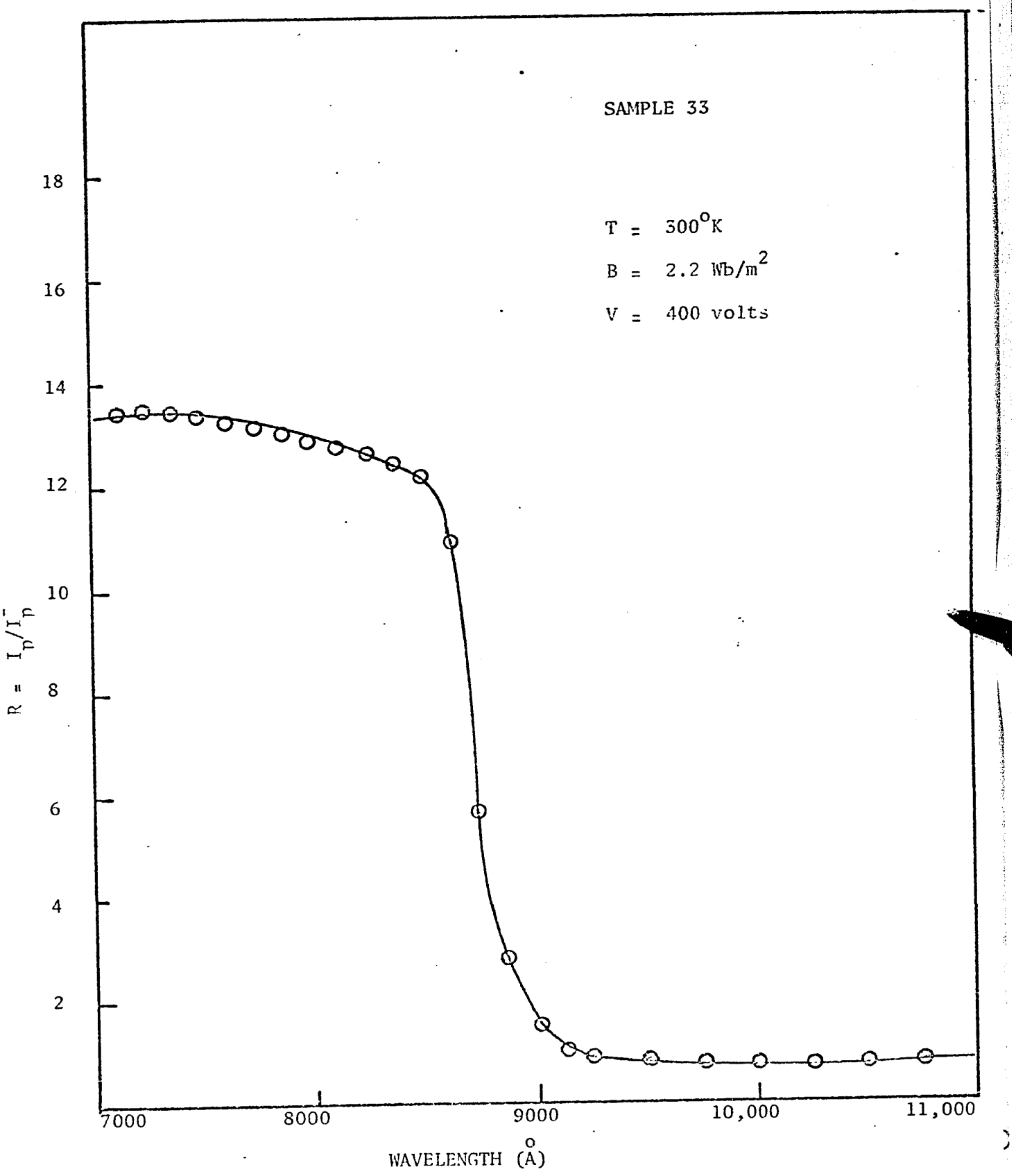

Figure 28 RECTIFICATION RATIO VERSUS WAVELENGTH

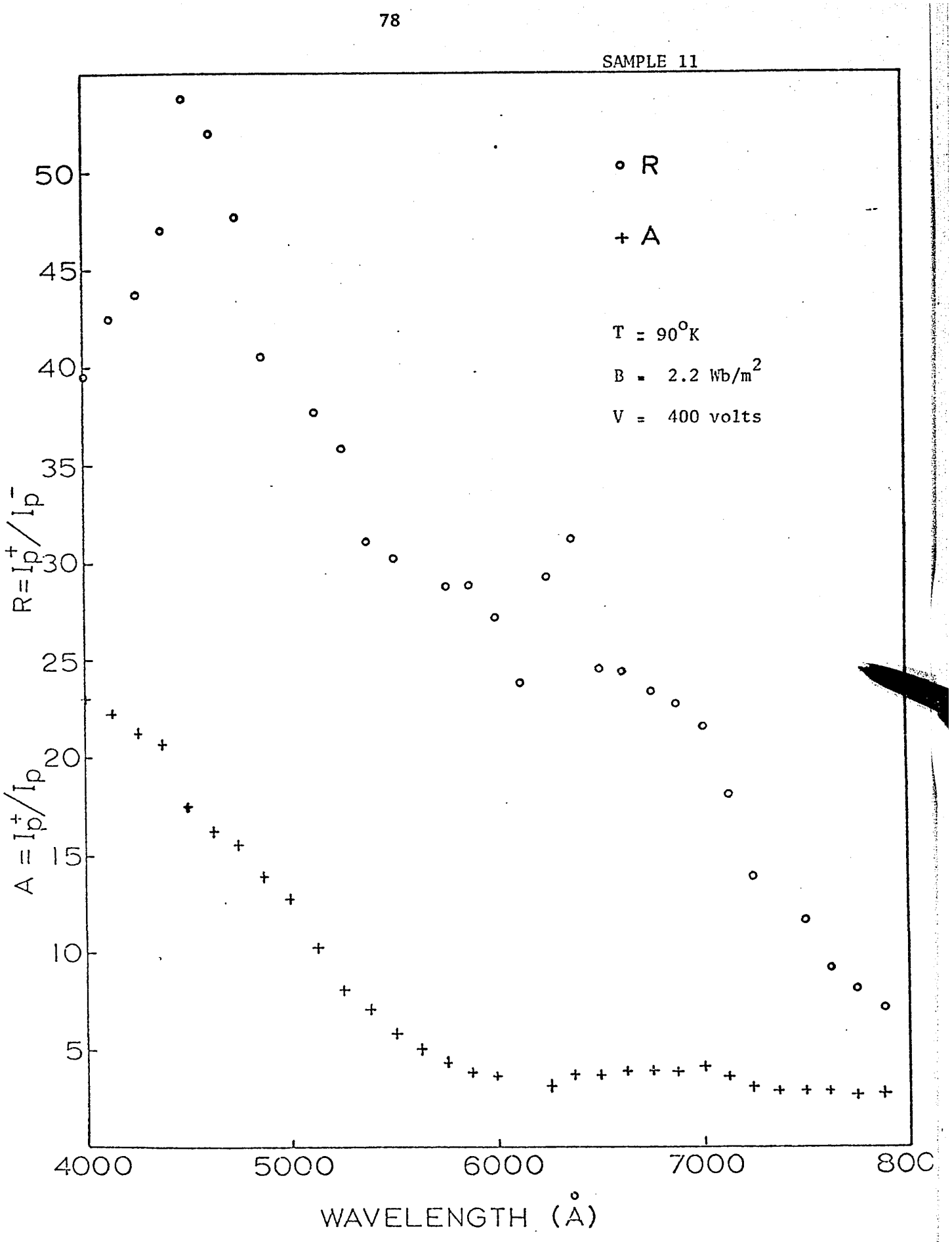

Figure 29 A AND R VERSUS WAVELENGTH

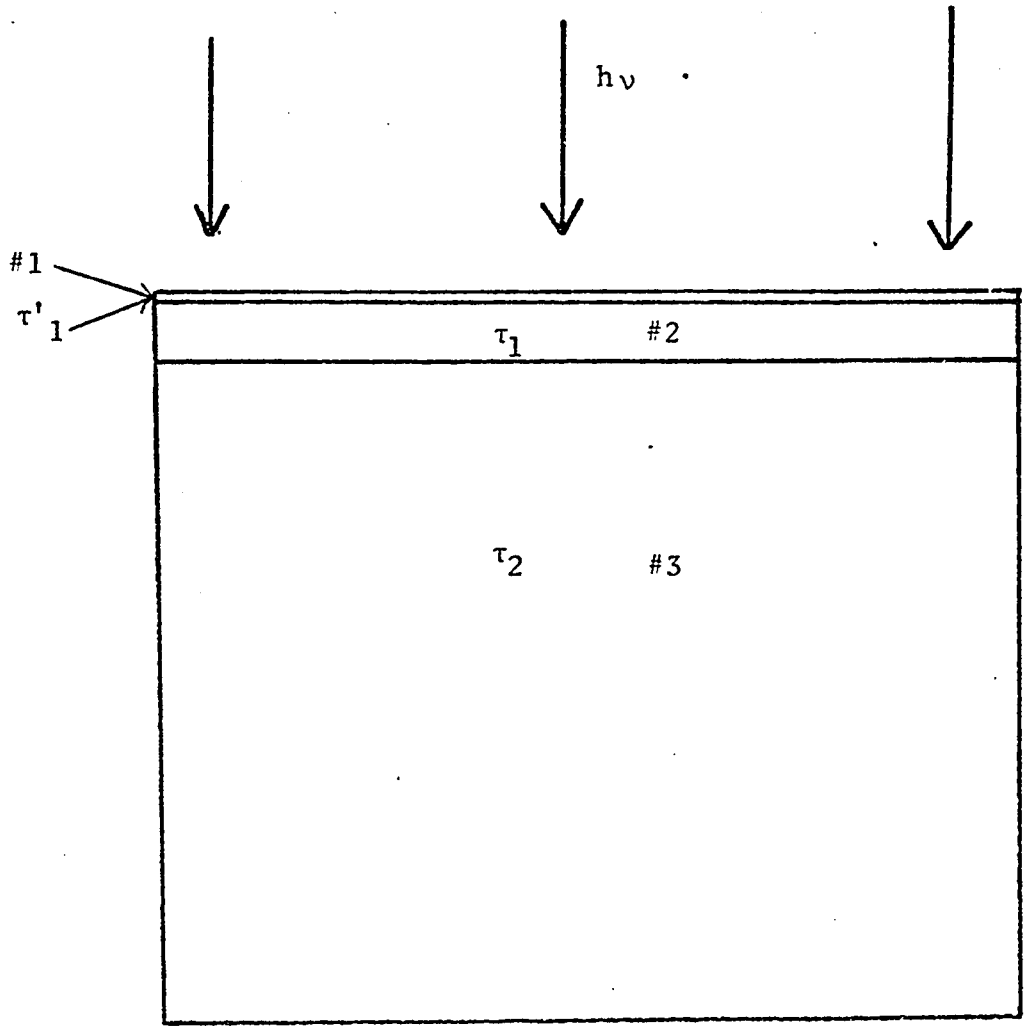

Figure 30 PHOTOCONDUCTING SLAB WITH A THIN FILM OF VERY SHORT LIFETIME τ'_1

A forward magnetic field (B) drives the photocarriers into regions no. 2 and no. 3 resulting in large amplification ratios since $\tau_2 > \tau_1 >> \tau_1'$. When B is reversed, the photocarriers excited in region no. 2 are forced into region no. 1; I_p^- is very small and hence a large increase in R ensues.

For longer wavelengths-deeper excitation, the majority of the photocarriers deflected towards the surface manage to reach only the top of region no. 2 giving values of I_p^- which are of about the same magnitude as those recorded in the original Sample 7. However, as illustrated in Fig. 31, the 10% increase in R could be due to the decrease in I_p^- caused by the small percentage of photocarriers which manage to reach region no. 1, when the carriers are deflected towards the illuminated surface.

PART II

This section gives a discussion of the results of the carrier mobility and lifetime measurements using the Photo-Hall and PEM effects. No Photo-Hall measurements were made at 90°K due to lack of the necessary apparatus (no attempt was made to build one since it formed a minor part of the project), but PEM measurements were made at both 300°K and 90°K. Photo-Hall results will be presented first.

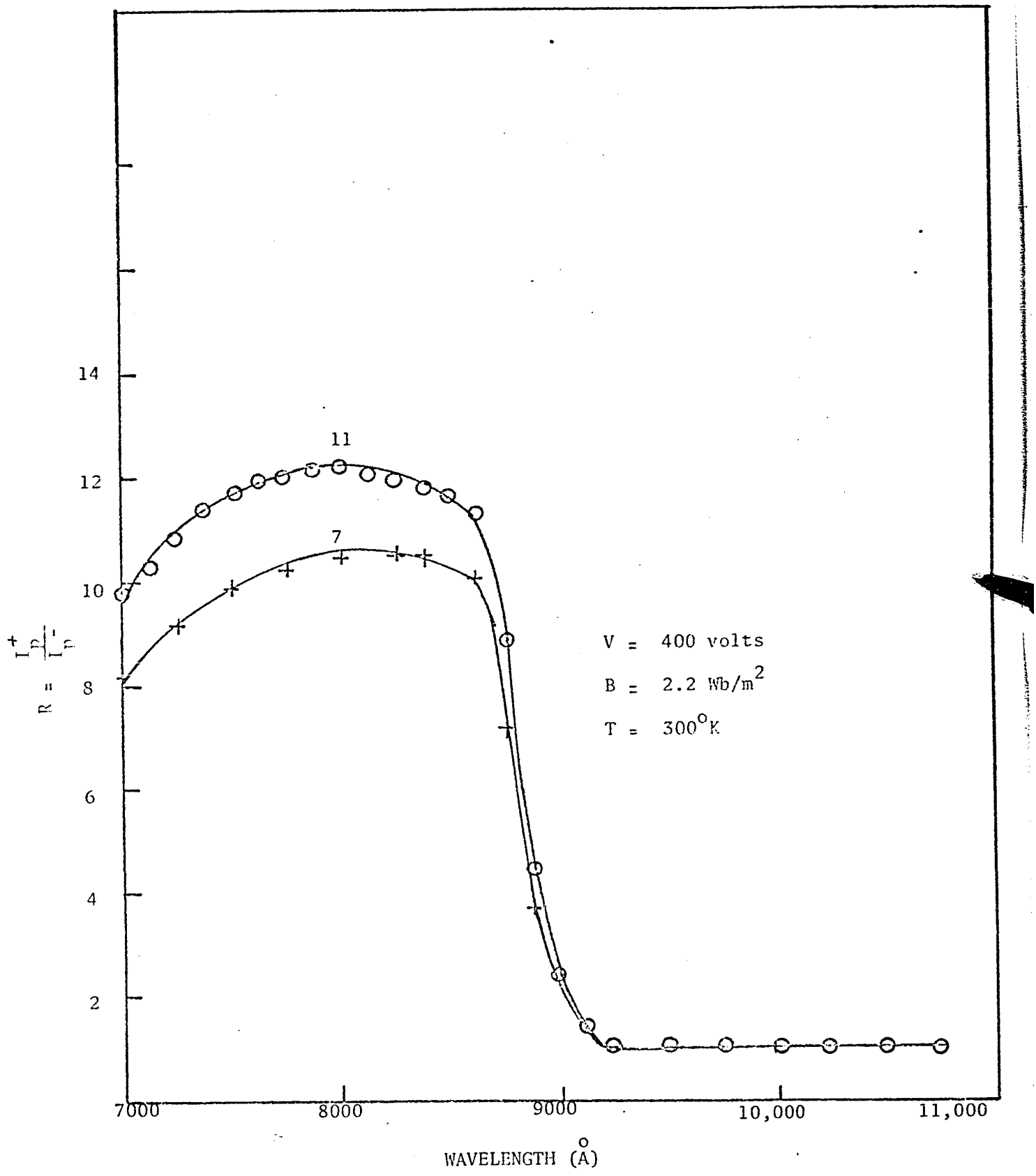

Figure 31 RECTIFICATION RATIO VERSUS WAVELENGTH FOR SAMPLES 11 AND 7

A. Photo-Hall

Photo-Hall measurements were made just to determine the mobility under illumination.

Fig (32) shows a graph of mobility as a function of intensity, in which the mobility increases from a dark value of $\mu = 0.25\ m^2$ $(volt\ sec)^{-1}$ saturating at higher intensities of excitation towards $\mu \sim 0.4\ m^2\ (volt\ sec)^{-1}$. This behaviour which has been previously observed by Blanc et al (15) is the result of a change in the scattering, i.e., a change in the occupancy of charged scattering centers, as a result of the motion of the steady-state fermi-level with photo-excitation. If we assume a scattering factor of unity, then $\mu_H = \mu_n$, and the electron mobilities indicated in Fig (32) are within the range of electron mobilities quoted in the literature: $\mu_n = 0.2 - 0.68\ m^2$ $(volt\ sec)^{-1}$ (21), $\mu_n = 0.3 - 0.8\ m^2\ (volt\ sec)^{-1}$ (22) and $\mu_n = 0.4\ m^2\ (volt\ sec)^{-1}$ (23).

Carrier concentration in s.i. GaAs is smaller than in s.c. GaAs and so the mobilities are smaller. This is related to the screening of ionized impurities by free-charge carriers and can be seen in the Brooks-Herring relation (22), by the dependence on both N_{ion} (concentration of ionized impurities) and the electron density n. For constant N_{ion}, μ_n decreases with n.

Now, since the Photo-Hall measurement gave the electron mobility, one would have expected the subsequent PEM measurements to give a hole mobility as the minority carrier mobility instead of the electron mobility which was obtained.

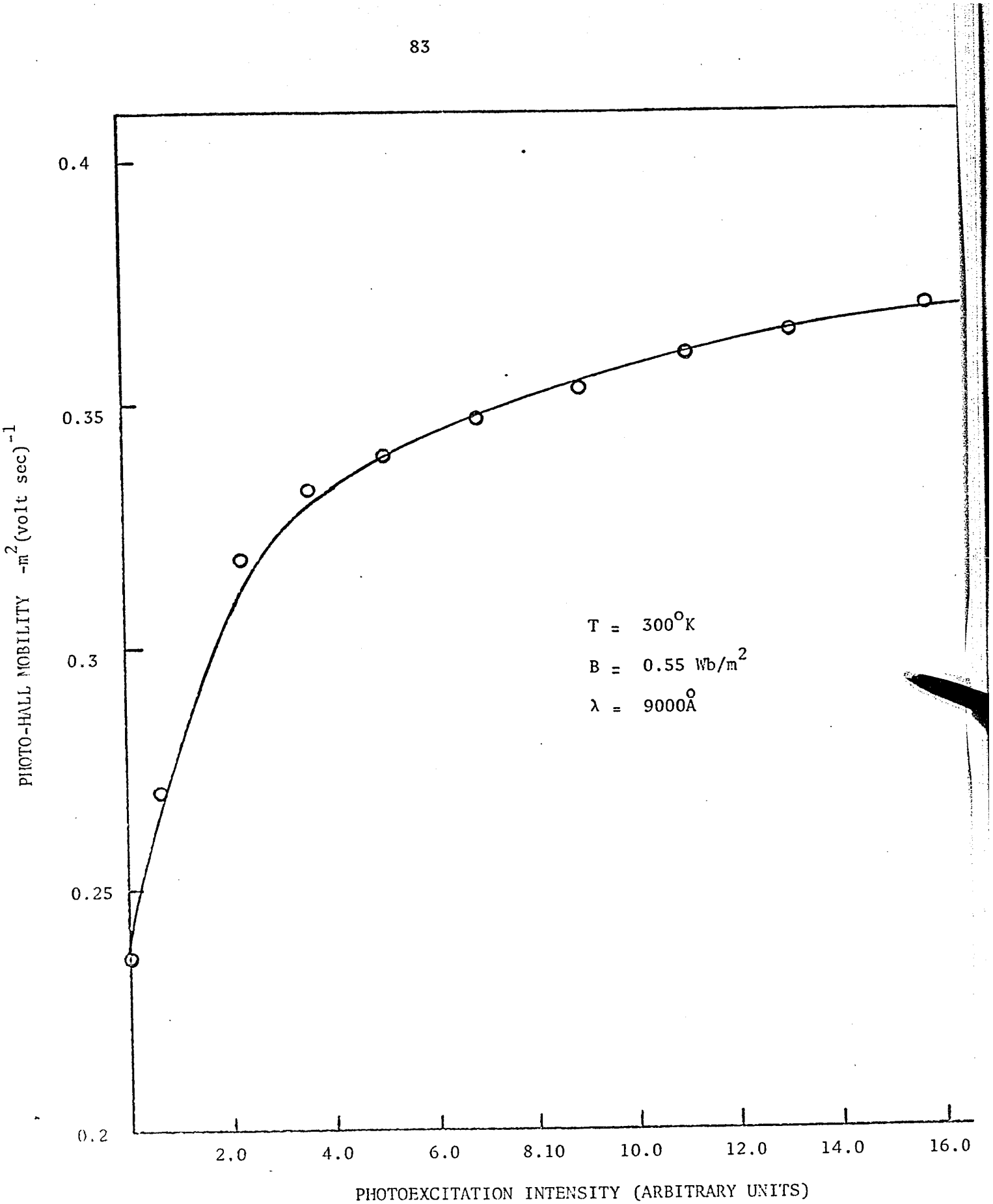

Figure 32 HALL MOBILITY AS A FUNCTION OF PHOTOEXCITATION INTENSITY.

The explanation is as follows: the Hall mobility for mixed conduction is given by

$$\mu_H = \frac{p\mu_p^2 - n\mu_n^2}{p\mu_p + n\mu_n}$$

but, since $\mu_n/\mu_p \sim 10$, $\mu_H \rightarrow \mu_n$ if $\rho < 10n$. The electrons would make a greater contribution towards the photoconductivity, even though in actual numbers there could be more holes than electrons. The photoconductivity may therefore be said to be "p-type" (i.e.: holes are the majority carriers), even though the sign of the Hall coefficient might indicate a predominance of electronic conduction.

PEM Measurements

Results of carrier mobility and lifetime measurements at 300°K will be given first.

Carrier Mobilities at 300°K

Fig (33) shows a plot of BV_{PEM}^{-1} versus B^2 at 300°K using eq. (2-11) in Chapter II. From the slope and intercept, C = 0.8, $\mu_n^2/C = 0.7/4.5$, hence $\mu_n = 0.32\ m^2\ volt^{-1}\ sec^{-1}$. This result is in good agreement with the photo-hall mobility value at the same intensity of photoexcitation (see Fig 32). Now assuming a mobility ratio $\mu_n/\mu_p = 10$, $\mu_p = 3.5 \times 10^{-2} m^2 volt^{-1} sec^{-1}$, and hence the mean harmonic of mobilities $\underline{\mu = 6.4 \times 10^{-2} m^2 volt^{-1} sec^{-1}}$. The Diffusion Constant $D = \mu KT/e = \underline{1.5 \times 10^{-3} m^2 sec^{-1}}$.

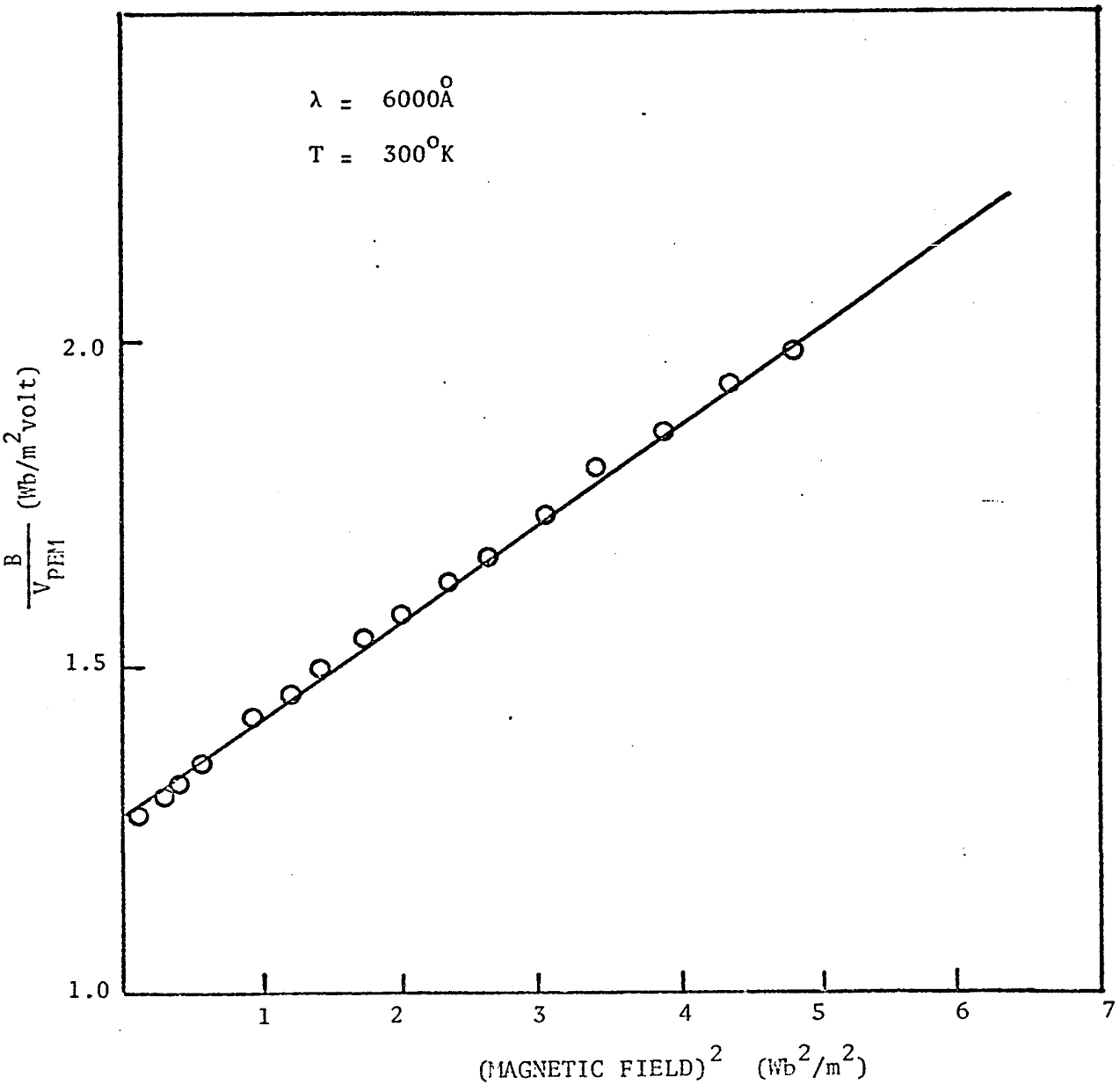

Figure 33 $\frac{B}{V_{PEM}}$ VERSUS B^2

Carrier Lifetimes at 300°K

Figs (34) and (35) show graphs of V_{PEM} as a function of Photoexcitation Intensity (I_o) and of V_{PEM}^{-1} versus I_o^{-1} at different wavelengths respectively using eq. (2-12) in Chapter II.

The values of A obtained at different wavelengths are summarized in Table I. In Table II are listed the I_{pc} and I_{PEM} currents at different wavelengths using B = 0.55 Wb/m^2, E = 2×10^4 $volt^{-1}$, and finally Table III gives a summary of the variation of lifetime with wavelength deduced from the two methods whose principles have been given in Chapter II, i.e., using eq. (2-18) and equations (2-12) and (2-15) respectively.

This is the first time that the method of lifetime measurements using the relation between the PEM voltage and Photoexcitation Intensity (eq. (2-12) - (2-15)), has been applied to GaAs and its agreement with the I_{pc}/I_{PEM} ratio method is remarkable. Also the values obtained are within an order of magnitude of the lifetimes previously measured in s.i. GaAs by Holeman and Hilsum (24) using a modified form of the I_{pc}/I_{PEM} ratio method. From other lifetime measurements made in normal semiconducting GaAs Amith (25) Hurd (26), it has been predicted by Madelung (27) that the lifetimes expected for trap-free GaAs lie between 3×10^{-9} and 5×10^{-7} sec. Thus, the lifetimes summarized in Table III are consistent with this prediction.

In the final evaluation of the mean surface lifetime τ_1 and mean volume lifetime τ_2 to be used in simple model, it is assumed that

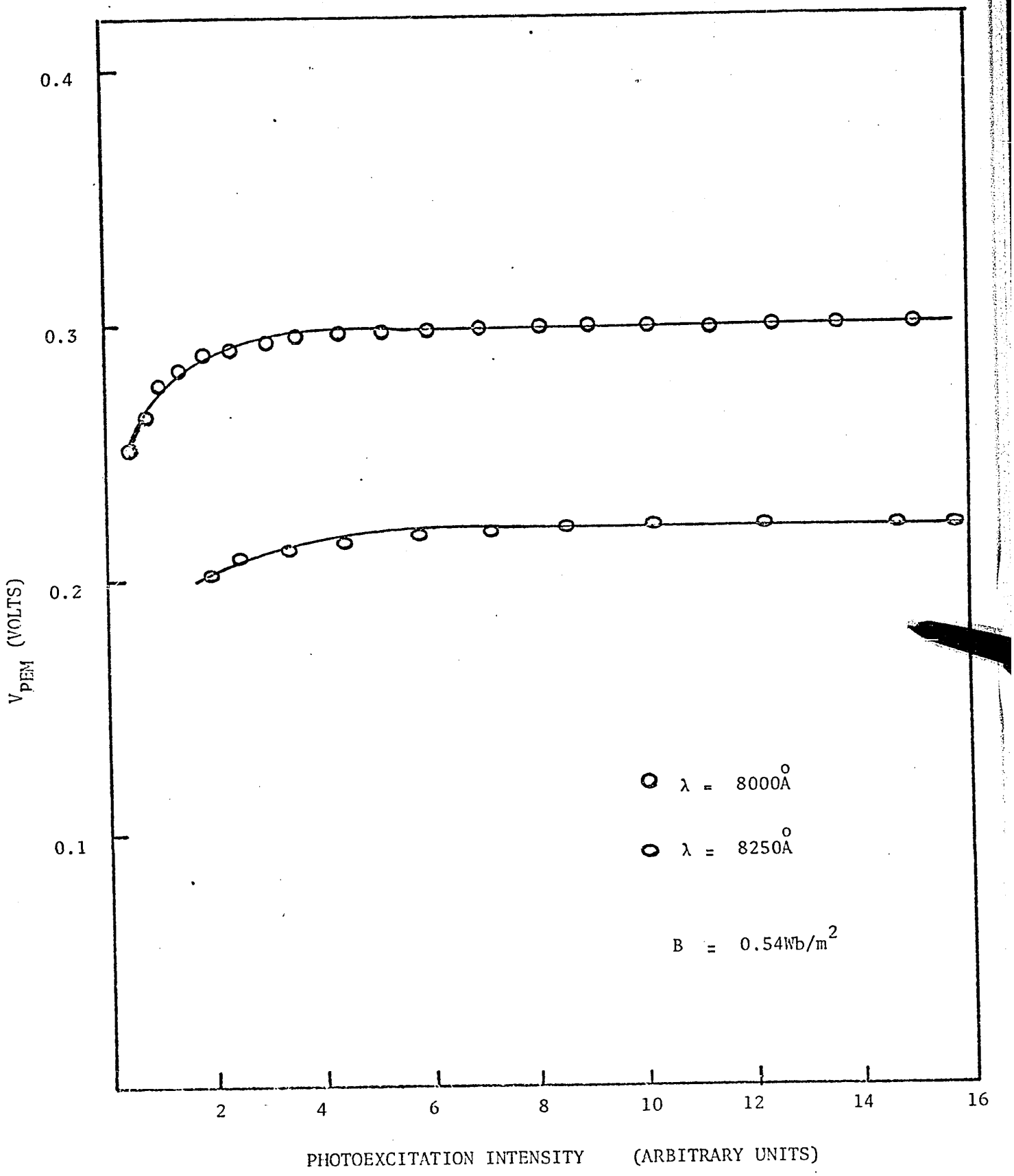

Figure 34 PEM VOLTAGE AS A FUNCTION OF PHOTOEXCITATION INTENSITY

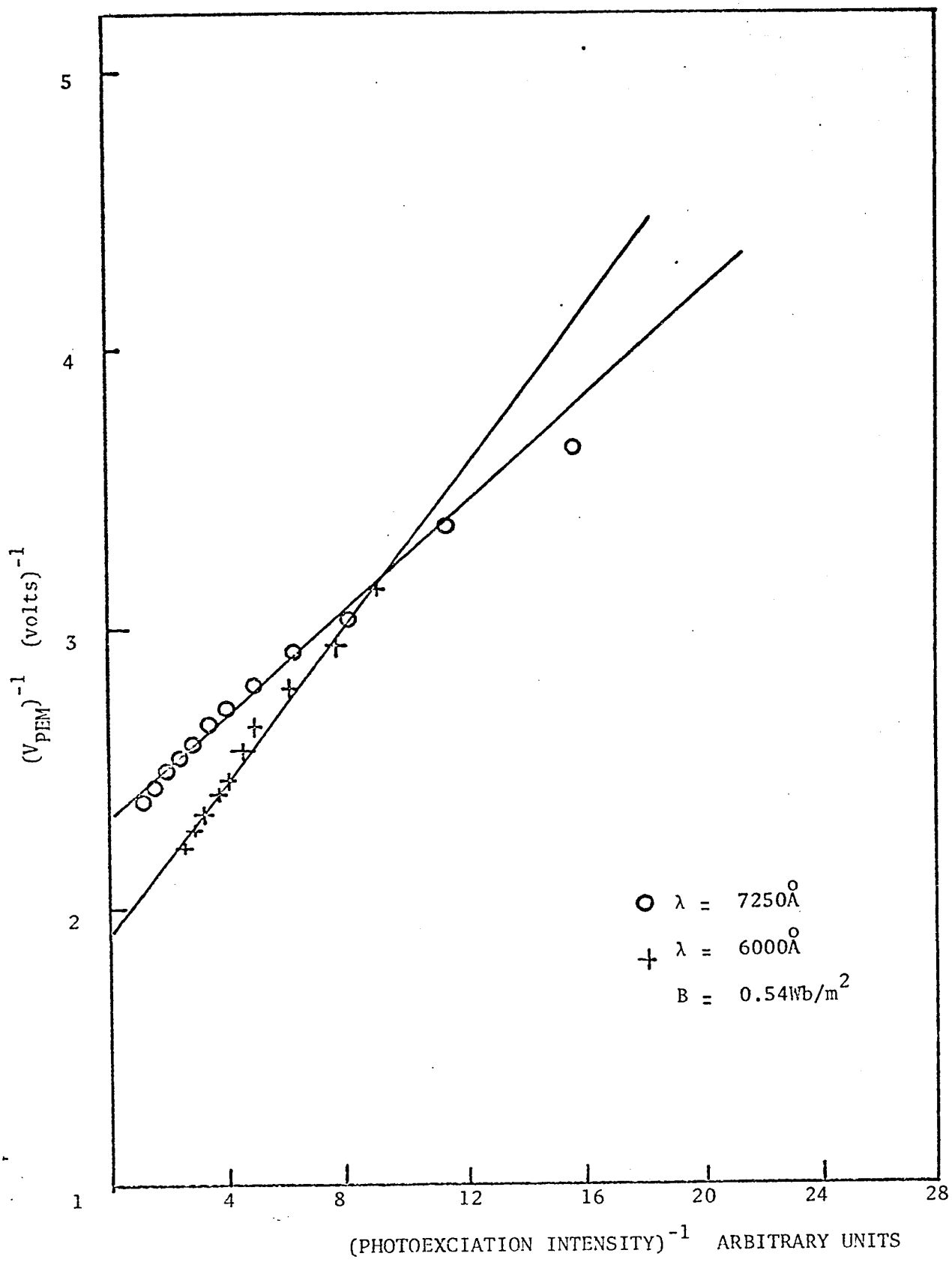

Figure 35 $(V_{PEM})^{-1}$ VERSUS (PHOTOEXCITATION INTENSITY)$^{-1}$

TABLE 1

Values Of A Obtained From Eq. (2-12) At Different Wavelengths

WAVELENGTH (Å)	A (volts)
5,000	0.53 0.01
6,000	0.53 0.01
7,250	0.43 0.01
8,000	0.30 0.01
8,250	0.23 0.01

TABLE 11

Ipc AND Ipem CURRENTS AT DIFFERENT WAVELENGTHS AT 300^{o} K

WAVELENGTH (Å)	PHOTOCURRENT Ipc (amp)	SHORT-CIRCUIT PEM CURRENT Ipem (amp)
5000	7.6×10^{-8}	2.7×10^{-10}
5250	8.9×10^{-8}	3.34×10^{-10}
5500	1.0×10^{-7}	3.9×10^{-10}
6000	1.19×10^{-7}	4.7×10^{-10}
7250	2.6×10^{-7}	7.3×10^{-10}
8000	3.8×10^{-7}	6.1×10^{-10}
8250	4.3×10^{-7}	6×10^{-10}
8500	5×10^{-7}	5.9×10^{-10}

TABLE III

Summary of Variation of Lifetime with Wavelength at $300^{o}K$

Wavelength λ(A)	$\tau = \frac{(B)}{(E)} D.\frac{(Ipc)}{(I_{pem})}$ (sec)	τ using equations (2.12)-(2.15) (sec)	MEAN τ_1 and τ_2 Calculated from the maximum Amplification condition $\mu^2 EB\tau_1 = Z_1$ (sec)
5000	9.8×10^{-8}	1×10^{-7}	$\tau \sim 9 \times 10^{-8}$
5250	9×10^{-8}		
5500	8.5×10^{-8}		
6000	9×10^{-8}	1×10^{-7}	
7250	1.6×10^{-7}	1.6×10^{-7}	
8000	4.3×10^{-7}	4.1×10^{-7}	$\tau_2 \sim 4 \times 10^{-7}$
8250	6×10^{-7}	5.9×10^{-7}	
8800	7×10^{-7}		

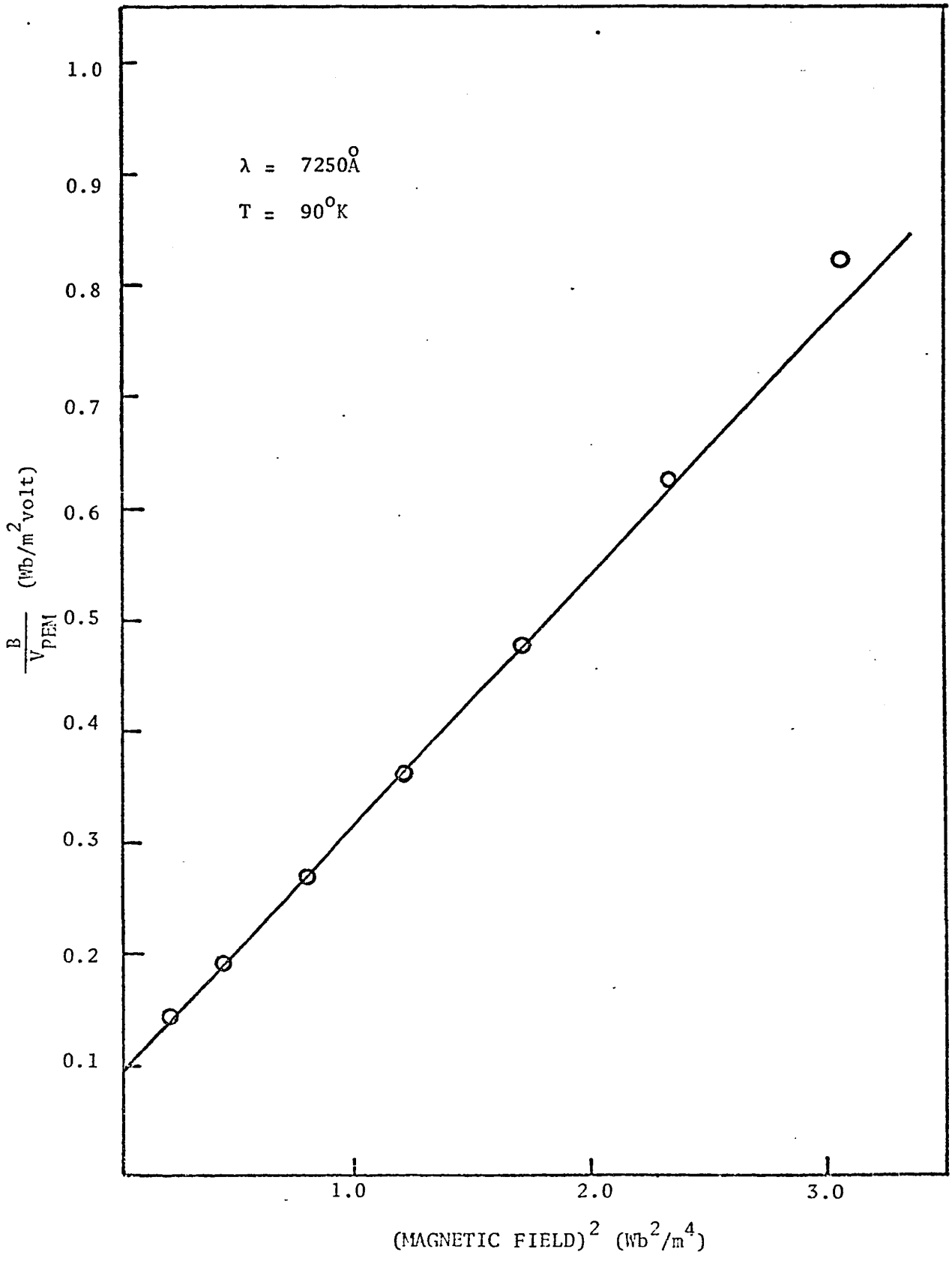

Figure 36 $\frac{B}{V_{PEM}}$ VERSUS B^2

TABLE IV

VALUES OF A AT DIFFERENT WAVELENGTHS CALCULATED FROM EQ.2.12 T = 90°K

WAVELENGTH (Å)	A (volts)
6000	5.5 ± 0.1
7250	3.6 ± 0.1
7500	3.8 ± 0.1
7750	3.7 ± 0.1
8000	2.7 ± 0.1
8250	0.27 ± 0.01

TABLE V

Ipc AND Ipem CURRENTS AT DIFFERENT WAVELENGTHS AT $90^{o}K$

WAVELENGTH (Å)	PHOTOCURRENT Ipc(amp)	PEM CURRENT Ipem(amp)
7250	3×10^{-8}	1.52×10^{-9}
7500	3.78×10^{-8}	1.95×10^{-9}

$B = 0.5 Wb/m^2$ $E = 8 \times 10^{3}$ Volt m^{-1}

TABLE VI

Summary of Carrier Lifetimes At $90^{o}K$

Wavelength (A)	τ using EQ (2-12)-(2-15) (sec)	τ using EQ (2-18) $\tau = (R/E)^2 .D. (I_{pc}/I_{PEM})^2$ (sec)	MEAN τ_1 & τ_2 Calculated From the Max. Amplification CONDITION $\mu^2 EB\tau_1 = Z_1$ (sec)
6000	1.3×10^{-9}		
7250	3.3×10^{-9}		
7500	2.9×10^{-9}	3.1×10^{-9}	$\tau_1 - 3 \times 10^{-9}$
7750	3.1×10^{-9}	3.1×10^{-9}	
8000	7×10^{-9}		$\tau_2 \sim 1.4 \times 10^{-8}$
8250	3.8×10^{-7}		

surface excitation predominates for wavelengths < 8,000Å, while volume excitation predominates for wavelengths > 8,000Å. Results from Table III then give $\tau_1 = 1.3 \times 10^{-7}$ sec and $\tau_2 = 6 \times 10^{-7}$ sec.

Now as stated in Chapter II, the model of section 2-1 predicts the maximum amplification conditions $\mu^2 EB\tau_1 = Z_1$ and also A (Maximum) $= \tau_2/\tau_1$. From the Amplification ratio as a function of magnetic field curve in Fig 15, and using μ from the mobility measurements, the above conditions give $\tau_1 \sim 9 \times 10^{-8}$ sec and $\tau_2 \sim 4 \times 10^{-7}$ sec. The agreement with the previous values seems quite satisfactory.

Carrier Lifetimes at 90°K

Fig (37) shows a graph of V_{PEM} as a function of Photoexcitation Intensity (I_o) at $\lambda = 8250$Å and Fig (38) a graph of V_{PEM}^{-1} versus I_o^{-1} at five different wavelengths. The values of A obtained using eq. (2-12) are summarized in Table IV. In Table V are listed the I_{pc} and I_{PEM} currents at two wavelengths and Table VI gives a summary of the variation of lifetimes with wavelength, i.e.: at different depths of excitation. Again these values are within the range of 3×10^{-9} - 5×10^{-7} sec, expected for trap-free GaAs (27).

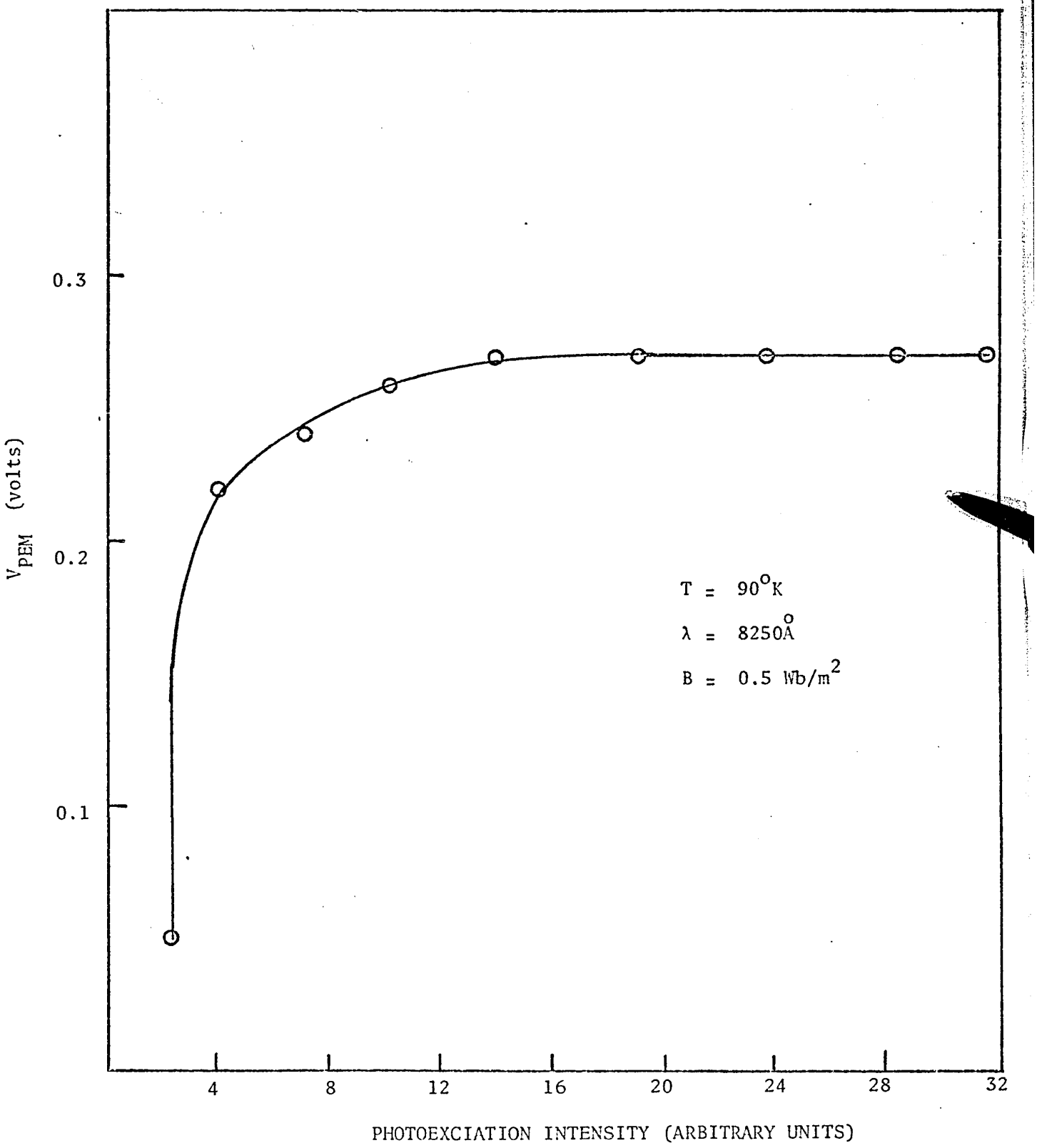

Figure 37 V_{PEM} VERSUS PHOTOEXCITATION INTENSITY.

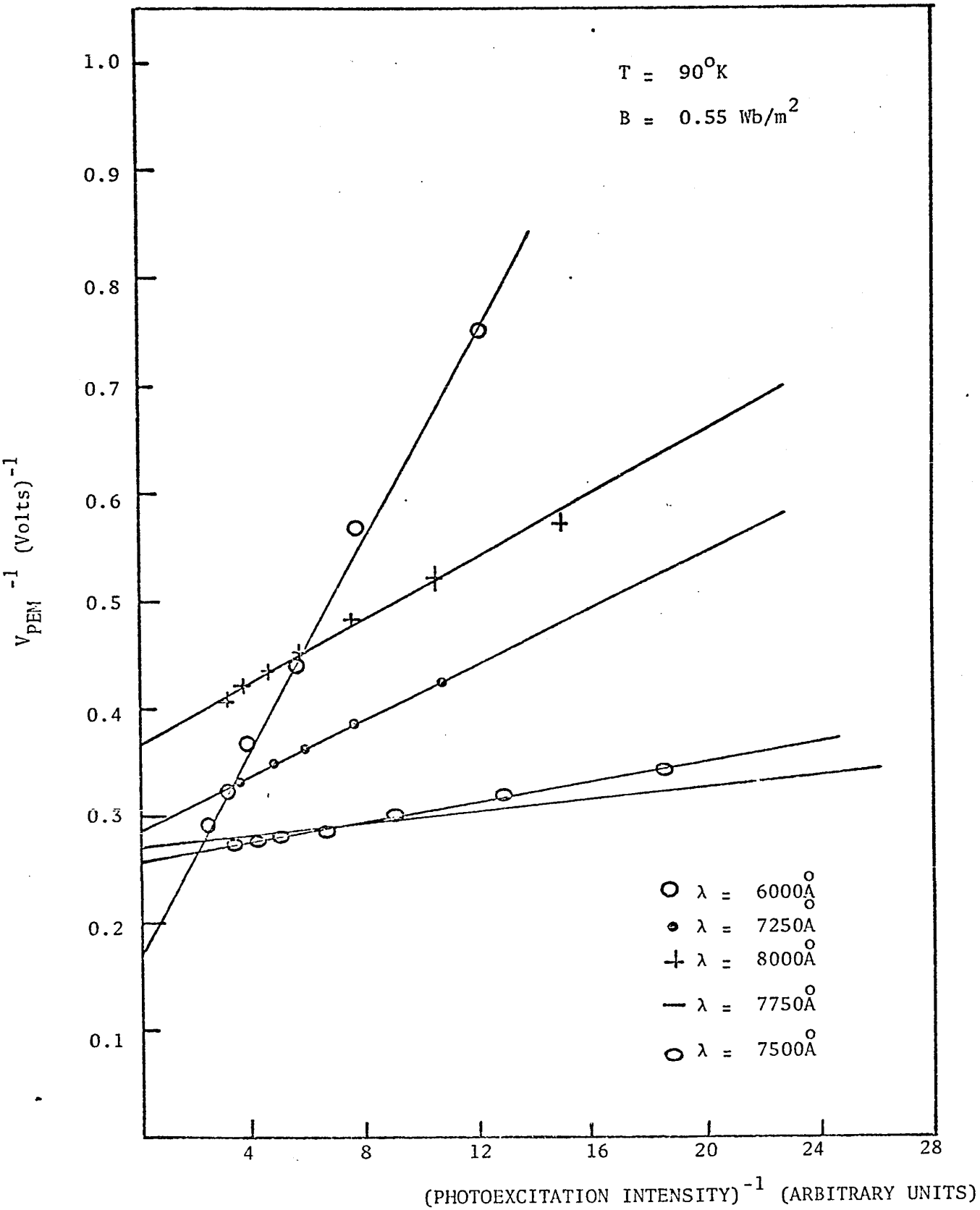

Figure 38 V_{PEM}^{-1} VERSUS (PHOTOEXCITATION INTENSITY)$^{-1}$ AT

B. Comparison Of Experimental Data With Simple Model

From the mobility and lifetime measurements at $300^{o}K$, the following were obtained.

A mean harmonic of mobilities $\mu = 6.4 \times 10^{-2} m^2$ (volt sec)$^{-1}$

A mean volume lifetime $\tau_2 = 6 \times 10^{-7}$ sec

A mean surface lifetime $\tau_1 = 1.3 \times 10^{-7}$ sec

A comparison will now be made between experimental data and values calculated from the simple model equation.

$$I_p^+ = I_p \frac{(1 + \mu^2 EB\tau_2/Z_1)}{(1 + \mu^2 EB\tau_1/Z_1)}$$

In the first case experimental values of I_p are compared with calculated values using the above equation and experimental values of I_p. μ, τ_2 and τ_1 are as given above: $Z_1 = 1/\alpha$ where α is the absorption coefficient at $\lambda = 9000\text{Å}$ ($= 10^5 m^{-1}$) when the amplification vanishes.

Substituting these values into the equation with $B = 1$ Wb/m^2 gives

$$I_p^+ = I_p \frac{(1 + 24E \times 10^{-5})}{(1 + 5.2E \times 10^{-5})}$$

I_p^+ is calculated from this equation for different values of E. Fig (39) is part of an I - V characteristic curve indicating experimental values of I_p and I_p^+, as well as calculated values of I_p^+: $\lambda = 6000\text{Å}$ and hence excitation is only in region no. 1 before the magnetic field is applied.

B. Comparison Of Experimental Data With Simple Model

From the mobility and lifetime measurements at $300^{o}K$, the following were obtained.

A mean harmonic of mobilities $\mu = 6.4 \times 10^{-2} m^2$ (volt sec)$^{-1}$

A mean volume lifetime $\tau_2 = 6 \times 10^{-7}$ sec

A mean surface lifetime $\tau_1 = 1.3 \times 10^{-7}$ sec

A comparison will now be made between experimental data and values calculated from the simple model equation.

$$I_p^+ = I_p \frac{(1 + \mu^2 EB\tau_2/Z_1)}{(1 + \mu^2 EB\tau_1/Z_1)}$$

In the first case experimental values of I_p are compared with calculated values using the above equation and experimental values of I_p. μ, τ_2 and τ_1 are as given above: $Z_1 = 1/\alpha$ where α is the absorption coefficient at $\lambda = 9000\text{Å}$ ($= 10^5 m^{-1}$) when the amplification vanishes.

Substituting these values into the equation with $B = 1$ Wb/m^2 gives

$$I_p^+ = I_p \frac{(1 + 24E \times 10^{-5})}{(1 + 5.2E \times 10^{-5})}$$

I_p^+ is calculated from this equation for different values of E. Fig (39) is part of an I - V characteristic curve indicating experimental values of I_p and I_p^+, as well as calculated values of I_p^+: $\lambda = 6000\text{Å}$ and hence excitation is only in region no. 1 before the magnetic field is applied.

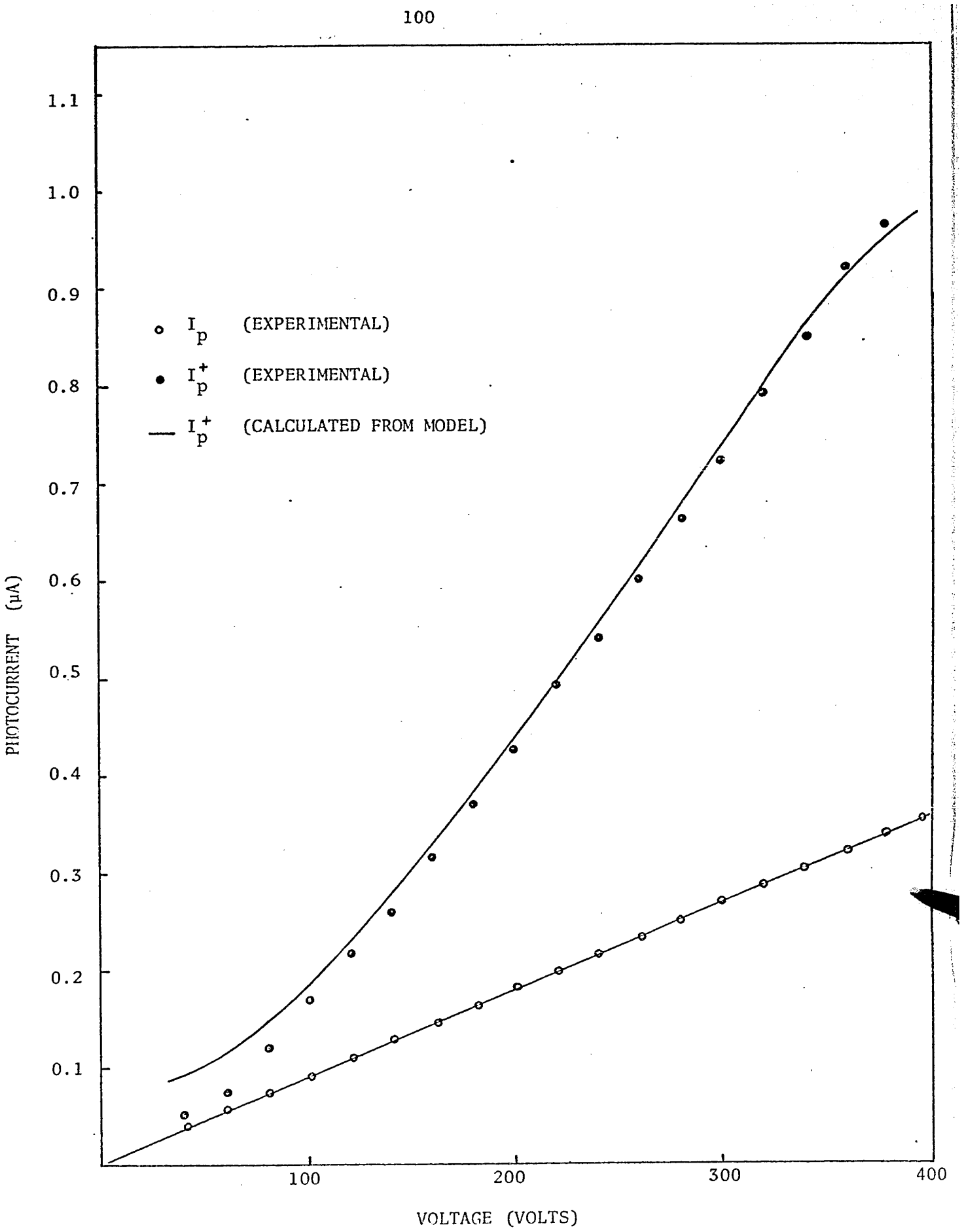

Figure 39 COMPARISON OF EXPERIMENTAL AND THEORETICAL VALUES OF I_p^+

A second comparison is made between the experimental and calculated values of the Amplification ratio as a function of magnetic field at constant electric field, $\lambda = 7500\text{Å}^{o}$ and again excitation is only in region no. 1, $E = 6 \times 10^{4}$ volt m^{-1}, and the equation takes on the form

$$A = \frac{I_p^+}{I_p} = \frac{(1 + 14.4B)}{(1 + 3.2B)}$$

Fig (40) indicates a satisfactory agreement between the experimental and calculated values of the Amplification ratio.

Also, the experimental maximum amplification ratio of 4.6 is equal to that predicted by the model which is

$$\tau_2/\tau_1 = \frac{6 \times 10^{-7}}{1.3 \times 10^{-7}} = 4.6$$

A second comparison is made between the experimental and calculated values of the Amplification ratio as a function of magnetic field at constant electric field, $\lambda = 7500\text{Å}$ and again excitation is only in region no. 1, $E = 6 \times 10^4$ volt m^{-1}, and the equation takes on the form

$$A = \frac{I_p^+}{I_p} = \frac{(1 + 14.4B)}{(1 + 3.2B)}$$

Fig (40) indicates a satisfactory agreement between the experimental and calculated values of the Amplification ratio.

Also, the experimental maximum amplification ratio of 4.6 is equal to that predicted by the model which is

$$\tau_2/\tau_1 = \frac{6 \times 10^{-7}}{1.3 \times 10^{-7}} = 4.6$$

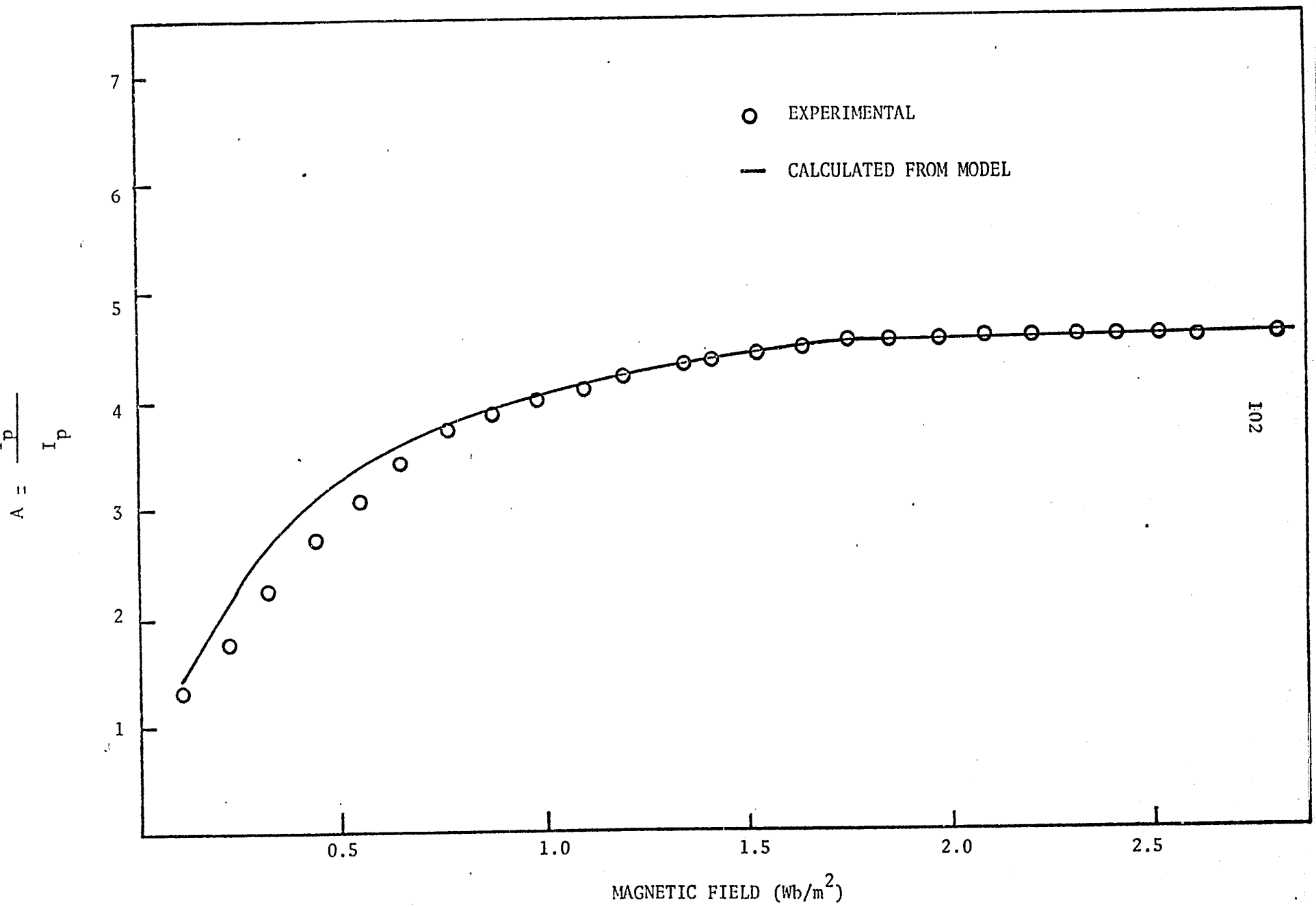

Figure 40 COMPARISON OF EXPERIMENTAL AND THEORETICAL VALUES OF A

CHAPTER V

CONCLUSION

1. A detailed study has been made for the first time of the changes of photocurrent of semi-insulating GaAs in a magnetic field. The effect was analysed quantitatively in terms of Amplification (A) and Rectification (R) ratios. The magnitudes of A and R depended upon the surface treatment given to the sample as well as on the temperature. However, for a particular surface treatment and at a fixed temperature, these ratios varied with wavelength of excitation (falling to unity at energies below the absorption edge), increases almost linearly with electric field, and saturated with increasing magnetic fields. The largest ratios obtained were $R = 54$, $A = 23$ for $B = 2.2\ Wb/m^2$, $E = 6 \times 10^4 Vm^{-1}$, $\lambda = 4500\ \mathring{A}$ and $T = 90^\circ K$. PEM studies made indicated that the short-circuit PEM current and the amplified photocurrent, varied in the same way with wave-length and intensity of photoexcitation as well as with the applied magnetic field. These results lend support to the initial hypothesis, that there existed some phenomenological similarities between the two effects.

Carrier mobilities and lifetimes were measured by two independent methods in each case (one of which has never been previously applied to s.i GaAs) with reasonable agreement between them. Also from the amplification effect carrier lifetimes were deduced the magnitudes of which agreed fairly with those obtained from the other two methods.

From these measurements were evaluated the principal parameters of the simple model derived: a comparison was then made between experimental data and values calculated from the model and the agreement was satisfactory.

2. The photocurrent amplification effect could have possible practical applications. In a photoconductor in which the carrier mobilities are almost the same; the effect could prove useful in measuring carrier mobilities, without having to use six contacts as in the Hall techniques. Provided the absorption coefficient at the wavelength when the amplification vanishes is known accurately, hence surface depth Z_1, a measurement of the maximum amplification ratio would yield the surface and volume lifetimes. In the field of device applications the effect could obviously provide photocurrent control, and flatten the spectral sensitivity curve of detectors. There is also the possibility of using the effect to measure magnetic fields. For example, if the values of the parameters measured are substituted into the model, then an amplification ratio of 3 would indicate a magnetic field of 0.5 Wb/m^2. A very thin high-resistivity layer (4μ thick) can be produced on the surface of the sample by proton bombardment using a Van de Graff generator (30). If the radiation damage is such that $\tau_2/\tau_1 = 100$, magnetic fields less than 0.05 Wb/m^2 could be measured accurately.

3. Although the simple model developed describes the amplification

effect satisfactorily, a better model could be deduced if fewer initial assumptions were made. In the model the carrier lifetime was assumed to be a function of Z only, while in actual practice it probably is a function of carrier concentration (ie: a function of illumination intensity) as well. Also, a step function was assumed for the depth dependence of the lifetimes, which in an actual photoconductor will be continuous.

For a photoconductor in which trapping effects are significant, trapping of minority carriers will be a limiting factor on the amplification. When carriers are trapped their effective mobility is zero as far as the amplification is concerned. In this case μ should be replaced by μ^1, where $\mu^1 < \mu$, the actual value depending on the relative amount of trapping involved. If all carriers of one sign are trapped, $\mu = 0$; if there is no trapping $\mu^1 = \mu$.

All these factors will tend to limit the ideal amplification expected from the simple model equation. Since the same factors also affect the magnitude of the PEM current, it is to be expected that a photoconductor giving a high PEM current may also be suitable for photocurrent amplification. Models that have been worked out for the PEM current in the presence of trapping could, therefore, probably be used as a starting point towards an improved model of the photocurrent amplification effect.

Finally, as to the ideas behind the simple model, a better test could be achieved, particularly with respect to the somewhat arbitrary use of the harmonic means of the mobilities, by a similar

study on a photoconductor where μ_n and μ_p are about the same; in this case, $\mu = \frac{2\mu_n\mu_p}{\mu_n + \mu_p} = \mu_n$ or μ_p.

High-resistivity GaP in which the room-temperature electron and hole mobilities are around 0.015 m^2 (volt sec)$^{-1}$ (31) (32) (33) may prove interesting in this respect.

LIST OF REFERENCES

1. Bube R. H. Phys. Rev. 101, 1668 (1956)
2. Shōji Tanaka, Taizo Masumi and Sigeru Irjima, J. Phys. Soc. Japan 11, 90-91 (1956)
3. Frankevitch E. L. and Balabanov E. I. Jept Letters 1, 169 (1965)
4. Frankevitch E. L. and Balabanov E. I. J.E.PT 23 No. 5, 814 (1966)
5. Zielinger J. P., Zouachi M., Fortin E. and Weichman F. L., Phys. Letters (Netherlands) Vol. 24A No. 7 397-399 (1967)
6. Fortin E., Phys. Stat. Sol 29 K153 (1968)
7. Smith R. A. Semiconductors 1959 Cambridge University Press, p. 310
8. Kurnick S. W. and Zitter R. N., J. Appl. Phys. 27, 278 (1956)
9. Aigrain P. and Bulliard H., Compte Rendus Acad. des Sciences 236, 595 (1953)
10. Aigrain P. and Bulliard H., Compte Rendus Acad. des Sciences 236, 673 (1953)
11. Bulliard H., Ann. de phys. 12^{e} Serie t. 9 p. 64 (Jan-Fev. 1954)
12. Bulliard H., Ann. de phys. 12^{e} Serie t. 9 p. 78 (1954)
13. Zielinger J. P., D-Sc Thesis, University of Strasbourg, (1969)
14. Hilsum C. and Holeman B., Proceedings of the International Conference on Semiconductor Physics Prague (1960) p. 962
15. Blanc J., Bube R. H., and MacDonald H. E., J. Appl. Phys. Vol 32 No. 9, 1674 (1961)
16. Bube R. H. Photoconductivity of Solids (1960) Wiley p. 386
17. Rose A., Concepts in Photoconductivity and Allied Problems (1963) Interscience Publishers, p. 56
18. Moss. Pincherle and Woodward, Proc. Phys. Soc. 66B 743 (1953)

19. Davis J. L. Bull. Ann. Phys. Soc. 6, 18

20. Flinn I., Surface Science Vol. 10, No. 1, p. 32 (1968)

21. Bube R. H., Photoconductivity of Solids (1960), Wiley p. 269

22. Madelung O. Physics of III - V, Compounds (1964), Wiley p. 133

23. Smith R. A., Semiconductors (1959) Cambridge University Press p. 408

24. Holeman B. R. and Hilsum C., J. Phys. Chem. Solids 22 19 (1961)

25. Amith A. Phys. Rev. 116 793 (1959)

26. Hurd C. M., Proc. Phys. Soc 79 42 (1962)

27. Madelung O., Physics of III - V, Compounds (1964), Wiley p. 220

28. Oliver D. J., Phys. Rev. 127 1045 (1962)

29. Weisberg L. R. Rose F. D. and Herkart P. G. (1960) Metallurgical Society Conferences Vol. 5, Properties of Elemental and Compound Semiconductors, Interscience Publishers, N.Y. p. 25

30. Lindley W. T., Wolfe C. M. Lincoln Lab. Report No. 2 p. 10 (1968)

31. Nasledov D. N., Slobotchikov S. V. Fiz. Tv. Tela 4, 2755, (1962)

32. Cherry R. J., Allen J. W. J., Phys. Chem. Solids 23, 163, (1962)

33. Johnson V. A., Lark-Horovitz K., Phys. Rev. 82, 977 (1951)